National Park Service
U.S. Department of the Interior

Natural Resource Stewardship and Science

Impacts of Fire Management on Aboveground Tree Carbon Stocks in Yosemite and Sequoia & Kings Canyon National Parks

Natural Resource Report NPS/SIEN/NRR—2015/910

ON THIS PAGE
Photograph of the aftermath of a high severity fire in Yosemite National Park, (Foresta area)
Photograph by Leland Tarnay

ON THE COVER
Photograph of high elevation landscape as seen looking northeast from Mt Hoffman, Yosemite NP
Photograph by Leland Tarnay

Impacts of Fire Management on Aboveground Tree Carbon Stocks in Yosemite and Sequoia & Kings Canyon National Parks

Natural Resource Report NPS/SIEN/NRR—2015/910

John R. Matchett[1], James A. Lutz[2], Leland W. Tarnay[3], Douglas G. Smith[3], Kendall M.L. Becker[2], and Matthew L. Brooks[1]

[1] U.S. Geological Survey
Western Ecological Research Center
Yosemite Field Station
40298 Junction Dr, Suite A
Oakhurst, CA 93644

[2] Utah State University
Wildland Resources
5230 Old Main Hill
Logan, UT 84322-5230

[3]National Park Service
Yosemite National Park
5083 Foresta Road
El Portal, CA 95318

January 2015

U.S. Department of the Interior
National Park Service
Natural Resource Stewardship and Science
Fort Collins, Colorado

The National Park Service, Natural Resource Stewardship and Science office in Fort Collins, Colorado, publishes a range of reports that address natural resource topics. These reports are of interest and applicability to a broad audience in the National Park Service and others in natural resource management, including scientists, conservation and environmental constituencies, and the public.

The Natural Resource Report Series is used to disseminate comprehensive information and analysis about natural resources and related topics concerning lands managed by the National Park Service. The series supports the advancement of science, informed decision-making, and the achievement of the National Park Service mission. The series also provides a forum for presenting more lengthy results that may not be accepted by publications with page limitations.

All manuscripts in the series receive the appropriate level of peer review to ensure that the information is scientifically credible, technically accurate, appropriately written for the intended audience, and designed and published in a professional manner.

This report received formal peer review by subject-matter experts who were not directly involved in the collection, analysis, or reporting of the data, and whose background and expertise put them on par technically and scientifically with the authors of the information.

Views, statements, findings, conclusions, recommendations, and data in this report do not necessarily reflect views and policies of the National Park Service, U.S. Department of the Interior. Mention of trade names or commercial products does not constitute endorsement or recommendation for use by the U.S. Government.

This report is available in digital format from Yosemite and Sequoia & Kings Canyon National Parks, and the Natural Resource Publications Management website (http://www.nature.nps.gov/publications/nrpm/). To receive this report in a format optimized for screen readers, please email irma@nps.gov.

Please cite this publication as:

Matchett, J. R., J. A. Lutz, L. W. Tarnay, D. G. Smith, K. M. L. Becker, and M. L. Brooks. 2015. Impacts of fire management on aboveground tree carbon stocks in Yosemite and Sequoia & Kings Canyon national parks. Natural Resource Report NPS/SIEN/NRR—2015/910. National Park Service, Fort Collins, Colorado.

NPS 104/127729, 102/127729, January 2015

Contents

Contents (continued)

Figures

Page

Tables

Appendices

Abstract

Forest biomass on Sierra Nevada landscapes constitutes one of the largest carbon stocks in California, and its stability is tightly linked to the factors driving fire regimes. Research suggests that fire suppression, logging, climate change, and present management practices in Sierra Nevada forests have altered historic patterns of landscape carbon storage, and over a century of fire suppression and the resulting accumulation in surface fuels have been implicated in contributing to recent increases in high severity, stand-replacing fires. For over 30 years, fire management at Yosemite (YOSE) and Sequoia & Kings Canyon (SEKI) national parks has led the nation in restoring fire to park landscapes; however, the impacts on the stability and magnitude of carbon stocks have not been thoroughly examined.

The purpose of this study is to quantify relationships between recent fire patterns and aboveground tree carbon stocks in YOSE and SEKI. Our approach focuses on evaluating fire effects on 1) amounts of aboveground tree carbon on the landscape, and 2) rates of carbon accumulation by individual trees. In 2010, we compiled a database of existing plot data for our analyses. In 2011, our field crews acquired vegetation data and collected tree growth cores from 105 plots. In 2012, we completed an interpretive component and began data analyses. In 2013, processing of tree cores began. In 2014, final processing of tree cores, data analyses, and manuscript preparation was conducted. The work for this project was facilitated through an interagency agreement between the National Park Service and the U.S. Geological Survey, and through a Cooperative Ecosystems Studies Unit (CESU) agreement with the University of Washington.

In order to accurately quantify landscape-level carbon stocks, our analyses accounted for major sources of measurement errors, propagating those errors as we scaled plot-based carbon density estimates up to landscape-level totals. Using Monte Carlo simulation methods, we found that vegetation type mapping error was the largest source of uncertainty, while measurement uncertainties contributed by tree diameter measurements and tree diameter–biomass allometry equations were relatively minor.

For some forest types, we found differences in aboveground tree carbon densities between burned and unburned areas. For example, mean carbon density in burned red fir forests was estimated to be ~29% lower versus unburned areas. Alternative measures of fire history, such as time since fire and number of times burned, were poorly related to carbon densities.

Within YOSE, we evaluated the stability of landscape carbon pools by quantifying carbon stocks in areas of varying degrees of departure from historic fire return intervals. Of the ~25 Tg of total aboveground tree carbon in YOSE, ~10 Tg is contained within relatively stable areas (the next fire is unlikely to be high severity and stand-replacing), ~10 Tg occurs in areas deemed moderately stable, and the remaining ~5 Tg within relatively unstable areas.

We compared our landscape carbon estimates in YOSE to remotely-sensed carbon estimates from the NASA–CASA project and found that the two methods roughly agree. Our analysis and comparisons suggest, however, that fire severity should be integrated into future carbon mapping efforts. We

illustrate this with an example using the 2013 Rim Fire, which we estimate burned an area containing over 5 Tg of aboveground tree carbon, but likely left a large fraction of that carbon on the landscape if one accounts for fire severity.

Acknowledgments

Funding was provided by the National Park Service's Climate Change Adaptation Program; the National Park Service's Fire and Aviation Management Research Fund; and the US Geological Survey's Terrestrial, Freshwater, and Marine Ecosystems Program. Remotely-sensed carbon stock data was provided by Chris Potter with the NASA–CASA program. Jan Van Wagtendonk, Phil Van Mantgem, Nate Benson, and Patrick Gonzalez provided critiques of early versions of this report, greatly improving the quality of the final document. Any use of trade, product, or firm names is for descriptive purposes only and does not imply endorsement by the US Government.

Introduction

The conversion of atmospheric carbon into biological matter is a process called biosequestration. This is in contrast to other forms of carbon sequestration involving physical (e.g. burial or deep ocean deposition) or chemical (e.g. mineral carbonation) processes. The distribution and abundance of biologically sequestered carbon on western North American landscapes is of crucial importance to land management issues involving fire (Hurteau and Brooks 2011) and climate (Swann et al. 2012). Carbon sequestration rates are also fundamental to understanding global gradients of ecosystem productivity (Chisholm et al. 2013). However, detailed carbon storage estimates have many sources of variation that are difficult to quantify for any particular landscape. In the Sierra Nevada, heterogeneity of carbon across landscapes is influence by multiple factors, such as species composition (Lutz et al. 2010), productivity gradients (Larson et al. 2008), history and magnitude of fire and wind (van Wagtendonk and Lutz 2007, Lutz and Halpern 2006, Lutz et al. 2011, North et al. 2007), fuels treatment and management (Hurteau and North 2009), dispersal and post-disturbance forest development (Halpern and Lutz 2013), and effects of insects and pathogens. Of these, fire is perhaps the most influential within Sierra Nevada forested ecosystems.

Fire—whether ignited naturally, accidentally, or purposely—is an indispensable tool for manipulating forest composition, structure, and function within Yosemite (YOSE) and Sequoia & Kings Canyon (SEKI) national parks. Wildfire suppression—starting 150 years ago and becoming very effective in the early 1900s (van Wagtendonk 2007)—has altered fuel structure, fire behavior, and fire regimes in ways that ultimately increase risks of damage to infrastructure, natural and cultural resources, watershed function, tourism, and local economies. Fire regimes in Sierra Nevada mixed-conifer forests prior to European settlement were characterized by low- and mixed-severity fires with short return intervals, while high-severity fires with long return intervals dominate contemporary regimes (Scholl and Taylor 2010). During the past three decades, fire has been systematically reintroduced—either by allowing naturally-ignited fires to burn under specified conditions or by management-ignited fires—into fire-adapted forests of YOSE and SEKI in an effort to reestablish historic regimes. The general objectives of these managed fires are to reduce surface and ladder fuels, minimize crown fires, restore pre-suppression era fire regimes, and increase resiliency of forests to projected climate change (YOSE and SEKI fire management plans[1]). In lower montane forests of the Sierra Nevada, the focus within national parks has been on increasing fire frequency, increasing overall landscape heterogeneity in burned areas (Hessburg et al. 2005), and restoring pre-suppression era fuels and fire regime characteristics.

Although fire is an important factor in forest carbon dynamics, the effect of contemporary fire regimes on carbon stocks has not been sufficiently evaluated. Fires convert large amounts of forest biomass into greenhouse gases—both immediately through combustion and over time as dead trees decompose—however, post-fire vegetation growth re-sequesters carbon (Hurteau and Brooks 2011).

[1]Available online at http://www.nps.gov/yose/parkmgmt/fireplan.htm and http://www.nps.gov/seki/naturescience/fic_ffmp.htm

The net change in carbon contained on the landscape relative to pre-fire levels depends on time since burning, fire severity, and the vegetation types that grow back (Hurteau 2013). It may take centuries for a forest experiencing high-severity fire to reach pre-fire carbon storage levels, while forests burned at lower severities can replace lost biomass within decadal timescales. The differing productivities of forests and their attendant regrowth rates (Larson et al. 2008), coupled with the characteristic fire return interval of each forest type, make it difficult to determine the conditions under which fires result in a net emission or assimilation of carbon at decadal and sub-decadal timescales. At broader spatial scales and multi-decadal timescales, recent research has shown frequent fire appears to create forest stands that are less dense, contain larger diameter trees, and store a greater mass of carbon per unit land area than the stands they replace (Fellows and Goulden 2008). In lower elevation forests of YOSE, high-severity fire may be associated with loss of large-diameter trees, whereas low- and moderate-severity fires do not cause noticeable declines in large-diameter tree density (Collins et al. 2011, Lutz et al. 2009). Additionally, forests composed of large-diameter, fire-resistant species have complex structure, which often includes high height-to-live-crown values, thus making them less susceptible to stand-replacing crown fires and promoting stability in long-term carbon storage (Hurteau et al. 2008).

In 2006 California passed the Global Warming Solutions Act (California Assembly 2006), which mandated statewide greenhouse gas emissions be reduced to 1990 levels. The California Air Resources Board was charged with developing and implementing a methodology for quantifying and monitoring greenhouse gas emissions from different industrial sectors, including the forestry sector. The immediate emissions from large wildfires can approach magnitudes equivalent to total annual emissions from medium to large cities, leading to the perception that such fires are significant threats to landscape carbon sequestration capacity. Even though this view only accounts for immediate and short-term fire effects, it still leads to the possibility that using fire as a management tool may be significantly limited if regulations restricting wildfire carbon emissions are implemented. However, if limitations on fire use result in further accumulation of surface and ladder fuels that increase the potential for high severity fire and thus unstable carbon stocks, such regulations may be counterproductive for long-term carbon management.

A more comprehensive and realistic view of forestry-sector carbon dynamics requires that initial losses from fire be placed in the context of longer-term forest productivity and stability, which could actually result in net gains in carbon stocks—or at least reduced potential for high-severity, stand-replacing fire—depending upon the amounts and types of biomass growing back post-fire (Hurteau and Brooks 2011, Hurteau 2013). Because forest regrowth can take decades to centuries, it is difficult to determine whether fires cause a net loss or gain of carbon over these longer timescales. Ultimately, the Earth's energy balance depends on how much carbon dioxide accumulates in the atmosphere over time. Year-to-year variations in annual emission budgets at small spatial scales (relative to the vegetated area of the planet) matter less than net accumulation of carbon dioxide and other greenhouse gases over decades, and any permanent diminishment of the amount and stability of carbons stocks in fire-adapted forest ecosystems has the potential to exceed sequestration gains made in other sectors by orders of magnitude. Protecting the characteristic composition, structure, and carbon dynamics of these potentially volatile and sensitive carbon pools must therefore be a high

priority for any comprehensive strategy that seeks to lessen the accumulation of atmospheric greenhouse gases.

In an effort to enhance our understanding of forest carbon dynamics in Sierra Nevada national parks and the influence of contemporary fire management, our objectives for this project were to 1) evaluate the relationships between fire and the aboveground tree carbon pool within YOSE and SEKI, and 2) quantify tree carbon assimilation rates and their relationships to fire. We addressed objective 1 by compiling existing vegetation plot data, collecting vegetation data in new plots, utilizing recent vegetation and fire history mapping data, compiling a set of species-specific biomass allometric equations, and developing a statistical analysis technique to assess uncertainties in landscape-scale carbon estimates. We are addressing objective 2 by using tree cores and dendro-chronological methods to document tree growth patterns and rates of carbon assimilation for five years before and after fires of low- to moderate-severity. Field data collection for objective 2 is complete, but laboratory analyses are still in progress, therefore the methods and results for that objective will be presented in a future manuscript.

Methods

Plot Dataset

We compiled a dataset of ground-based tree measurements using data collected by various vegetation projects throughout the parks. These projects included natural resource inventories (Peggy Moore, Ecologist, USGS Yosemite Field Station and Sylvia Haultain, Plant Ecologist, Sequoia/Kings Canyon National Park personal communications), vegetation mapping (Keeler-Wolf et al. 2012; Sylvia Haultain, Plant Ecologist, Sequoia/Kings Canyon National Park personal communication), fire effects monitoring (Gus Smith, Fire Ecologist, Yosemite National Park and Tony Caprio, Fire Ecologist, Sequoia/Kings Canyon National Park personal communications), fuels studies (van Wagtendonk and Moore 2010), a Smithsonian-affiliated demography study (Lutz et al. 2012, 2013), and this project. Plots in forested vegetation types were primarily 0.1 ha in size, within which tree species and diameter at breast height (DBH) were recorded. Our compiled dataset consisted of 2590 total plots, with 1646 plots within the forested vegetation types we used in our analysis (Table 1). Plot measurement years ranged from 1982 to 2011.

Table 1. Number of sampling plots located within each vegetation type.

Forested Vegetation Type	# Plots
Deciduous Oak Forest and Woodland	88
Douglas-fir Forest	7
Evergreen Oak Forest and Woodland	110
Foothill Pine Woodland	11
Foxtail Pine Forest	58
Giant Sequoia Forest	42
High Woodland	89
Jeffrey Pine Forest	111
Lodgepole Pine Forest	190
Mountain Hemlock Forest	38
Pinyon Pine Woodland	27
Ponderosa Pine Forest	123
Ponderosa Pine Woodland	13
Red Fir Forest	116
Riparian Forest	87
Riparian Shrub	23
Shrub	258
Western White Pine Forest	27
Western White Pine Woodland	4
White Fir - Sugar Pine Forest	224
Total	1646

Field Data Collection

We supplemented the pre-existing plot data by establishing 105, 0.1-ha circular plots in YOSE (67 plots) and SEKI (48 plots). The plot locations were stratified by five different forest types (white fir–sugar pine, red fir, lodgepole pine, Jeffrey pine, and ponderosa pine) and two fire histories (burned at low to moderate severity since 1984, or unburned in recorded history; Table 2). The new plots were selected from adjacent portions of forests that had been either burned or unburned in an attempt to control for local variation. Plot locations were selected by GIS analysis to achieve maximum areal coverage given the labor allocated (i.e., more over-dispersed than random), with slightly lower representation in those areas far from roads. Additionally, the new plots were positioned >50 m

Table 2. Numbers of newly established plots by park, forest type, and burn history.

	White Fir		Red Fire		Lodgepole Pine		Jeffrey Pine		Ponderosa Pine		
Park	**B[1]**	**U[2]**	**B**	**U**	**B**	**U**	**B**	**U**	**B**	**U**	**Total**
YOSE	11	15	4	4	4	0	4	5	9	11	67
SEKI	1	0	10	8	3	1	10	2	2	1	38
Total	12	15	14	12	7	1	14	7	11	12	105

[1]B = burned; [2]U = unburned

inside the mapped boundary of the intended forest type and burn patch, on slopes between 0° and 35°, and >100 m from roads, streams, and trails. Upon arriving at a site, field crews assessed the intended forest type and burn status, and relocated the plot if it did not meet the intended specifications. Plots were also relocated if there were fewer than 10 trees >8 cm DBH within 46.5 m of the plot center.

Field crews visited plots between June and September 2011. They recorded plot center coordinates (measured with consumer-grade GPS receivers), slope, aspect, topographic position (slope position: low, mid, upper slope; level position: low, mid, or high level; hydrology: inter-fluvial, channel, wall, basin floor) and slope configuration (convex or concave). Additionally, two plot photos (north and south view) and a panoramic video were taken from the plot center. Crews ocularly estimated canopy cover by species for each plot quadrant. They recorded percentage cover by shrub species for any species occupying ≥1% of one plot quadrant. Species and DBH of all live trees and snags >15 cm DBH were recorded within the entire plot, and species and DBH were recorded for all live trees and snags between 2.5 cm and 15 cm DBH in at least one plot quadrant.

Allometric Equations

In order to calculate tree biomass, we compiled a set of allometric equations developed by prior studies. For each tree species, we first examined existing equations and selected the most appropriate equation(s) by considering the tree species, location of the original study, tree age range (where reported), tree diameter range, site productivity, site climate, and sample size. When available, we used species-specific equations from studies geographically closest to our study region (e.g., Westman 1998 for fir). None of the allometric equations were developed from trees within the parks. If a species-specific equation wasn't available, we chose an equation from a species with a similar growth form or used one of the generalized equations developed by Jenkins et al. (2003). In some cases, such as high elevation woodlands, the Jenkins et al. (2003) generalized equations may not be appropriate because of the compact and stunted morphology of high elevation pine and hemlock species. In many cases, the diameter range of trees used to develop an equation did not extend throughout the diameter range of trees in our dataset. YOSE and SEKI contain some of the largest known individuals of ponderosa pine, sugar pine, white fir, red fir, and giant sequoia (Van Pelt 2001). Because destructive sampling is generally enjoined in the parks, allometric equations using large diameter trees do not exist. For these situations we created blended equations using the species-specific equations over the diameter range of trees from which the equation was developed, then switched to equations from similar species and growth forms that covered the necessary diameter range. Appendix A provides a detailed listing of equations used for each species.

All biomass equations were originally expressed in, or converted to, the form $\ln(biomass) = a + b \times \ln(DBH)$, with *biomass* expressed in kg and *DBH* in cm. Each equation included a standard error of the estimate (SEE), which is the standard deviation of the normally-distributed error around the predicted biomass while expressed on a log scale. The SEE can be used to calculate a bias correction factor when exponentiating the log-scaled biomass to an arithmetic value. Tree carbon mass was assumed to be 50% of biomass based on the proportion of carbon found in cellulose, hemicellulose, and lignin, but without regard for the various proportions of carbon

present in species-specific complex organic compounds (e.g. polyphenols and extractives). Although the proportion of carbon differs by species and tissue (wood, bark, and foliage), conifer species have a mean wood carbon value variously reported as 50.8% (Thomas and Martin 2012), or 47–55% (Lamlom and Savidge 2003). The 50% figure provides an acceptable average—generally, firs (*Abies* spp.) have carbon content slightly less than 50%, pines (*Pinus* spp.) slightly greater than 50%, and cedars (Cupressaceae family) around 52%. However, similar to the situation with allometric equations, very few carbon analyses have been done on the species prevalent in YOSE and SEKI.

Analyses

Assigning Forest Types

Although the number of plots in the study was large, the number of plots in many mapped vegetation community types was small. In order to increase sample sizes and improve our carbon density estimates within a given forest type, we aggregated mapped community types based on tree species composition, tree morphology, and characteristic fire regime. For example, there were several high elevation woodland communities which all have a very long fire return interval and characteristic tree morphology (short, compact boles of Sierra juniper, whitebark pine, and mountain hemlock), therefore we assigned a single forest type to those vegetation communities (see Appendix B for community–forest type assignments). We assigned plots to forest types by spatially intersecting their locations with the vegetation maps. We inspected these assigned forest types and plot species composition, and discovered that in some cases there were incorrect assignments, presumably because plot geographic coordinates were incorrect or the map polygon was incorrectly classified. We then identified potentially misclassified plots by conducting a k-means clustering of plots using their tree species composition, assigning the resulting clusters to our aggregated forest types, then looking for mismatches between the mapped-based and cluster-based forest types. When a mismatch was found, we manually assessed the plot's species composition and assigned it to the appropriate forest type.

Density and Total Carbon

We estimated tree carbon density (kg/m^2) and total carbon (Tg) for each forest type within each park. Our definition of trees included living trees and standing snags. In addition to the typical uncertainty in estimated statistical parameters arising from sampling a population, we also explored the influence of various other measurement errors on carbon estimates and their uncertainties. These measurement errors included repeatability in tree diameter measurements, uncertainties in allometric equation diameter–biomass relationships, and classification accuracies in vegetation maps. We developed a Monte Carlo simulation that repeatedly calculated carbon densities and total carbon while taking into account those uncertainties. For tree diameter, a normally-distributed error with mean 0 and standard deviation 0.027 (based on the root mean squared error of duplicated tree diameter measurements reported by Gonzalez et al. [2010]) was added to each tree DBH measurement. Tree biomass—on a log scale—was calculated using the assigned allometric equations plus a normally-distributed error with mean 0 and standard deviation equal to the equation's standard error of the estimate. Typically, when making a single prediction using a log–log equation, a bias correction is added to the value so that when it is exponentiated it is closer to the arithmetic mean (the arithmetic values tend to be log-normally distributed and exponentiating the log value without bias correction will place the

prediction closer to the distribution's median; Baskerville 1972). However, during a Monte Carlo simulation, the distribution of multiple arithmetic predictions will realize the lognormal distribution, so a bias correction is not needed. Log-scaled tree biomass values were exponentiated, multiplied by the carbon content value (0.5), summed within a plot, and divided by the plot area to produce a carbon density value (kg/m^2). A bootstrapped sample (a random sample with replacement equal in size to the original sample) of all plots was taken in order to incorporate uncertainty from statistical sampling. We then fit a linear regression model to predict carbon density (log + 1 transformed) using forest type, forest canopy cover class, and their interaction as explanatory variables. Forest canopy cover classes were taken from the forest type maps, where each mapped polygon had been assigned a canopy cover class during photo interpretation. Three forest types (Douglas-fir Forest, Foothill Pine Woodland, and Western White Pine Woodland) did not have enough plots across a range of canopy covers, so their carbon estimates are a simple mean. These steps for predicting carbon densities utilized plots pooled across all parks.

We used the park vegetation maps to calculate the total areas for each combination of forest type and canopy cover class. To take into account uncertainties in vegetation mapping, we used the accuracy assessment matrices to generate uncertainties in forest type areas. The vegetation type assigned to each polygon was randomly assigned using the numbers of ground-based truth plots as weights. For example, if a particular vegetation type had 100 ground-based accuracy assessment plots with 70 determined to be the correctly classified type, 20 determined to be another type, and 10 determined to be a third type, then the probabilities of vegetation type assignment for that polygon were randomly assigned to the three types based on the proportions 0.7, 0.2, and 0.1, respectively. If a vegetation type had four or fewer accuracy assessment plots, we did not randomly reassign types. We then cross-walked the polygon vegetation types to our forest types, summed the total areas for each combination of forest type and canopy cover class, and multiplied by the predicted carbon densities to produce estimates of total carbon (Tg). These steps were done separately for each park, including using the park-specific accuracy assessment matrix (Keeler-Wolf et al. 2012; USGS–NPS Vegetation Characterization Program), in order to produce park-specific carbon estimates. Estimates of mean carbon densities for individual forest types (without regards to canopy cover) were calculated by taking a weighted average of the canopy cover class-specific estimates, with the weights equal to the total area of each canopy cover class.

We also explored simplifying the incorporation of allometric equation errors. Since individual trees within a plot are summed together to calculate carbon density, individual tree errors can also be summed together to produce a plot-level error. Tree biomass errors are expressed, and normally distributed about the prediction, while on a log-scale; however, they can be approximately converted to an arithmetic scale (equation 9 in Baskerville 1972). There are then two options for summing the resulting tree errors: a simple sum and a sum in quadrature (the square root of the sum of squared errors). If errors are assumed to be random and independent of each other, then summing in quadrature is appropriate, whereas the simple sum is a more conservative approach if independence cannot be assumed. Tree errors within a plot are likely dependent—for example a tree with a smaller-than-predicted bole biomass likely has smaller-than-predicted branch and leaf biomasses; or, tree biomasses in a plot might all be higher than predicted if wood density tends to be greater due to

slower growth at a low-productivity site. More importantly, the allometric equations we used were developed from tree sub-populations outside the parks (sometimes from a considerable distance away), and it is very likely that the tree morphologies differ between the sample location and the parks, forming a consistent (but unknown) bias in the allometric equations. For these plot-level summaries, tree biomass was calculated using a bias correction factor since only a single prediction is being made. The benefit of using plot-level errors is that in each Monte Carlo realization random errors need only be generated for thousands of plots as opposed to hundreds of thousands trees, greatly reducing computation time.

Carbon density and total carbon estimates, plus their standard errors and 95% confidence intervals (CI), were based on the means, standard deviations, and 2.5 and 97.5 percentiles of the distributions from a Monte Carlo simulation of 10,000 realizations. The simulations were programmed in R (R Core Team 2013), graphs developed using ggplot (Wickham 2009) and base R graphics packages, spatial data managed using PostGIS (PostGIS Development Team 2013), and maps produced using QGIS (QGIS Development Team 2013).

Fire History and Carbon Density

We investigated the influence of fire history on carbon density for forest types that experience regular, natural wildfire and for which we had sufficient sample sizes—specifically red fir, white fir–sugar pine, ponderosa pine, Jeffrey pine, and lodgepole pine forests. We intersected plots within those forest types with fire history polygon data (~1920 to present) from each park and derived three fire history metrics for each plot: 1) burned vs. unburned, 2) years since the last fire, and 3) number of times burned. For plots without a recorded history of fire, we set years since last fire to 100. We evaluated potential relationships between each of those burn metrics and forest type carbon density by developing a set of statistical models and comparing them using an information-theoretic approach. We defined seven candidate models: one model having just forest type as an explanatory variable, and six others that included one of the three burn history metrics either in addition to or interacting with forest type as explanatory variables (Table 3). Carbon density (log + 1 transformed) was the response variable. Model AIC scores (adjusted for sample size) were used to compare the predictive performances of the candidate models. For the best model, we estimated model parameter values, carbon densities, and compared differences in predicted responses to fire history using a Markov Chain–Monte Carlo procedure. These models didn't incorporate tree biomass measurement uncertainties (arising from tree diameter and allometry equation errors) because, as we discuss below, those uncertainties were negligible compared to the uncertainties due to statistical sampling.

Carbon Stock Stability

We evaluated relative carbon stock stabilities in relation to wildfire risk by overlaying our carbon density map with a fire regime interval departure (FRID) map (van Wagtendonk et al. 2002). FRID is the number of fires missed (relative to the expected number of fires given a historically natural fire regime) at a particular point in the landscape over a given time span. An area with a high FRID has burned less frequently than expected under natural conditions, and the resulting build-up of surface and ladder fuels presumably increases the risk of intense, stand-replacing crown fire. We calculated the amount of carbon within each forest type within various FRID levels (specifically median FRIDs)

using the 2012 YOSE FRID map (Kent van Wagtendonk, YOSE Fire GIS specialist, personal communication). A FRID map for SEKI has not been developed; therefore, our carbon stability summaries are applicable to only YOSE.

Comparison with Another Carbon Accounting Effort

The NASA–CASA program has developed a 250-m resolution, California-wide product that estimates current carbon stocks by applying remotely-sensed net primary productivity estimates to baseline biomass stocks (Potter 2010). Within YOSE, we compared our carbon estimates to the NASA–CASA estimates and evaluated potential limitations in how the NASA–CASA method accounts for carbon losses due to wildfire, using 2013's Rim Fire as a specific example.

Results and Discussion

Error Propagation and Sources of Uncertainty

Carbon estimates rely on plot-based tree allometry equations linking biomass to tree diameter measurements, then scaling them up to the landscape level. There are uncertainties associated with every step in these measurement and scaling processes. For a given forest type, tree inventories are converted to areal carbon estimates using allometric equations, and landscape level values are calculated based on the area of that forest type. It is therefore just as important to understand the aggregate uncertainties of carbon estimates, as it is to understand their mean values. Specifically, there are five potentially large sources of error associated with this process:

1. Uncertainty embedded within allometric equations

The existing tree allometric equations themselves have error associated with them because they are typically derived from a small number of trees (usually <25, but often <10; Jenkins et al. 2004). These small sample sizes relative to the variation in diameter–biomass relationships result in considerable standard errors of typically 10% to 30% throughout the range of tree diameters used to develop them.

2. Site-specific tree morphology

Site-specific tree morphologies are not constant and trees sampled for allometric equations are usually gathered from one limited portion of the species range. When equations generated within one biophysical context are applied elsewhere, differences in site productivity, disturbances, climate, and land use histories can yield errors due to different morphologies of the sampled and target populations.

3. Lack of equations for large-diameter trees

Growth rates of trees vary over time and the range of tree sizes used to develop allometric equations should conservatively define the range of tree sizes to which they are applied. The paucity of large diameter trees in the development of most allometric equations (very few contain trees >100 cm DBH) is especially problematic since most carbon within Sierra Nevada forests is contained in these large trees (Lutz et al. 2012). As a result, the biomass of large-diameter trees must be estimated either from those few proxy species that have been sampled at large diameters or by extrapolating well beyond the range of tree diameters used for developing the species-specific equation. The problem of accurately calculating the biomass of large-diameter trees is magnified by their more complex and variable crown architecture compared to smaller trees (Sillett and Van Pelt 2007, Van Pelt and Sillett 2008). In areas where large-diameter trees constitute a large proportion of the tree population (for example where smaller trees are routinely eliminated by fire), or in areas where species reach maximum sizes much greater than any previously dissected, biomass estimates could potentially have large uncertainties.

4. Landscape heterogeneity

Landscapes are heterogeneous, containing gradients of biophysical conditions (particularly relating to the site water balance) that can affect diameter–biomass relationships. To be accurate, landscape

level estimates of carbon must be based on a sufficient number and distribution of plots to capture the range of these conditions.

5. Vegetation type mapping error

The vegetation maps used to scale-up carbon estimates for forest types contain their own degree of error associated with vegetation cover assignment. Georeferencing uncertainties between plot locations (e.g., poor plot location information from older GPS units, difficult topography, or multipath GPS reception cause by high tree density) and vegetation cover polygons (e.g., poor aerial photograph georectification, incorrect vegetation type identification, or polygon edge error during data input) can add further error.

We evaluated the relative contribution of these five sources of error, and found that in general uncertainties associated with repeated measurements of tree diameters and choice of diameter–biomass allometric relationships had very little effect on the standard errors and confidence intervals of tree carbon density and total carbon estimates (however, better allometric equations constructed from dissections of large numbers of individual trees may reduce these uncertainties). The widths of

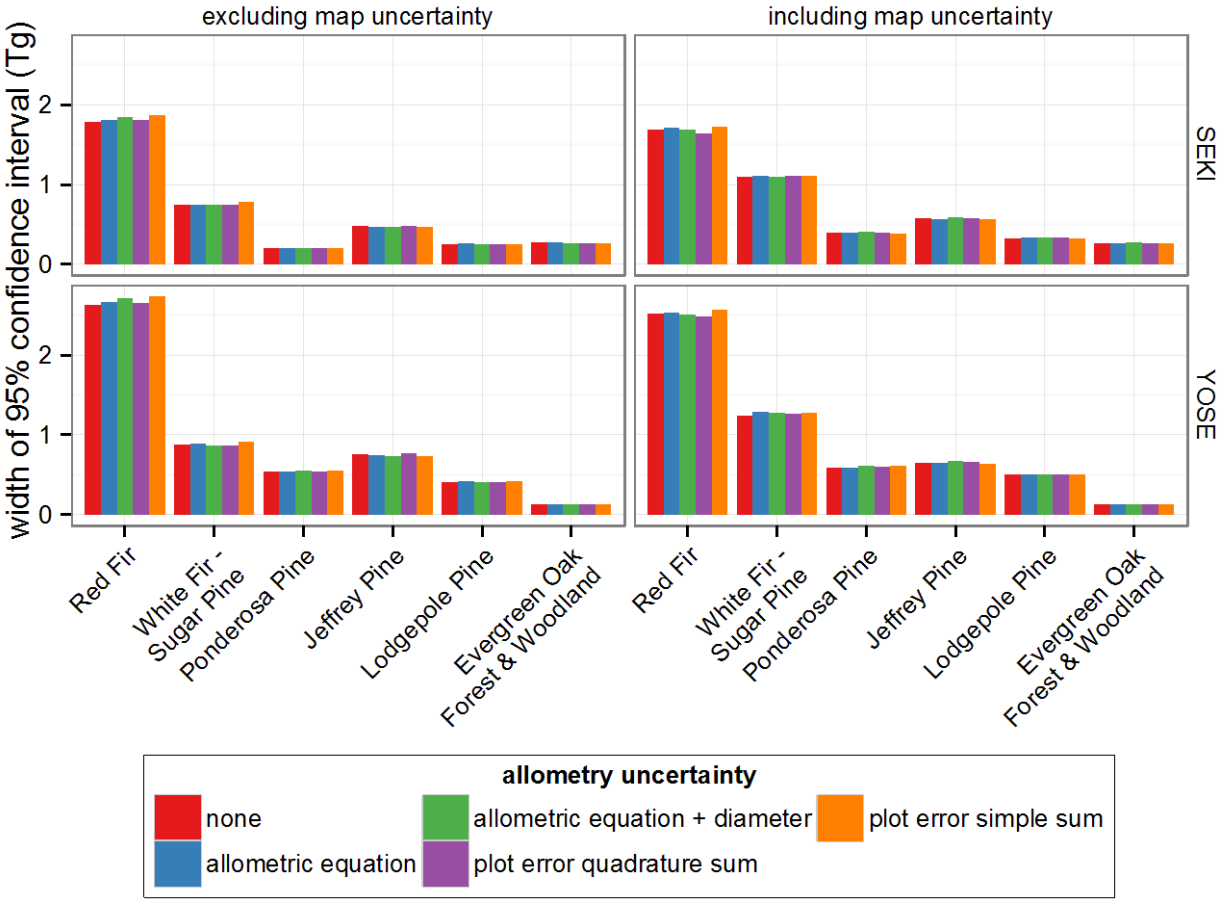

Figure 1. Comparisons of uncertainties in total carbon estimates for 6 forest types in Sequoia & Kings Canyon (SEKI) and Yosemite (YOSE) national parks.

the 95% confidence intervals for total carbon in several major forest types within both parks differed only slightly among the different methods of accounting for allometry error (Figure 1). The typical uncertainty arising from sampling a population—especially a very heterogeneous one—appears much more important for our dataset.

Forest type classification uncertainties, however, were an important component of uncertainty in total carbon estimates. We observed that Monte Carlo-estimated areas differed from observed mapped-based areas for several forest types. For example, a single summation of red fir forest polygons from YOSE's vegetation map yields 41,315 ha, while the Monte Carlo estimate is ~13% lower at 36,052 ha (95% CI: 34,655–37,723), suggesting that this forest type is currently over-mapped. Other forest types appear to be under-mapped, for example the high woodland type, which occurs on 26,602 ha in YOSE according to the vegetation map, while the Monte Carlo estimate is ~9% higher at 28,995 ha (95% CI: 28,307–29,953). These differences in area estimates noticeably affected total carbon estimates for some forest types, and usually widened the total carbon confidence intervals, although can also narrow the confidence intervals in some types (for example red fir) because the reduction in total area of the type leads to lower total carbon and confidence intervals generally become more narrow as the estimate gets smaller.

Given these responses, the Monte Carlo simulation used to produce the carbon estimates throughout the remainder of this report used the 'plot error simple sum' method to propagate error and incorporate allometric uncertainty (mainly as a conservative approach, because this method tended to produce the widest 95% confidence intervals) and incorporated the vegetation mapping uncertainty. A bootstrapped sample of plots was taken in each Monte Carlo realization to incorporate sampling uncertainty.

Aboveground Tree Carbon

Accounting for the uncertainties as described above, we estimate total aboveground tree carbon in YOSE to be 25 Tg (95% CI: 23–27 Tg) and for SEKI to be 20 Tg (95% CI: 18–21 Tg). The total across both parks is about 4.1% of the total standing carbon estimated in the Sierra Nevada (Potter et al. 2010). Over the area (YOSE has an area of 3,052 km^2 and SEKI has an area 3,503 km^2) of both parks, the range of aboveground tree carbon is 41–48 Tg (mean of 45 Tg), which is nearly 10% of the total standing wood in the Sierra Nevada (Potter et al. 2010).

Densities of aboveground tree carbon varied from a low of nearly 0 kg/m^2 in shrub vegetation types to over 55 kg/m^2 in giant sequoia forests (Figure 2). Although the carbon densities for vegetation types were very similar between parks, the total carbon in many vegetation types differed substantially since the areal extents of the vegetation types differed (Figure 3). For example, in SEKI the namesake giant sequoia forests alone account for 10–17% of total tree carbon, while in YOSE they account for 0.2–0.4%. Red fir forest accounted for ⅓ of total tree carbon in both parks (32–36% in SEKI; 37–42% in YOSE), with YOSE (8.8–11.5 Tg) having nearly double the amount of carbon in its red fir than SEKI (5.7–7.6 Tg). White fir–sugar pine forests for both parks accounted for about 19–22% of their respective total tree carbon (3.5–4.7 Tg for SEKI; 4.4–5.7 Tg for YOSE). Further summaries for each forest type are provided in Appendix C.

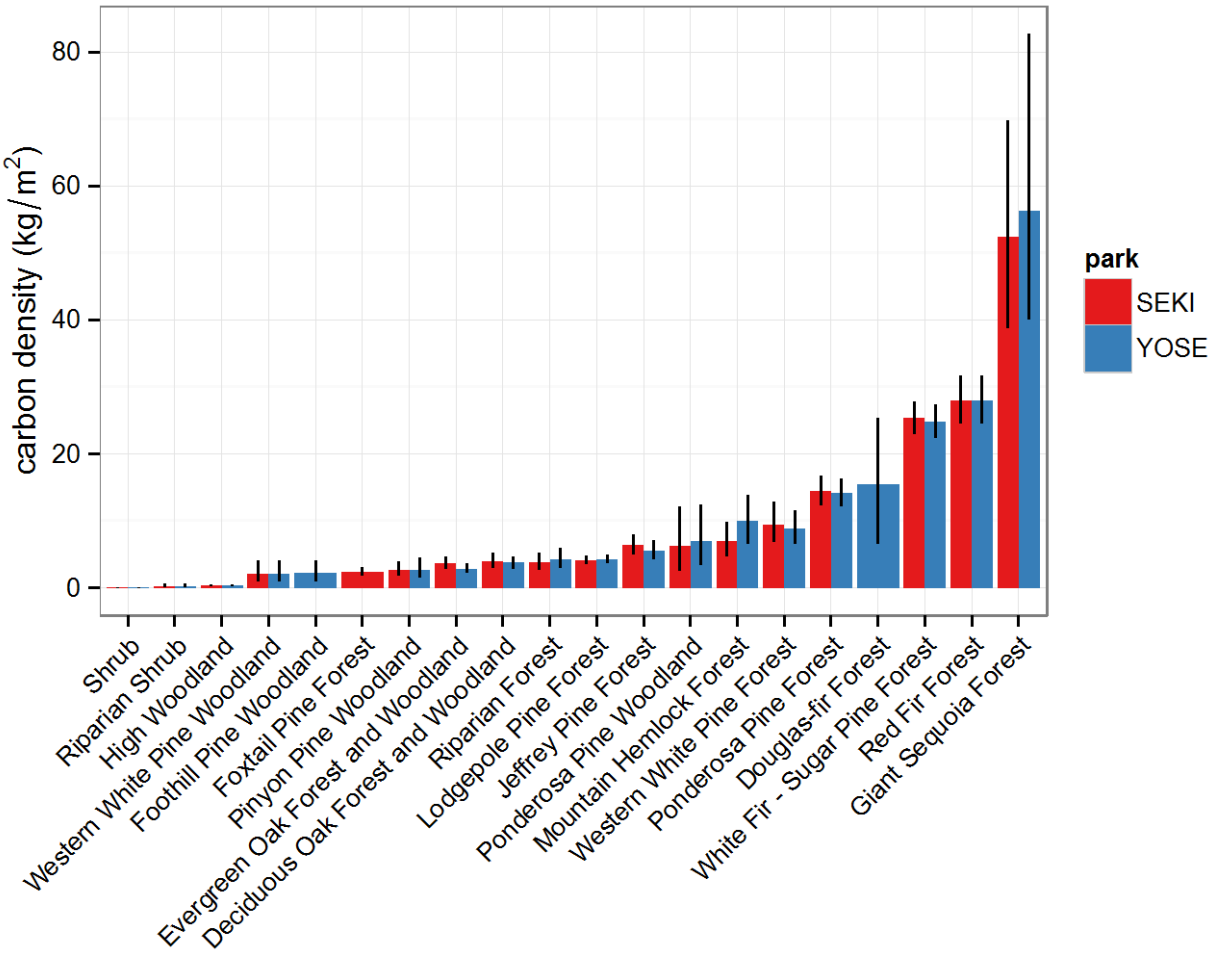

Figure 2. Aboveground tree carbon densities (means and 95% confidence intervals) for vegetation types in Yosemite (YOSE) and Sequoia & Kings Canyon (SEKI) national parks.

Here we should note a fundamental uncertainty and decision point in estimating carbon stocks: the plot carbon values that underpin total landscape carbon estimates within each vegetation type are not normally distributed. A small proportion of plots have very high carbon—probably because of large-diameter trees—and this skews the calculated mean. For example, Figure 4 shows the cumulative distribution of carbon densities for 116 red fir plots in YOSE. The red line is the simple mean, the blue line is the median, and the green line is the mean calculated using log-transformed values that are then exponentiated back to arithmetic values. The different means for this extremely important forest type can vary by ~7 kg/m^2 depending upon how they are calculated. Taken over the area of YOSE covered by red fir, this variation in estimated carbon density can result in a ~4 Tg swing in total carbon for the park. The same principle applies to other vegetation types with large, old-growth trees (e.g., white fir–sugar pine and giant sequoia forests), although they cover less area and therefore contribute less to potential differences in total tree carbon.

Though problematic from a computational and statistical standpoint, there is a growing body of literature suggesting that this skewed distribution toward large trees is a valuable and desired forest

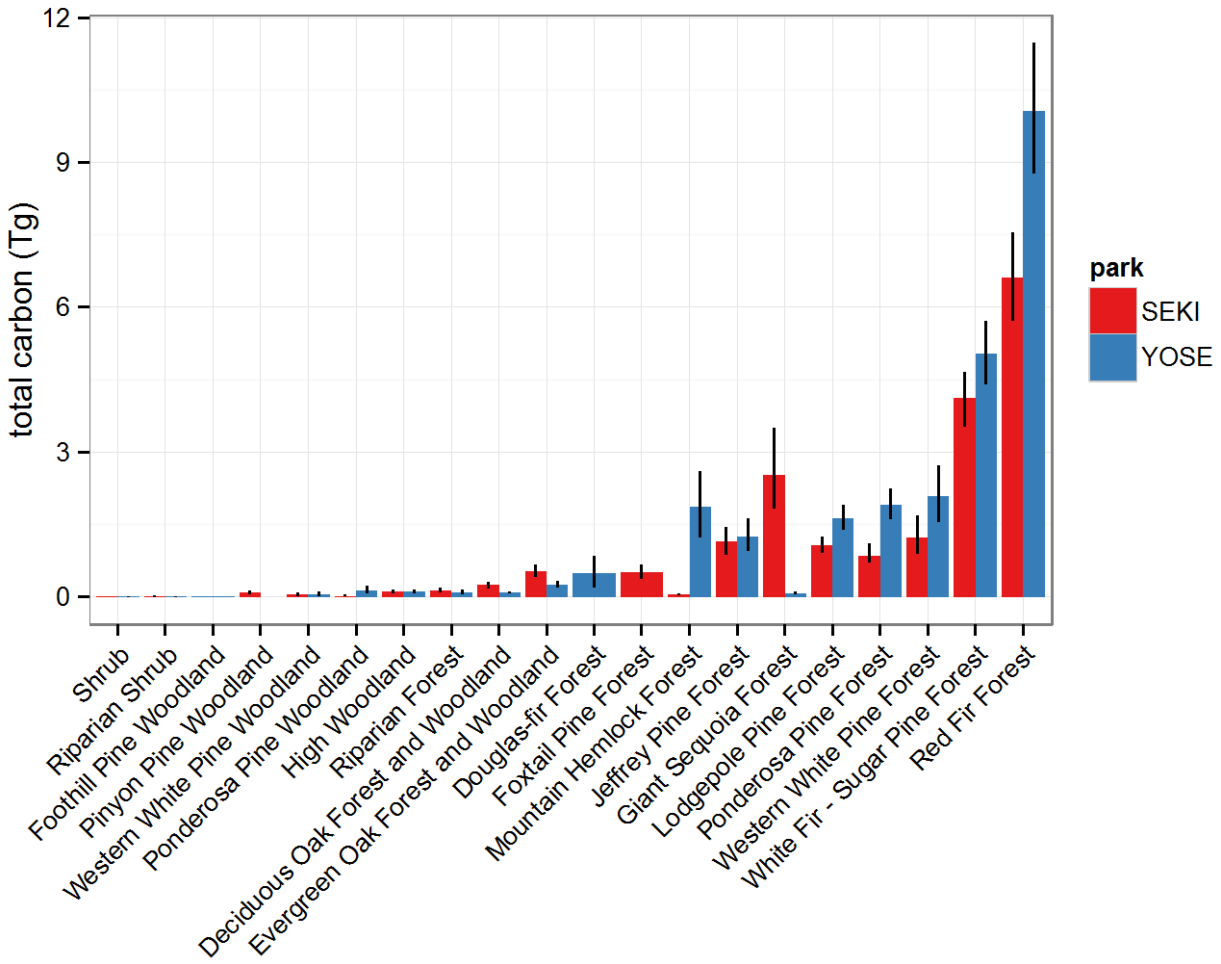

Figure 3. Aboveground tree carbon totals (means and 95% confidence intervals) for vegetation types in Yosemite (YOSE) and Sequoia & Kings Canyon (SEKI) national parks.

characteristic (e.g., Hurteau et al. 2011, Lutz et al. 2012, 2013) from a carbon, fire management, and a forest function perspective. For example, Lutz et al. (2012) found that although large-diameter live trees (≥100 cm DBH) accounted for 1.4% of the individuals, they comprised 49.4% of total biomass (white fir and sugar pine comprised 93% of large-diameter trees at their study site). Kane et al. (2013) demonstrated that fires "thin from below" by removing much of the canopy area in the 2–8 m canopy strata. Thus, while fire removes biomass from forests, it disproportionately removes the understory at lower fire severity, leaving the large-diameter trees containing a greater proportion of carbon. These large-diameter trees are perhaps the defining feature of these two parks. They are uniquely able to withstand all but the highest severity fires, and are of considerable ecological and social interest (including giving rise to the name of Sequoia National Park itself). Dendro-chronological evidence confirms that these large trees developed under frequent fire regimes, with high severity fire patches limited in extent (Scholl and Taylor 2010). The resilience of large-diameter trees to damage from fires characteristic of the pre-suppression era suggests that their preservation is important to overall forest composition and structure, and most probably will continue to be so even under projected climate change scenarios (e.g. Lutz et al. 2010).

Fire History and Tree Carbon Density

The statistical model containing forest type, whether a plot was burned or unburned, and burning's interaction with forest type had the greatest support (lowest AIC value) out of our seven candidate models (Table 3). However, the statistical support for that model was only slightly greater than the model containing only forest type (AIC difference of only being ~3). The other candidate models using the other burn history metrics (number of times burned and years since most recent fire), either alone or interacting with forest type, did not have much support.

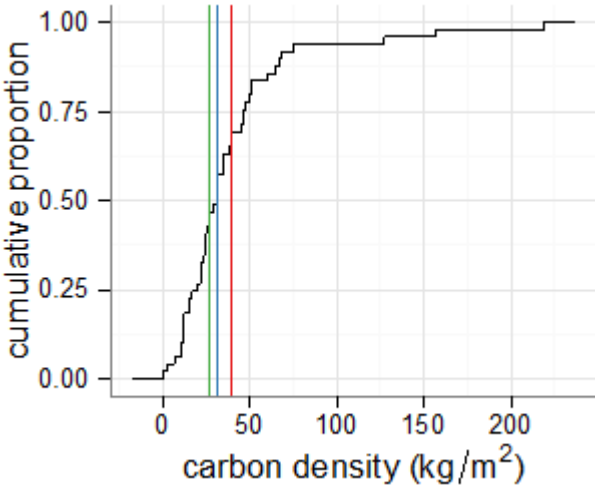

Figure 4. Distribution of carbon densities for red fir forest plots in Yosemite. Red line is the simple mean, blue line is the median, and green line is mean of log-transformed values.

Aboveground tree carbon density estimates using the best model (forest type + burned + forest type × burned) indicated the burn history effect was inconsistent across forest types (Figure 5). The most substantial difference was in red fir forest, where carbon density was ~29% lower if burned (absolute difference of 8.9 kg/m^2 with a 95% CI of 0.4–16.9). Carbon densities were ~15% lower in burned versus unburned within ponderosa pine (difference 2.6 kg/m^2; 95% CI -1.8–7.0) and white fir–sugar pine (difference 3.9 kg/m^2; 95% CI -1.8–9.4) forests, while Jeffrey pine forests had ~40% higher density within burned areas (difference 2.0 kg/m^2; 95% CI -0.2–4.4). Those differences included 0 within their 95% confidence intervals, and thus are not strongly significant. Burned lodgepole pine forests also appeared to have slightly higher carbon density (difference 2.4 kg/m^2; 95% CI -0.6–6.3), but there was substantial uncertainty around the burned estimate, primarily because of small sample size.

This analysis of fire history impacts on forest carbon storage is admittedly simplistic, and a more sophisticated view would account for fire severity and its effect on carbon accumulation rates (e.g., Hurteau and North, 2012). In addition, it should be noted that the context of our burned versus unburned contrast was for plots that were sampled with medians ranging from 14–16 years since last fire, with very few plots having >30 years since last fire. General effects of fire at longer times since burning could not be addressed with the data on hand. We are currently examining fire severity and carbon dynamics relationships (to be published in Becker, K.M.L., Smith, D.G., and Lutz, J.A. In prep. Trends and variability in the effects of fire on forest structure in the Sierra Nevada). Given the

Table 3. Tree carbon density and fire history model comparisons.

Model Effects	AIC	AIC – Minimum AIC
forest type	1698.6	2.97
forest type + burned	1699.6	3.93
forest type + burned + forest type x burned	1695.7	0.00
forest type + times burned	1700.6	4.96
forest type + times burned + forest type x times burned	1698.7	2.98
forest type + years since fire	1699.9	4.26
forest type + years since fire + forest type x years since fire	1696.7	1.01

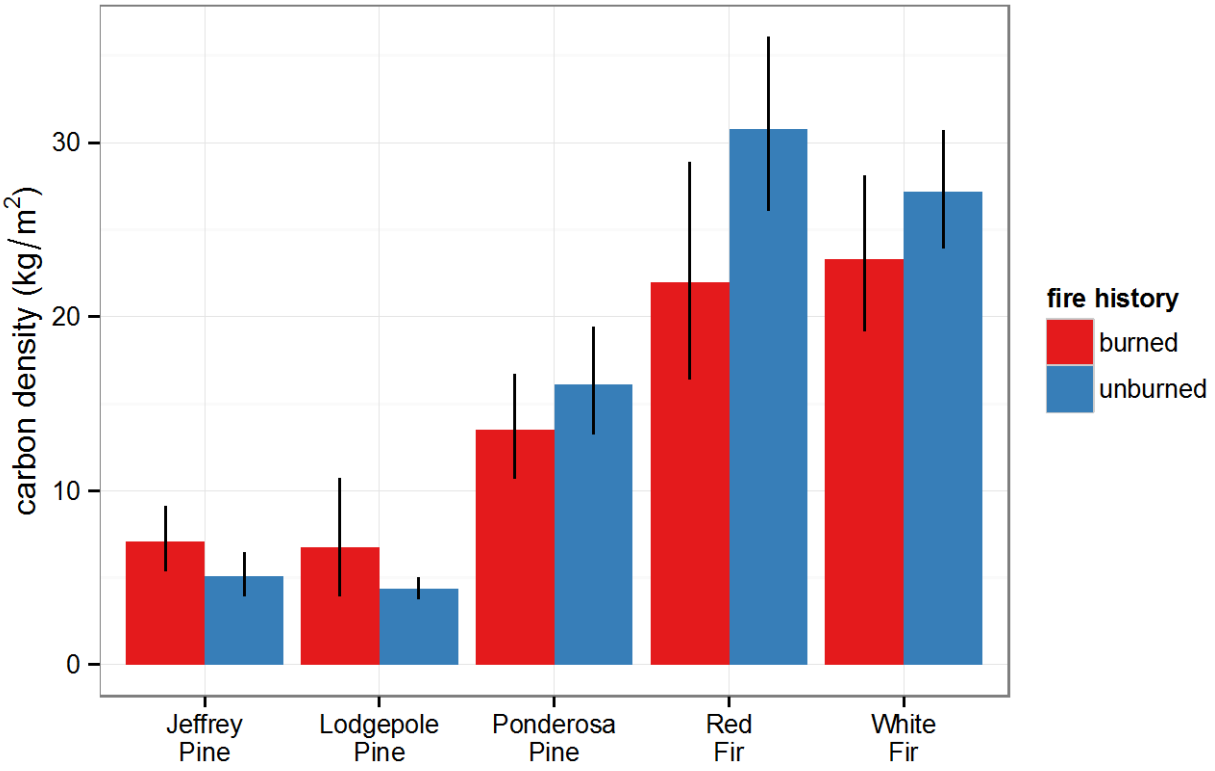

Figure 5. Aboveground tree carbon totals (means and 95% confidence intervals) for vegetation types in Yosemite (YOSE) and Sequoia & Kings Canyon (SEKI) national parks.

limited number of plots and range of fire severity within each vegetation type, preliminary results do not point to a large and statistically significant effect of low- to moderate-severity fire. The results presented in the current report therefore focus on the burned/unburned alternatives on which policy is currently based, and whether that metric provides any useful information on the effects of fire on carbon stocks. The work still in progress will help bound the effects of low severity fire on forest composition and structure.

Additionally, our analysis potentially underestimates carbon losses in cases where fire caused a drastic change in vegetation composition. For example, if a plot classified as a shrub community (according to its composition and the vegetation map) had been a forest community prior to a fire, then the change in tree carbon following fire for that plot wouldn't be part of the estimated change for the forest community because there is no way of knowing the plot's pre-fire vegetation classification. This situation most likely occurs following high-severity fire; therefore, our estimated differences in burned versus unburned carbon densities are most applicable for low- to moderate-severity fires.

Yosemite Carbon Stability Using Fire Return Interval Departure

How much of the Yosemite carbon stock is at risk? One proxy for the risk of carbon loss in fire is the fire return interval departure (FRID), which indicates the degree to which the recent fire return interval for a given stand deviates from the expected fire return interval under a naturally occurring fire regime (van Wagtendonk et al. 2002). Forest stands that have not experienced a fire for a longer

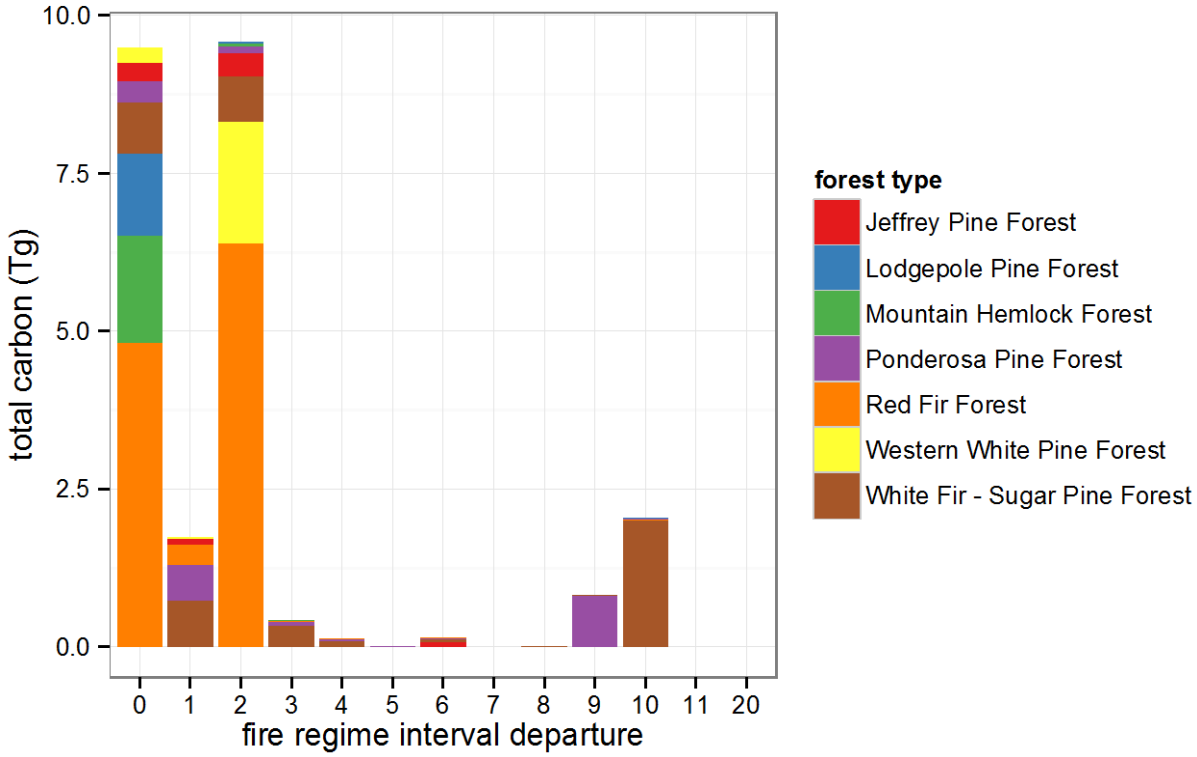

Figure 6. Aboveground tree carbon stored in forest types at fire regime interval departures within Yosemite National Park.

than characteristic interval have elevated fuel loadings, higher densities, and likely more contiguous surface and ladder fuels accumulating beneath the forest canopy. This in turn increases the risk of high severity fire and concomitant high losses of carbon. We used our carbon map to estimate the amount of carbon sequestered in areas with various FRID values (Figure 6). FRID values of less than two probably do not represent a risk of a fire of much higher than characteristic severity. However, FRID values of 3 or higher would indicate a higher risk of substantial high severity patches within fire perimeters. These classifications are consistent with fire risk condition classes used throughout California (e.g., Safford and Van de Water 2014), with both FRID (used by the National Park Service), and Percent FRID (PFRID; used by the USDA Forest Service; Hann and Strohm 2003, Safford et al. 2011) considering departures of three times the fire return interval and greater being high risk. Although FRID and PFRID are used as proxies for the likely severity of the next fire, more quantitative calibration of the metrics is needed to better quantify risk. For YOSE, ~10 Tg of the 25 Tg total aboveground tree carbon is contained within areas where the next fire is unlikely to be high severity and stand-replacing (low departures from historic fire return intervals), another ~10 Tg occurs in areas deemed moderately stable (up to two fire return intervals have been missed), and the remaining ~5 Tg of carbon is within relatively unstable areas (three or more fire return intervals have been missed).

Comparisons with NASA–CASA Biomass Estimates

Overall, our total YOSE tree carbon estimate of 25 Tg is ~17% lower than the 2009 NASA–CASA estimate of 30 Tg, and the NASA–CASA estimate is beyond the upper bound of our estimate's 95% confidence interval (27 Tg). The NASA–CASA estimates do not include errors, so it's difficult to judge the certainty to which the two estimates differ, but there are a few possible reasons why differences should be expected. One potential underestimation in our method is that it excludes shrub biomass, as we were focused exclusively on tree carbon and unable to find adequate shrub cover–biomass allometry equations. In forests with older trees (~500 years) that have experienced frequent low-severity fire, shrubs constitute ~1% of total aboveground biomass, while shrub biomass can be a much higher percentage in stands that experienced high-severity fire (Lutz et al. 2012). When broken down by vegetation types (Figure 7), this difference is evident in the shrub and woodland vegetation categories, which might explain at least 2 Tg of the difference between the two estimates, and brings a NASA–CASA estimate without shrubs (28 Tg) very close to the upper end of our plot-based estimate (27 Tg). We recognized the importance of shrubs in carbon dynamics—particularly because

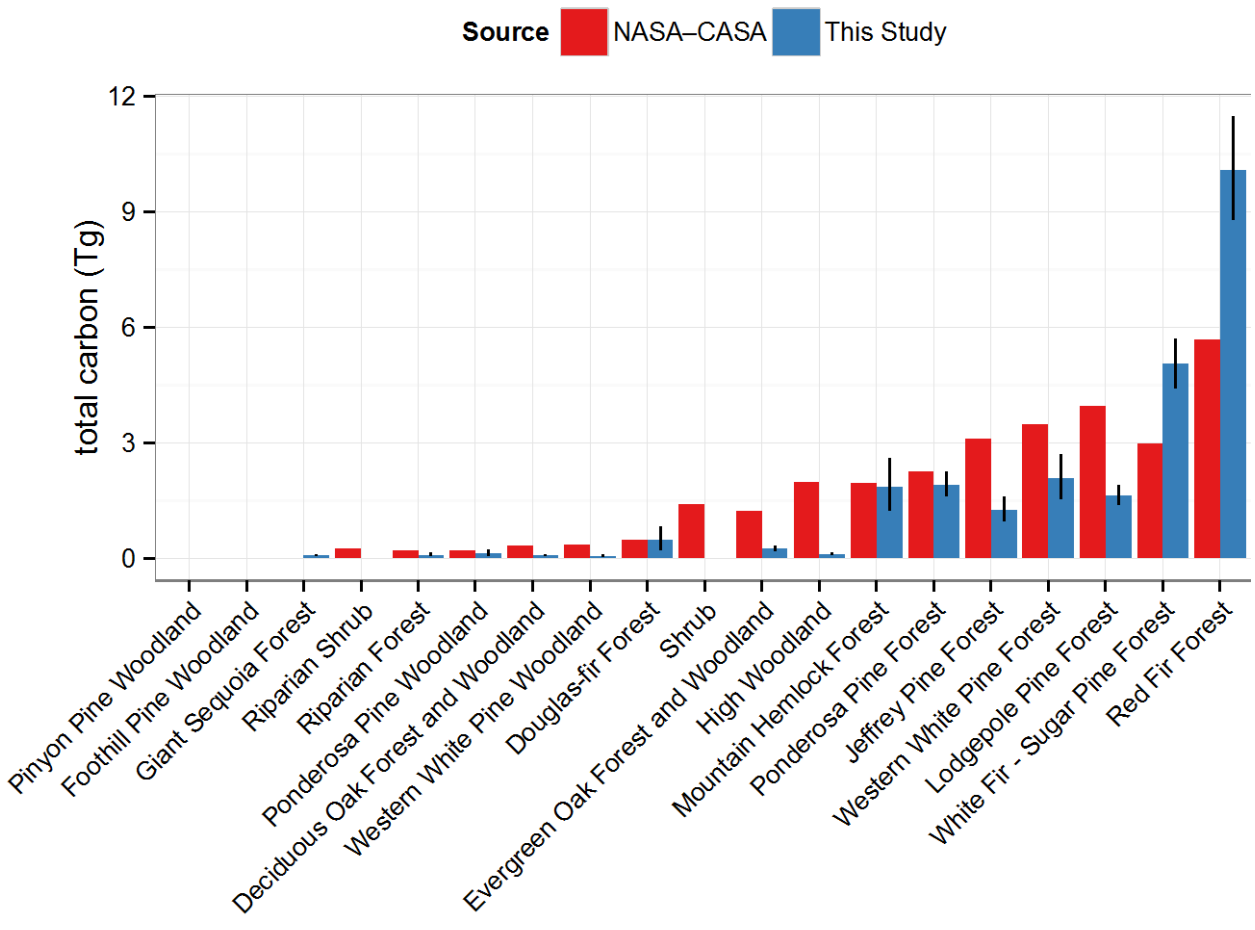

Figure 7. NASA–CASA total carbon estimates versus total aboveground tree carbon estimates from this study for various vegetation types in Yosemite National Park.

they are often fully consumed by fire—and developed allometric equations for three shrub species (Lutz et al. submitted), and encourage other researchers to extend the number of Sierra Nevada shrub species for which high quality (i.e., sample size >25) allometric equations exist.

In high elevation woodlands, NASA–CASA estimates fall well above ours. Inappropriate allometric equations may play a role. High elevation pines, especially those with larger diameters, are much more limited in their height at a given bole diameter when compared to low elevation pines. It is not uncommon for high elevation junipers and whitebark pines to have a DBH of 100 cm and a height less than 10 m. The baseline biomass calculations for NASA–CASA utilized generic pine allometric equations (Pan et al. 2011, and references therein), and therefore almost certainly overestimate biomass of high elevation forests in the Sierra Nevada. We used equations based on arid juniper species (Miller et al. 1981), which have a height-constrained growth form similar to high elevation pines.

Our YOSE carbon estimates are based on the vegetation map developed using aerial photography from 1997, and most of our field plots are from that time period. Unfortunately, NASA–CASA data are available for YOSE during only 2009, though eventually maps going back to 2000 will be produced (Potter 2010). Eleven years of tree growth between 1997 and 2009 may lead the NASA–

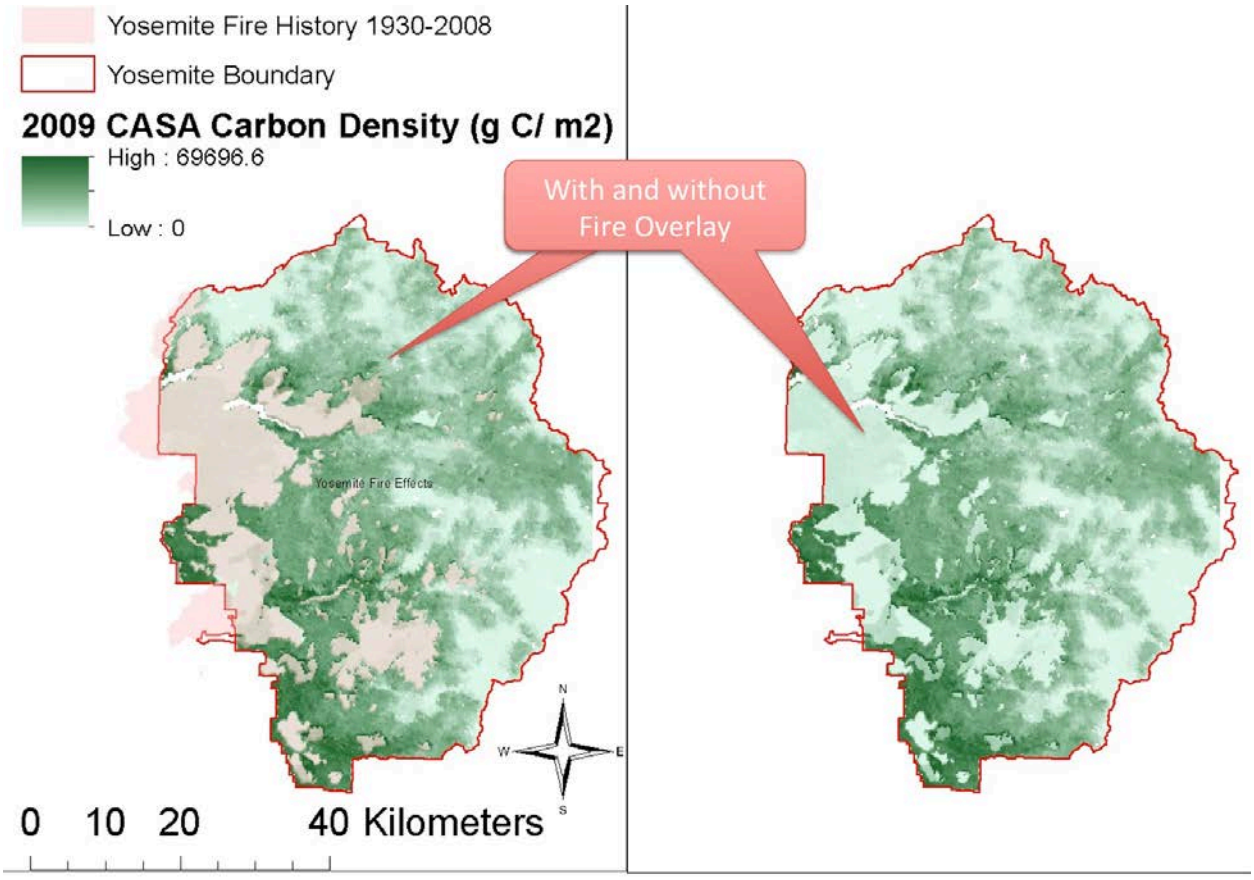

Figure 8. NASA–CASA aboveground carbon and its relationship to fire history.

CASA estimates to be higher than ours simply because of time. Reconciling the two will require the use of established succession schemes (Davis et al. 2009), and the development of a downscaled NASA–CASA raster developed for the YOSE (and potentially SEKI) areas for the year 2000.

The current NASA–CASA scheme incorporates fire impacts on forest carbon stocks by basically assuming a reset back to a low, shrub-based value following a fire. The effect of using this method is visually evident in the map, especially when compared to an overlay of Yosemite fire history (Figure 8). Fires do not uniformly reduce carbon over the area within a fire perimeter—except in the most extreme high severity scenarios—rather, there is a range of severities that produce a range of carbon loss to the atmosphere and transfer to the standing dead pool (van Wagtendonk and Lutz 2007, Lutz et al. 2009, Hurteau and North 2010, Carlson et al. 2012, Kolden et al. 2012). Figure 9 presents a basic model of carbon fluxes immediately following wildfire and provides a computational framework for post-fire carbon loss accounting using fire severity data. Results from our carbon–fire history analysis—which showed only slight differences in carbon densities inside vs. outside fire perimeters—also support this notion of a mixed severity regime, where fire doesn't result in significant overall tree mortality. Fire typically produces a heterogeneous mix of carbon reductions, much of which (at least in the low to moderate severity areas) is returned to the landscape by tree or

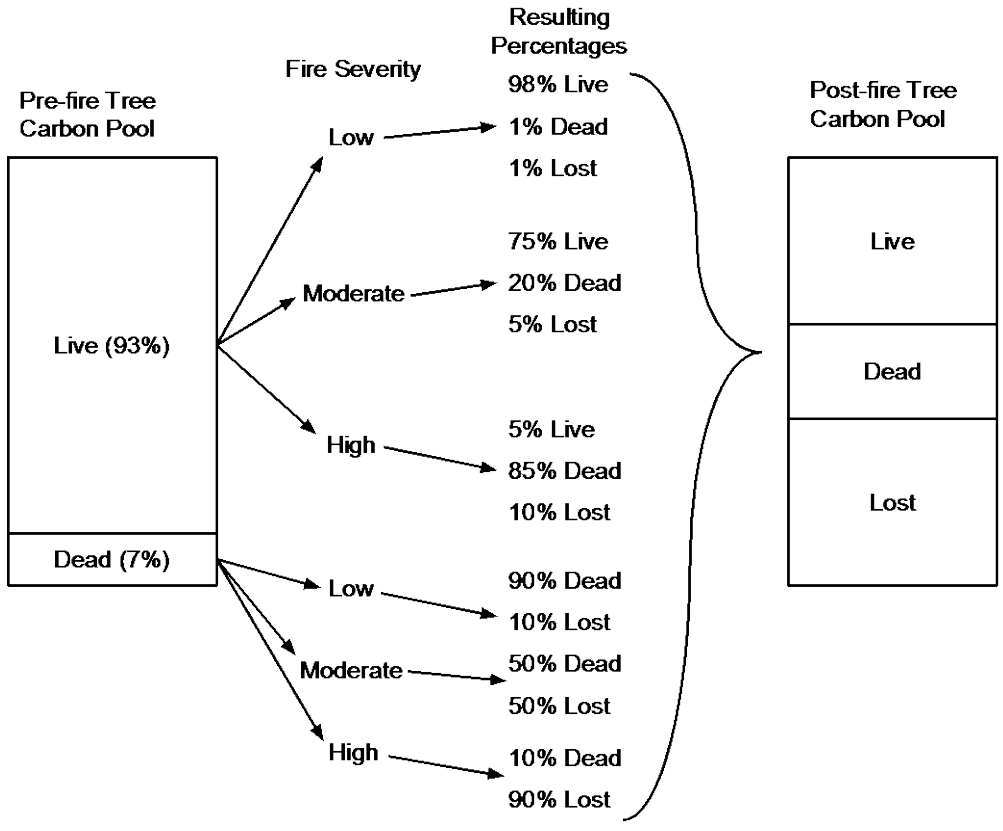

Figure 9. Scheme for changes in tree carbon in response to fire severity.

shrub regeneration within a decade or two (Hurteau et al. 2010). It is likely that an ecosystem carbon dynamics model which incorporates fire severity variables is better suited for quantifying responses in fire-prone landscapes, and would better compare contrasting fire management scenarios. We recommend a severity-based approach and illustrate its potential bias in the next section as a way to better quantify actual stock changes in fire-prone landscapes like YOSE, and reconcile those changes with NASA–CASA remote sensing.

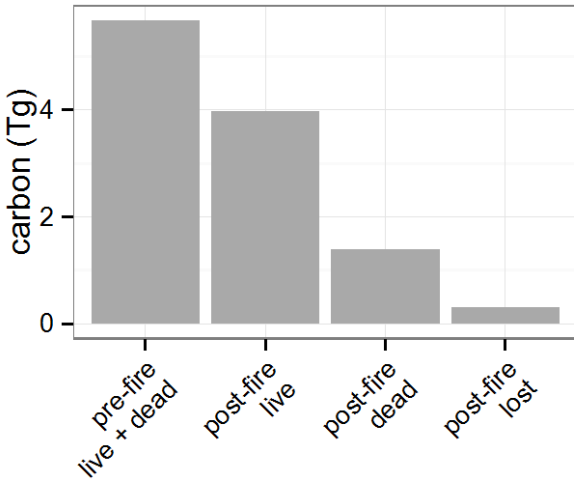

Figure 10. Total aboveground tree carbon within the Rim Fire footprint within Yosemite National Park.

Potential for Overestimating Losses Due to Fire: the Rim Fire of 2013

Using the scheme in Figure 9, remotely-sensed burn severity for the Rim Fire[2], and our tree carbon calculations, we estimate aboveground carbon in live tree biomass within the Rim fire footprint within YOSE was reduced from ~5 Tg before the fire to ~4 Tg after the fire, with ~1.4 Tg as standing dead, and ~0.3 Tg immediately lost to the atmosphere (Figure 10). NASA–CASA assumes a 100% loss of all pre-fire live and dead standing tree biomass. Our values are based on a hypothetical carbon loss by severity scheme, and we use this only as a means to illustrate the potential difference in estimated losses, not to provide definitive numbers for actual Rim fire carbon losses. Measurements of ground-based plots and extended severity assessments one year after the fire will likely provide better estimates of responses in tree carbon pools to the Rim Fire.

Approach and Scope Limitations

This work focuses exclusively on standing live and dead tree carbon. Shrubs were excluded because of very few cover–biomass allometric equations available in the literature. Equations based on metrics such as basal stem diameter or crown diameter/height/volume are more common—see for example McGinnis et al. 2010, Halpern and Lutz 2013, Lutz et al. submitted—unfortunately, none of those were measured for shrubs in the datasets we used. Shrub carbon usually accounts for a relatively small fraction of total aboveground carbon on landscapes dominated by trees. For example, shrub biomass within late-successional, lower mixed-conifer forests of the Sierra Nevada was approximately 1% of ecosystem biomass (Lutz et al. 2012), and in early seral systems (those responding to extreme severity fire in the study area), shrub biomass declined from about 33% of total biomass 20 years after stand-initiating disturbance to about 6% of total biomass 40 years later (Halpern and Lutz 2013). We also excluded herbaceous (grasses, forbs, mosses, and lichens) biomass from our calculations, again due to a dearth of species-specific cover–biomass equations.

[2] US Forest Service's Rapid Assessment of Vegetation Condition After Wildfire (RAVG) product (http://www.fs.fed.us/postfirevegcondition)

Belowground carbon was excluded primarily because there are insufficient studies of total carbon in late-successional systems, especially those with large-diameter trees. Although fire removes large roots from previously dead trees and volatilizes some surface carbon, belowground stores of carbon are less changeable in response to fire than aboveground carbon. We acknowledge the importance of belowground carbon stocks and the need for further research in this area.

We determined that the first step to understanding carbon dynamics and the role of fire was to evaluate aboveground dynamics. We plan to leverage our existing plots, pairing them with belowground carbon measurements, as part of a future study.

Conclusions

- We used an extensive ground-based plot dataset, the most applicable biomass allometry equations, and a robust statistical analysis to estimate aboveground tree carbon densities and total stocks, plus the uncertainty around those estimates, for Yosemite and Sequoia & Kings Canyon national parks.
- We found aboveground tree carbon density responded inconsistently to fire history across forest types. Red fir forests were the most impacted by fire, with ~29% lower carbon density in burned areas. The other forest types we analyzed appeared to be less affected by fire history.
- With allowances for likely biases in both methodologies, our results are comparable to aboveground carbon estimates utilizing remotely-sensed data (NASA–CASA) in Yosemite. Our efforts have the potential to refine how carbon stocks are adjusted for fire effects in the California greenhouse gas inventory.
- Incorporating fire severity (using either ground-based or satellite-derived metrics) into our analyses and into NASA–CASA estimates would likely provide better estimates of wildfire effects on forest carbon storage.

Recommendations for Future Carbon Accounting

This work has shown that—even with thousands of measurement plots—there is substantial uncertainty in carbon estimates over large landscapes. Tracking fire severity may be required to refine our understanding of carbon dynamics across park landscapes.

No one method completely and definitively quantifies tree carbon. However, given the current state of vegetation mapping and allometric equations, we have bounded the uncertainty in carbon estimates and have provided a means for comparison with remote sensing techniques. This can assist in updating mapped carbon estimates as carbon continues to accumulate and disturbances like fire alter carbon densities. Combining these plot-based methods and the tree coring work to calibrate pre- and post-fire recovery rates with remotely-sensed carbon estimates is likely to provide the best way forward for managers to update carbon inventory maps.

Deliverables and Project Completion Plan

The original proposal listed these delivery goals: 1) a peer-reviewed journal article and an accompanying 1-page publication brief summarizing its management implications for each of the two project objectives, 2) presentation of results in at least one workshop for NPS staff and in at least one national conference, and 3) an interpretive component focused on educating the public about the value of forest carbon stocks and the impacts of fire. The following activities have been completed to meet these goals, with additional deliverables beyond the requirements (completed or planned) also listed:

Peer-reviewed manuscripts

- Lutz, J. A., K. A. Schwindt‡, T. J. Furniss, J. A. Freund, M. E. Swanson, K. I. Hogan‡, G. E. Kenagy‡, and A. J. Larson. 2014. Community composition and allometry of *Leucothoe davisiae*, *Cornus sericea*, and *Chrysolepis sempervirens*. Canadian Journal of Forest Research 44(6): 677-683.

- Lutz, J. A., J. R. Matchett, L. W. Tarnay, D. G. Smith, K. M. L. Becker†, and M. L. Brooks. In prep. The uncertainty of carbon sequestered in forest ecosystems of Yosemite and Sequoia & Kings Canyon National Parks, California, USA. To be submitted to Forest Ecology and Management.

- Becker†, K. M. L., D. G. Smith, and J. A. Lutz. In prep. Effects of fire severity, time since fire, and climatic water balance on species composition in Yosemite and Sequoia & Kings Canyon National Parks, California, USA. This manuscript will detail the compositional analysis from the paired (burned and unburned) plots established during this study.

- Becker†, K. M. L., D. G. Smith, and J. A. Lutz. In prep. Structural equivalence in a regional species pool may mitigate anthropogenic change. To be submitted to Ecology Letters.

- Lutz, J. A., J. R. Matchett, L. W. Tarnay, D. G. Smith, K. M. L. Becker†, and M. L. Brooks. In prep. Pre-fire and post-fire carbon assimilation rates in montane forests of Yosemite and Sequoia & Kings Canyon National Park differs by severity, time since fire, and site water balance.

Presentations

- Impacts of fire on carbon stocks in Yosemite, Sequoia, and Kings Canyon national parks. Presented by J. R. Matchett at the Southern Sierra Nevada Fire Science Workshop, Yosemite National Park, May 2014.

- Carbon sequestration and fire. Presented by M. L. Brooks and M. Hurteau at the Southern Sierra Nevada Fire Science Workshop, Yosemite National Park, May 2014.

- Effects of low-severity fire on structural attributes and radial tree growth in *Abies concolor*-dominated forests, Yosemite National Park, California. Presented by J. Wilson‡ for the Senior Capstone Program on the Environment, University of Washington, May 22, 2013.

- Effects of fire on *Abies concolor* and *Abies magnifica* vegetation communities, forest structure, and carbon sequestration in Yosemite and Sequoia & Kings Canyon National Parks. Presented by K. M. L. Becker† for Masters thesis defense public presentation, University of Washington, Seattle, March 12, 2014.

†Graduate or ‡undergraduate advisee who participated in the research as part of outreach and training

Education and outreach

- Yosemite National Park's educational team has developed a "Parks as Classrooms" program focused on fire ecology, which includes curriculum based educational content and activities

focused on impacts of fire on the carbon cycle. Although these products are not complete because all the analyses for interpretation are not complete, the products will be finalized once more results are available.

- A master's thesis at the University of Washington. Becker, K. M. L. 2014. Effects of low-severity fire on species composition and structure in montane forests of the Sierra Nevada, California, USA. Masters thesis, University of Washington, Seattle, Washington.
- A video "Carbon: Forests and Fire" (http://www.youtube.com/watch?v=HIN8iY40Hl8), by K. Song, Yosemite Leadership Internship Program.
- Project data has also been used in four undergraduate student senior projects at the University of Washington.

Literature Cited

Baskerville, G. L. 1972. Use of logarithmic regression in the estimation of plant biomass. Canadian Journal of Forest Research 2:49–53.

California Assembly. 2006. Bill No. 32: An act to add Division 25.5 (commencing with Section 38500) to the Health and Safety Code, relating to air pollution. Approved by Governor 9/27/2006.

Carlson, C. H., S. Z. Dobrowski, and H. D. Safford. 2012. Variation in tree mortality and regeneration affect forest carbon recovery following fuel treatments and wildfire in the Lake Tahoe Basin, California, USA. Carbon Balance and Management 7:7.

Chisholm, R. A., H. C. Muller-Landau, K. A. Rahman, D. P. Bebber, Y. Bin, S. A. Bohlman, et al. 2013. Scale-dependent relationships between species richness and ecosystem function in forests. Journal of Ecology 101:1214–1224.

Collins, B. M., R. G. Everett, and S. L. Stephens. 2011. Impacts of fire exclusion and recent managed fire on forest structure in old-growth Sierra Nevada mixed-conifer forests. Ecosphere 2:article 51.

Davis, B. H., J. Beck, and J. Van Wagtendonk. 2009. Modeling fuel succession. Fire Management Today 69:18-21

Fellows, A. W., and M. L. Goulden. 2008. Has fire suppression increased the amount of carbon stored in western U.S. forests? Geophysical Research Letters 35(12):L12404.

Gonzalez, P., G. P. Asner, J. J. Battles, M. A. Lefsky, K. M. Waring, and M. Palace. 2010. Forest carbon densities and uncertainties from Lidar, QuickBird, and field measurements in California. Remote Sensing of Environment 114:1561–1575.

Halpern, C. B., and J. A. Lutz. 2013. Canopy closure exerts weak controls on understory dynamics: a 30-year study of overstory-understory interactions. Ecological Monographs 83:19–35.

Hann, W. J., and D. J. Strohm. 2003. Fire regime condition class and associated data for fire and fuels planning: methods and applications. Pages 397-434 in: Omi, P. N., L. A. Joyce (editors) Fire, fuel treatments, and ecological restoration. Conference proceedings RMRS-P-29. U.S.D.A. Forest Service, Rocky Mountain Research Station, Fort Collins, CO

Hessburg, P. F., J. K. Agee, and J. F. Franklin. 2005. Dry forests and wildland fires of the inland Northwest USA: contrasting the landscape ecology of the pre-settlement and modern eras. Forest Ecology and Management 211:117–139.

Hurteau, M. D. 2013. Effects of wildland fire management on forest carbon stores. Pages 359–380 in D. G. Brown, D. T. Robinson, N. H. F. French, and B. C. Reed (editors) Land use and the carbon cycle: science applications in human environment interactions. Cambridge University Press, Cambridge UK.

Hurteau, M. D., and M. L. Brooks. 2011. Short- and long-term effects of fire on carbon in US dry temperate forest ecosystems. BioScience 61:139–146.

Hurteau, M. D., and M. P. North. 2009. Fuel treatment effects on tree-based forest carbon storage and emissions under modeled wildfire scenarios. Frontiers in Ecology and the Environment 7:409–414.

Hurteau, M. D., and M. North. 2010. Carbon recovery rates following different wildfire risk mitigation treatments. Forest Ecology and Management 260:930-937

Hurteau, M. D., M. T. Stoddard, and P. Z. Fule. 2011. The carbon costs of mitigating high-severity wildfire in southwestern ponderosa pine. Global Change Biology 17:1516-1521

Jenkins, J. C., D. C. Chojnacky, L. S. Heath, and R. A. Birdsey. 2003. National-scale biomass estimators for United States tree species. Forest Science 49:12–35.

Kane, V. R., J. A. Lutz, S. L. Roberts, D. F. Smith, R. J. McGaughey, N. A. Povak, and M. L. Brooks. 2013. Landscape-scale effects of fire severity on mixed-conifer and red fir forest structure in Yosemite National Park. Forest Ecology and Management 287:17–31.

Keeler-Wolf, T., P. E.Moore, E. T. Reyes, J. M. Menke, D. N. Johnson and D. L. Karavidas. 2012. Yosemite National Park vegetation classification and mapping project report. Natural Resource Technical Report NPS/YOSE/NRTR—2012/598. National Park Service, Fort Collins, Colorado.

Kolden, C. A., J. A. Lutz, C. H. Key, J. T. Kane, and J. W. van Wagtendonk. 2012. Mapped versus actual burned area within wildfire perimeters: characterizing the unburned. Forest Ecology and Management 286:38–47.

Lamlom, S. H., and R. A. Savidge. 2003. A reassessment of carbon content in wood: variation within and between 41 North American species. Biomass and Bioenergy 25: 381–388.

Larson, A. J., J. A. Lutz, R. F. Gersonde, J. F. Franklin, and F. F. Hietpas. 2008. Productivity influences the rate of forest structural development. Ecological Applications 18:899–910.

Lutz, J. A., K. A. Schwindt, T. J. Furniss, J. A. Freund, M. E. Swanson, K. I. Hogan, G. E. Kenagy, and A. J. Larson. Submitted. Community composition and allometry of *Leucothoe davisiae*, *Cornus sericea*, and *Chrysolepis sempervirens*. Canadian Journal of Forest Research.

Lutz, J. A., and C. B. Halpern. 2006. Tree mortality during early forest development: a long-term study of rates, causes, and consequences. Ecological Monographs 76:257–275.

Lutz, J. A., C. H. Key, C. A. Kolden, J. T. Kane, and J. W. van Wagtendonk. 2011. Fire frequency, area burned, and severity: A quantitative approach to defining a normal fire year. Fire Ecology 7:51–65.

Lutz, J. A., A. J. Larson, M. E. Swanson, and J. A. Freund. 2012. Ecological importance of large-diameter trees in a temperate mixed-conifer forest. PLoS ONE 7:e36131.

Lutz, J. A, A. J. Larson, J. A. Freund, M. E. Swanson, and K. J. Bible. 2013. The ecological importance of large-diameter trees to forest structural heterogeneity. PLoS ONE 8:e82784.

Lutz, J. A., J. W. van Wagtendonk, A. E. Thode, J. D. Miller, and J. F. Franklin. 2009. Climate, lightning ignitions, and fire severity in Yosemite National Park, California, USA. International Journal of Wildland Fire 18:765–774.

Lutz, J. A., J. W. van Wagtendonk, and J. F. Franklin. 2009. Twentieth-century decline of large-diameter trees in Yosemite National Park, California, USA. Forest Ecology and Management 257: 2296–2307.

Lutz, J. A., J. W. van Wagtendonk, J. F. Franklin. 2010. Climatic water deficit, tree species ranges, and climate change in Yosemite National Park. Journal of Biogeography 37:936–950.

McGinnis, T. W., C. D. Shook, and J. E. Keeley. 2010. Estimating aboveground biomass for broadleaf woody plants and young conifers in Sierra Nevada, California, Forests. Western Journal of Applied Forestry 25:203–209.

Miller, L. M., R. O. Meeuwig, and J. D. Budy. 1981. Biomass of singleleaf pinyon and Utah juniper. USDA Forest Service, Intermountain Forest and Range Experimental Station Research Paper INT-273. Ogden, Utah.

North, M. J., J. Innes, and H. Zald. 2007. Comparison of thinning and prescribed fire restoration treatments to Sierran mixed-conifer historic conditions. Canadian Journal of Forest Research 37:331–342.

Pan, Y., R. A. Birdsey, J. Fang, R. Houghton, P. E. Kauppi, et al. 2011. A large and persistent carbon sink in the world's forests. Science 333: 988-993.

Potter, C. 2010. The carbon budget of California. Environmental Science & Policy 13:373–383.

PostGIS Development Team. 2013. PostGIS, version 2.1. http://postgis.net.

QGIS Development Team. 2013. QGIS, version 2.4. http://qgis.net

R Core Team. 2013. R: A language and environment for statistical computing, version 3.0. R Foundation for Statistical Computing, Vienna, Austria. http://www.R-project.org/

Safford, H. D., and K. M. Van de Water. 2014. Using fire return interval departure (FRID) analysis to map spatial and temporal changes in fire frequency on national forest lands in California. U.S.D.A. Forest Service, Pacific Southwest Research Station, Research Paper PSW-RP-266.

Safford, H. D., K. Van de Water, and D. Schmidt. 2011. California Fire Return Interval Departure (FRID) map, 2010 version. U.S.D.A. Forest Service, Pacific Southwest Region, and The Nature Conservancy – California. http://www.fs.usda.gov/main/r5/landmanagement/gis/.

Scholl A. E, and A. H. Taylor. 2010. Fire regimes, forest change, and self-organization in an old-growth mixed-conifer forest, Yosemite National Park, USA. Ecological Applications 20:362–380.

Sillett, S.C., Van Pelt, R. 2007. Trunk reiteration promotes epiphytes and water storage in an old-growth redwood forest canopy. Ecological Monographs 77:335–359.

Swann, A. L. S, I. Y. Fung, J. C. H. Chiang. 2012. Mid-latitude afforestation shifts general circulation and tropical precipitation. Proceedings of the National Academy of Sciences of the USA 109:712–716.

Thomas, S. C., and A. R. Martin. 2012. Carbon content of tree tissues: A synthesis. Forests 3: 332-352.

Van Pelt, R. 2001. Forest giants of the Pacific coast. University of Washington Press, Seattle, Washington.

Van Pelt, R., and S. C. Sillett. 2008. Crown development throughout the lifespan of coastal *Pseudotsuga menziesii*, including a conceptual model for tall conifers. Ecological Monographs 78:283–311.

van Wagtendonk, J. W., K. A. van Wagtendonk, J. B. Meyer, and K. J. Paintner. 2002. The use of geographical information for fire management planning in Yosemite National Park. The George Wright Forum 19:19–39.

van Wagtendonk, J. W. 2007. The history and evolution of wildland fire use. Fire Ecology 3:3–17.

van Wagtendonk, J. W., and J. A. Lutz. 2007. Fire regime attributes of wildland fires in Yosemite National Park, USA. Fire Ecology 3:34–52.

van Wagtendonk, J. W., and P. E. Moore. 2010. Fuel deposition rates of montane and subalpine conifers in the central Sierra Nevada, California, USA. Forest Ecology and Management 259:2122–2132.

Westman, W. E. 1998. Aboveground biomass, surface area, and production relations of red fir (*Abies magnifica*) and white fir (*A. concolor*). Canadian Journal of Forest Research 17:311–319.

Wickham, H. 2009. ggplot2: elegant graphics for data analysis. Springer, New York.

Appendix A. Allometric equations.

scientific name	minumum applied DBH (cm)	maximum applied DBH (cm)	ceiling DBH (cm)	component	equation species	a	b	SEE	reference ID
Abies concolor	0	6.9999	1000	tree	small conifer	-1.8516	2.3701	0.1191	15
Abies concolor	7	98	1000	tree	Abies concolor	-2.5521	2.5043	0.16805	2
Abies concolor	98.0001	1000	1000	bole	Abies procera	-3.0319	2.5812	0.1841	4
Abies concolor	98.0001	1000	111	branch live	Abies pooled	-4.9318	2.5585	0.454	8
Abies concolor	98.0001	1000	111	foliage	Abies pooled	-3.5458	1.9278	0.399	8
Abies	0	27.5	1000	tree	small conifer	-1.8516	2.3701	0.1191	15
Abies	27.5001	100	1000	tree	Abies magnifica	-4.3136	2.9121	0.22074	2
Abies	100.0001	1000	1000	bole	Abies procera	-3.0319	2.5812	0.1841	4
Abies	100.0001	1000	111	branch live	Abies pooled	-4.9318	2.5585	0.454	8
Abies	100.0001	1000	111	foliage	Abies pooled	-3.5458	1.9278	0.399	8
Abies magnifica	0	27.5	1000	tree	small conifer	-1.8516	2.3701	0.1191	15
Abies magnifica	27.5001	100	1000	tree	Abies magnifica	-4.3136	2.9121	0.22074	2
Abies magnifica	100.0001	1000	1000	bole	Abies procera	-3.0319	2.5812	0.1841	4
Abies magnifica	100.0001	1000	111	branch live	Abies pooled	-4.9318	2.5585	0.454	8
Abies magnifica	100.0001	1000	111	foliage	Abies pooled	-3.5458	1.9278	0.399	8
Acer macrophyllum	0	7.5999	1000	tree	soft maple/birch	-2.0332	2.3651	0.491685	16
Acer macrophyllum	7.6	1000	1000	bole bark	Acer macrophyllum	-4.5757	2.574	0.058	7
Acer macrophyllum	7.6	1000	1000	bole wood	Acer macrophyllum	-3.4931	2.723	0.014	7
Acer macrophyllum	7.6	1000	1000	branch dead	Acer macrophyllum	-3.8495	1.092	1.862	7
Acer macrophyllum	7.6	1000	1000	branch live	Acer macrophyllum	-4.2613	2.43	0.225	7
Acer macrophyllum	7.6	1000	1000	foliage	Acer macrophyllum	-3.7701	1.617	0.101	7
Aesculus californica	0	1000	1000	tree	mixed hardwood	-2.545	2.4835	0.360458	16
Alnus rhombifolia	0	1000	1000	tree	aspen/alder/cottonwood/willow	-2.3381	2.3867	0.507441	16
Arctostaphylos viscida	0	1000	1000	tree	mixed hardwood	-2.545	2.4835	0.360458	16
Arctostaphylos viscida ssp. viscida	0	1000	1000	tree	mixed hardwood	-2.545	2.4835	0.360458	16
Betula occidentalis	0	1000	1000	tree	soft maple/birch	-2.0332	2.3651	0.491685	16
Calocedrus decurrens	0	1000	1000	tree	cedar/larch	-2.077	2.2592	0.294574	16
Cercocarpus betuloides	0	1000	1000	tree	mixed hardwood	-2.545	2.4835	0.360458	16

scientific name	minumum applied DBH (cm)	maximum applied DBH (cm)	ceiling DBH (cm)	component	equation species	a	b	SEE	reference ID
Cercocarpus ledifolius	0	1000	1000	tree	mixed hardwood	-2.545	2.4835	0.360458	16
Cercis occidentalis	0	1000	1000	tree	mixed hardwood	-2.545	2.4835	0.360458	16
Corylus cornuta var. californica	0	1000	1000	tree	mixed hardwood	-2.545	2.4835	0.360458	16
Cornus nuttallii	0	1000	1000	tree	mixed hardwood	-2.545	2.4835	0.360458	16
Fraxinus dipetala	0	1000	1000	tree	mixed hardwood	-2.545	2.4835	0.360458	16
Fraxinus latifolia	0	1000	1000	tree	mixed hardwood	-2.545	2.4835	0.360458	16
Fraxinus velutina	0	1000	1000	tree	mixed hardwood	-2.545	2.4835	0.360458	16
Juniperus occidentalis	0	1000	1000	tree	Juniperus occidentalis	-5.6604	2.2462	0.1433	8
Juniperus occidentalis var. australis	0	1000	1000	tree	Juniperus occidentalis	-5.6604	2.2462	0.1433	8
Juniperus osteosperma	0	1000	1000	tree	Juniperus occidentalis	-5.6604	2.2462	0.1433	8
Malus	0	1000	1000	tree	mixed hardwood	-2.545	2.4835	0.360458	16
Pinus albicaulis	0	10	1000	tree	Pinus albicaulis	-0.389	1.1585	0.4045	3
Pinus albicaulis	10.0001	20	1000	bole	Juniperus occidentalis	-8.3826	2.6378	0.159	8
Pinus albicaulis	10.0001	20	1000	canopy	Pinus albicaulis	-1.3017	1.2991	0.483	3
Pinus albicaulis	20.0001	1000	1000	tree	Juniperus occidentalis	-5.6604	2.2462	0.1433	8
Pinus attenuata	0	1000	1000	tree	pine	-2.5678	2.4349	0.253781	16
Pinus balfouriana ssp. austrina	0	10	1000	tree	Pinus albicaulis	-0.389	1.1585	0.4045	3
Pinus balfouriana ssp. austrina	10.0001	20	1000	bole	Juniperus occidentalis	-8.3826	2.6378	0.159	8
Pinus balfouriana ssp. austrina	10.0001	20	1000	canopy	Pinus albicaulis	-1.3017	1.2991	0.483	3
Pinus balfouriana ssp. austrina	20.0001	1000	1000	tree	Juniperus occidentalis	-5.6604	2.2462	0.1433	8
Pinus contorta var. murrayana	0	19.9999	1000	tree	Pinus contorta	-2.095	2.3909	0.4786	26
Pinus contorta var. murrayana	20	1000	1000	tree	Pinus contorta	-1.0386	1.9294	0.3205	1
Pinus jeffreyi	0	22.3999	1000	tree	small conifer	-1.8516	2.3701	0.1191	15
Pinus jeffreyi	22.4	133.1	1000	bole	Pinus jeffereyi	-5.1108	2.952	0.204834	4
Pinus jeffreyi	22.4	1000	162	branches dead	Pseudotsuga menziesii	-3.794	1.7503	0.728	8

scientific name	minumum applied DBH (cm)	maximum applied DBH (cm)	ceiling DBH (cm)	component	equation species	a	b	SEE	reference ID
Pinus jeffreyi	22.4	1000	162	branches live	Pseudotsuga menziesii	-3.8938	2.1382	0.632	8
Pinus jeffreyi	22.4	1000	162	foliage	Pseudotsuga menziesii	-3.0877	1.7009	0.695	8
Pinus jeffreyi	133.1001	1000	1000	bole	Pseudotsuga menziesii	-2.2765	2.4247	0.2415	4
Pinus lambertiana	0	8.6999	1000	tree	small conifer	-1.8516	2.3701	0.1191	15
Pinus lambertiana	8.7	179.6	1000	bole	Pinus lambertiana	-3.6973	2.6863	0.193513	4
Pinus lambertiana	8.7	1000	162	branches dead	Pseudotsuga menziesii	-3.794	1.7503	0.728	8
Pinus lambertiana	8.7	1000	162	branches live	Pseudotsuga menziesii	-3.8938	2.1382	0.632	8
Pinus lambertiana	8.7	1000	162	foliage	Pseudotsuga menziesii	-3.0877	1.7009	0.695	8
Pinus lambertiana	179.6001	1000	1000	bole	Pseudotsuga menziesii	-2.2765	2.4247	0.2415	4
Pinus monophylla	0	1000	1000	tree	pine	-2.5678	2.4349	0.253781	16
Pinus monticola	0	19.9999	1000	tree	Pinus contorta	-2.095	2.3909	0.4786	26
Pinus monticola	20	1000	1000	tree	Pinus contorta	-1.0386	1.9294	0.3205	1
Pinus	0	1000	1000	tree	pine	-2.5678	2.4349	0.253781	16
Pinus ponderosa	0	15.4999	1000	tree	small conifer	-1.8516	2.3701	0.1191	15
Pinus ponderosa	15.5	79.5	1000	tree	Pinus ponderosa	-3.2673	2.582	0.1266	8
Pinus ponderosa	79.5001	1000	1000	bole	Pseudotsuga menziesii	-2.2765	2.4247	0.2415	4
Pinus ponderosa	79.5001	1000	162	branches dead	Pseudotsuga menziesii	-3.794	1.7503	0.728	8
Pinus ponderosa	79.5001	1000	162	branches live	Pseudotsuga menziesii	-3.8938	2.1382	0.632	8
Pinus ponderosa	79.5001	1000	162	foliage	Pseudotsuga menziesii	-3.0877	1.7009	0.695	8
Pinus sabiniana	0	1000	1000	tree	pine	-2.5678	2.4349	0.253781	16
Platanus racemosa	0	1000	1000	tree	mixed hardwood	-2.545	2.4835	0.360458	16
Populus balsamifera	0	1000	1000	tree	aspen/alder/cottonwood/willow	-2.3381	2.3867	0.507441	16
Populus balsamifera ssp. trichocarpa	0	1000	1000	tree	aspen/alder/cottonwood/willow	-2.3381	2.3867	0.507441	16
Populus tremuloides	0	36	1000	tree	Populus tremuloides	-2.1461	2.242	0.3205	11
Populus tremuloides	36.0001	1000	1000	tree	aspen/alder/cottonwood/willow	-2.3381	2.3867	0.507441	16
Prunus emarginata	0	1000	1000	tree	mixed hardwood	-2.545	2.4835	0.360458	16
Prunus virginiana var. demissa	0	1000	1000	tree	mixed hardwood	-2.545	2.4835	0.360458	16

scientific name	minumum applied DBH (cm)	maximum applied DBH (cm)	ceiling DBH (cm)	component	equation species	a	b	SEE	reference ID
Pseudotsuga menziesii	0	1000	1000	tree	Pseudotsuga menziesii	-2.2543	2.4435	0.218712	16
Quercus chrysolepis	0	1000	1000	tree	hard maple/oak/hickory/beech	-2.0407	2.4342	0.236483	16
Quercus douglasii	0	1000	1000	tree	hard maple/oak/hickory/beech	-2.0407	2.4342	0.236483	16
Quercus kelloggii	0	1000	1000	tree	hard maple/oak/hickory/beech	-2.0407	2.4342	0.236483	16
Quercus lobata	0	1000	1000	tree	hard maple/oak/hickory/beech	-2.0407	2.4342	0.236483	16
Quercus x moreha	0	1000	1000	tree	hard maple/oak/hickory/beech	-2.0407	2.4342	0.236483	16
Quercus wislizeni	0	1000	1000	tree	hard maple/oak/hickory/beech	-2.0407	2.4342	0.236483	16
Quercus wislizeni var. wislizeni	0	1000	1000	tree	hard maple/oak/hickory/beech	-2.0407	2.4342	0.236483	16
Rhamnus californica	0	1000	1000	tree	mixed hardwood	-2.545	2.4835	0.360458	16
Rhamnus ilicifolia	0	1000	1000	tree	mixed hardwood	-2.545	2.4835	0.360458	16
Salix laevigata	0	1000	1000	tree	aspen/alder/cottonwood/willow	-2.3381	2.3867	0.507441	16
Salix lasiolepis	0	1000	1000	tree	aspen/alder/cottonwood/willow	-2.3381	2.3867	0.507441	16
Salix	0	1000	1000	tree	aspen/alder/cottonwood/willow	-2.3381	2.3867	0.507441	16
Salix lucida	0	1000	1000	tree	aspen/alder/cottonwood/willow	-2.3381	2.3867	0.507441	16
Salix lucida ssp. lasiandra	0	1000	1000	tree	aspen/alder/cottonwood/willow	-2.3381	2.3867	0.507441	16
Salix melanopsis	0	1000	1000	tree	aspen/alder/cottonwood/willow	-2.3381	2.3867	0.507441	16
Salix scouleriana	0	1000	1000	tree	aspen/alder/cottonwood/willow	-2.3381	2.3867	0.507441	16
Sequoiadendron giganteum	0	96.7999	1000	tree	cedar/larch	-2.077	2.2592	0.294574	16
Sequoiadendron giganteum	96.8	1000	1000	bole	Sequoiadendron giganteum	-2.8134	2.4019	0.254442	4
Torreya californica	0	1000	1000	tree	mixed hardwood	-2.545	2.4835	0.360458	16
generic tree species	0	1000	1000	tree	pine	-2.5678	2.4349	0.253781	16
Tsuga mertensiana	0	11.4999	1000	tree	small conifer	-1.8516	2.3701	0.1191	15
Tsuga mertensiana	11.5	1000	1000	bole	Tsuga mertensiana	-3.2801	2.5915	0.195028	4
Tsuga mertensiana	11.5	1000	1000	branch live	Tsuga mertensiana	-5.2655	2.6045	0.122	8
Tsuga mertensiana	11.5	1000	1000	branches dead	Tsuga mertensiana	-9.951	3.2845	0.11	8
Tsuga mertensiana	11.5	1000	1000	foliage	Tsuga mertensiana	-3.8294	1.9756	0.158	8
Umbellularia californica	0	1000	1000	tree	Umbellularia californica	-2.1313	2.3996	0.2497	21

References:

1 Pearson JA, Fahey TJ, Knight DH (1984) Biomass and leaf area in contrasting lodgepole pine forests. Canadian Journal of Forest Resources 14:259-265

2 Westman WE (1987) Aboveground biomass, surface area, and production relations of red fir (Abies magnifica) and white fir (A. concolor). Canadian Journal of

Forest Resources 17:311-319

3 Brown JK (1978) Weight and density of crowns of Rocky Mountain conifers. USFS Research Paper INT-197:56

4 Means JE, Hansen HA, Koerper GJ, Alaback PB, Klopsch MW (1994) Software for computing plant biomass--BIOPAK users guide. USFS Research Paper PNW-GTR-340

5 Jenkins JC, Chojnacky DC, Heath LS, Birdsey RA (2004) Comprehensive database of diameter-based biomass regressions for north american tree species. USFS Research Paper GTR NE-319

6 Ter-Mikaelian MT, Korzukhin MD (1997) Biomass equations for sixty-five North American tree species. Forest Ecology and Management 97:1-24

7 Grier CC, Logan RS (1977) Old-growth Pseudotsuga menziesii communities of a western Oregon watershed: biomass distribution and production budgets. Ecological Monographs 47:373-400

8 Gholz HL, Grier CC, Campbell AG, Brown AT (1979) Equations for estimating biomass and leaf area of plants in the Pacific Northwest. Oregon State University School of Forestry Research Paper 41:39

9 Chojnacky DC, Moisen GG (1993) Converting wood volume to biomass for pinyon and juniper. USFS Research Paper INT-411

10 Miller E, Meeuwig R, Budy J (1981) Biomass of singleleaf pinyon and Utah juniper. USFS Research Paper INT-273

11 Johnston RS, Bartos DL (1977) Summary of nutrient and biomass data from two aspen sites in western United States. USFS Research Paper INT-277:15

12 Perala DA, Alban DH (1994) Allometric biomass estimation for aspen-dominated ecosystems in the Upper Great Lakes. USFS Research Paper NC-134:38

13 Boerner REJ, Kost JA (1986) Biomass equations for flowering dogwood, Cornus florida L.. Castane 51:153-154

14 Helgerson O, Cromack K, Stafford S, Miller R, Slagle R (1988) Equations for estimating aboveground components of young Douglas-fir and red alder in a coastal Oregon plantation. Canadian Journal of Forest Research 18:1082-1085

15 Gower ST, Vogt KA, Grier CC (1992) Carbon dynamics of rocky mountain douglas-fir: Influence of water and nutrient availability. Ecological Monographs 62:43-65

16 Jenkins JC, Chojnacky DC, Heath LS, Birdsey RA (2003) National-scale biomass estimators for United States tree species. Forest Science 49:12-35

17 Lambert MC, Ung CH, Raulier F (2005) Canadian national tree aboveground biomass equations. Canadian Journal of Forest Research 35:1996-2018

18 Chojnacky DC (1984) Volume and biomass for curlleaf Cercocarpus in Nevada. USFS Research Paper INT-332

21 Coltrin WR (2010) Biomass quantification of live trees in a mixed evergreen forest using biomass diameter-based allometric equations. Master's Thesis, Humboldt State University 52 pp

22 Harmon M (1994) Mark Harmon, Forest Science Dept., Ore State Univ. fit the equation.. x x

23 Pastor J, Aber JD, Melillo JM (1984) Biomass prediction using generalized allometric regressions for some northeast tree species. Forest Ecology and Management 7:265-274

24 Halpern CB, Miller EA, Melora (1996) Equations for predicting above-ground biomass of plant species in early successional forests of the western cascade range, Oregon. Northwest Science 70:306-320

26 Gower ST, Grier CG, Vogt DJ, Vogt KA (1987) Allometric relations of deciduous (Larix occidentalis) and evergreen conifers (Pinus contorta and Pseudotsuga menziesii) of the Cascade Mountains in Central Washington. Canadian Journal of Forest Resources 17:63

Appendix B. Community type assignments.

Mapping Code	Mapping Community Type	Carbon Type
0	none	unassigned
100	Alpine Talus Slope	No Biomass
200	Alpine Scree Slope	No Biomass
300	Alpine Snow Patch Communities	Herbaceous
400	Alpine Fell-field	No Biomass
500	Mesic Rock Outcrop	No Biomass
700	Boulder Field	No Biomass
910	Conifer Reproduction	Successional Conifer
920	Conifer Plantation	Successional Conifer
940	Sparsely Vegetated Undifferentiated	No Biomass
941	Sparsely Vegetated Riverine Flat	Herbaceous
950	Non-alpine Talus	No Biomass
961	Sparsely Vegetated to Non-vegetated Exposed Rock	No Biomass
963	Dome	No Biomass
964	Fissured Rock Outcrop	No Biomass
965	Sparsely Vegetated Rocky Streambed	No Biomass
970	Alpine Permanent Snowfield/Glacier	No Biomass
980	Water	No Biomass
981	Permanently Flooded, Emergent, or Floating Vegetation Mapping Unit	No Biomass
990	Urban/Developed	No Biomass
1020	Canyon Live Oak Forest Alliance	Evergreen Oak Forest and Woodland
1021	Canyon Live Oak/Birchleaf Mountain Mahogany Forest Mapping Unit	Evergreen Oak Forest and Woodland
1022	Canyon Live Oak/Whiteleaf Manzanita Forest Association	Evergreen Oak Forest and Woodland
1023	Canyon Live Oak-(Ponderosa Pine-Incense-cedar) Forest Superassociation	Evergreen Oak Forest and Woodland
1024	Canyon Live Oak-California Laurel Forest Superassociation	Evergreen Oak Forest and Woodland
1026	Canyon Live Oak-Foothill Pine Forest Association	Evergreen Oak Forest and Woodland
1029	Canyon live oak/Greenleaf Manzanita Forest Association	Evergreen Oak Forest and Woodland
1040	Interior Live Oak Woodland Alliance	Evergreen Oak Forest and Woodland
1043	Interior Live Oak-Canyon Live Oak Woodland Association	Evergreen Oak Forest and Woodland

Mapping Code	Mapping Community Type	Carbon Type
1044	Interior Live Oak-California Buckeye/Birchleaf Mountain Mahogany-California Redbud Forest Association	Evergreen Oak Forest and Woodland
1510	Canyon Live Oak/California Buckeye Woodland & Interior Live Oak-California Buckeye S	Evergreen Oak Forest and Woodland
1520	Blue Oak-(Interior Live Oak-Foothill Pine/Buckbrush/Annual Grass) Woodland Mapping U	Evergreen Oak Forest and Woodland
1530	Interior Live Oak Woodland & Shrubland Superalliance	Evergreen Oak Forest and Woodland
2010	Quaking Aspen Forest Alliance	Riparian Forest
2011	Quaking Aspen/California False Hellebore Forest Association	Riparian Forest
2013	Quaking Aspen/Willow spp. Forest Mapping Unit	Riparian Forest
2014	Quaking Aspen/Willow spp. Talus Mapping Unit	Riparian Forest
2015	Quaking Aspen-Jeffrey Pine/(Big Sagebrush) Forest Association	Riparian Forest
2016	Quaking Aspen/Big Sagebrush Forest Superassociation	Riparian Forest
2017	Quaking Aspen/Meadow Mapping Unit	Riparian Forest
2020	California Black Oak Forest Alliance	Deciduous Oak Forest and Woodland
2021	California Black Oak/Greenleaf Manzanita Forest Association	Deciduous Oak Forest and Woodland
2022	California Black Oak-Incense-cedar Forest Association	Evergreen Oak Forest and Woodland
2025	California Black Oak/(Bracken Fern) Forest Mapping Unit	Deciduous Oak Forest and Woodland
2030	Blue Oak Woodland Alliance	Deciduous Oak Forest and Woodland
2033	Blue Oak/Brome spp.-American Wild Carrot Woodland Association	Deciduous Oak Forest and Woodland
2034	Blue Oak-Interior Live Oak/Brome spp.-American Wild Carrot Woodland Association	Deciduous Oak Forest and Woodland
2038	Blue Oak-California Buckeye-(Interior Live Oak) Woodland Mapping Unit	Deciduous Oak Forest and Woodland
2040	Valley Oak Woodland Alliance	Deciduous Oak Forest and Woodland
2050	Black Cottonwood Temporarily Flooded Forest Alliance	Riparian Forest
2052	Black Cottonwood-Quaking Aspen-(Jeffrey Pine)/Willow spp. Mapping Unit	Riparian Forest
2053	Black Cottonwood Forest Association	Riparian Forest
2060	White Alder Temporarily Flooded Forest Alliance	Riparian Shrub
2061	White Alder-Red willow-California Sycamore Forest Association	Riparian Shrub
2070	Mountain Alder Mapping Unit	Shrub
2080	Bigleaf Maple Forest Alliance	Deciduous Forest
2100	California Sycamore Temporarily Flooded Woodland Alliance	Riparian Forest
2102	California Sycamore-(Canyon Live Oak-Interior Live Oak) Forest Mapping Unit	Riparian Forest
2110	California Buckeye Woodland Alliance	Evergreen Oak Forest and Woodland

Mapping Code	Mapping Community Type	Carbon Type
2114	California Buckeye-Canyon Live Oak Woodland Association	Evergreen Oak Forest and Woodland
2503	Montane Broadleaf Deciduous Trees Mapping Unit	Deciduous Forest
2510	Willow spp. Forest Mapping Unit	Riparian Shrub
2520	White Alder & Bigleaf Maple Forest Superalliance	Riparian Forest
2530	Montane Broadleaf Deciduous Trees Mapping Unit	Deciduous Forest
3010	Sierra Lodgepole Pine-Quaking Aspen-(Jeffrey Pine) Forest Alliance	Lodgepole Pine Forest
3012	Sierra Lodgepole Pine-Quaking Aspen/(Kentucky Bluegrass) Forest Mapping Unit	Lodgepole Pine Forest
3020	Sierra Lodgepole Pine Forest Alliance	Lodgepole Pine Forest
3022	Sierra Lodgepole Pine/(Bog Blueberry) Forest Mapping Unit	Lodgepole Pine Forest
3026	Sierra Lodgepole Pine Rocky Woodlands Superassociation	Lodgepole Pine Forest
3027	Sierra Lodgepole Pine/(Big Sagebrush-Roundleaf Snowberry-Currant-Red Mountainheather	Lodgepole Pine Forest
3028	Sierra Lodgepole Pine-(Whitebark Pine)/(Ross Sedge-Shorthair Sedge) Forest Superassociation	Lodgepole Pine Forest
3034	Sierra Lodgepole Pine/Big Sagebrush Forest Association	Lodgepole Pine Forest
3047	Sierra Lodgepole Pine/(Big Sagebrush)/(Kentucky Bluegrass) Forest Mapping Unit	Lodgepole Pine Forest
3048	Sierra Lodgepole Pine Mesic Forest Superassociation	Lodgepole Pine Forest
3049	Sierra Lodgepole Pine Xeric Forest Superassociation	Lodgepole Pine Forest
3050	Ponderosa Pine Woodland Alliance	Ponderosa Pine Woodland
3053	Ponderosa Pine-California Black Oak/Whiteleaf Manzanita Woodland Association	Ponderosa Pine Woodland
3060	Ponderosa Pine-Incense-cedar Forest Alliance	Ponderosa Pine Forest
3061	Ponderosa Pine-Incense-cedar-Canyon Live Oak/Mountain Misery Forest Association	Ponderosa Pine Forest
3062	Ponderosa Pine-Incense-cedar/Mountain Misery Forest Association	Ponderosa Pine Forest
3063	Ponderosa Pine-Incense-cedar-California Black Oak Forest Association	Ponderosa Pine Forest
3066	Ponderosa Pine-Incense-cedar-(California Black Oak-Canyon Live Oak)	Ponderosa Pine Forest
3070	Jeffrey Pine Woodland Alliance	Jeffrey Pine Forest
3072	Jeffrey Pine/Greenleaf Manzanita Woodland Association	Jeffrey Pine Forest
3073	Jeffrey Pine/Whitethorn Ceanothus Woodland Association	Jeffrey Pine Forest
3075	Jeffrey Pine/Huckleberry Oak Woodland Association	Jeffrey Pine Forest
3076	Jeffrey Pine/Antelope Bitterbrush Woodland Association	Jeffrey Pine Forest
3081	Jeffrey Pine?Singleleaf Pinyon Pine Woodland Association	Jeffrey Pine Forest
3082	Jeffrey Pine/Curl-leaf Mountain Mahogany Woodland Association	Jeffrey Pine Forest

Mapping Code	Mapping Community Type	Carbon Type
3083	Jeffrey Pine-White Fir/Roundleaf Snowberry/Squirreltail Woodland Association	Jeffrey Pine Forest
3084	Jeffrey Pine-Canyon Live Oak/Whiteleaf Manzanita Woodland Association	Jeffrey Pine Forest
3085	Jeffrey Pine-California Red Fir Woodland Association	Jeffrey Pine Forest
3090	Foothill Pine Woodland Alliance	Foothill Pine Woodland
3097	Foothill Pine-Interior Live Oak/(Whiteleaf Manzanita-Buckbrush-Chamise) Woodland Sup	Foothill Pine Woodland
3101	Knobcone Pine/Whiteleaf Manzanita Woodland Association	Shrub
3102	Knobcone Pine-Canyon Live Oak Woodland Mapping Unit	Shrub
3105	Knobcone Pine/Chamise Woodland Association	Shrub
3110	Single-leaf Pinyon Pine Woodland Alliance	Pinyon Pine Woodland
3112	Singleleaf Pinyon Pine/Curl-leaf Mountain Mahogany-Big Sagebrush-Antelope Bitterbrus	Pinyon Pine Woodland
3113	Singleleaf Pinyon Pine/(Desert Gooseberry-Big Sagebrush/Squirreltail) Woodland Super	Pinyon Pine Woodland
3114	Single-leaf Pinyon Pine-Canyon Live Oak/Whiteleaf Manzanita Woodland Association	Pinyon Pine Woodland
3130	Western White Pine Woodland Alliance	Western White Pine Woodland
3131	Western White Pine/Western Needlegrass Woodland Mapping Unit	Western White Pine Woodland
3133	Western White Pine/(Greenleaf Manzanita-Bush Chinquapin-Oceanspray) Woodland Mapping Unit	Western White Pine Woodland
3140	Whitebark Pine Woodland Alliance	High Woodland
3142	Whitebark Pine/Davidsons Penstemon Woodland Association	High Woodland
3143	Whitebark Pine/(Ross Sedge-Shorthair Sedge) Woodland Superassociation	High Woodland
3144	Whitebark Pine/Shorthair Sedge Woodland Association	High Woodland
3147	Whitebark Pine-Mountain Hemlock Woodland Association	High Woodland
3148	Whitebark Pine-Mountain Hemlock Woodland Association	High Woodland
3149	Whitebark Pine-(Sierra Lodgepole Pine-Mountain Hemlock) Krummholz Conifer Mapping Un	High Woodland
3150	Limber Pine Woodland Alliance	High Woodland
3200	Foxtail Pine Woodland Alliance	Foxtail Pine Forest
3202	Foxtail Pine/Bush Chinquapin Woodland Association	Foxtail Pine Forest
3203	Foxtail Pine Woodland Superassociation	Foxtail Pine Forest
3204	Foxtail Pine-Western White Pine Woodland Superassociation	Foxtail Pine Forest
3205	Dead Foxtail Pine Mapping Unit	Foxtail Pine Forest
3520	(Foxtail Pine-Sierra Lodgepole Pine-Whitebark Pine) Krummholz Woodland Mapping Unit	Foxtail Pine Forest
3530	Whitebark Pine-Foxtail Pine-Lodgepole Pine Woodland Superalliance	High Woodland

Mapping Code	Mapping Community Type	Carbon Type
3540	Foxtail Pine-Lodgepole Pine Woodland Superalliance	Foxtail Pine Forest
4010	Incense-cedar Forest Alliance	Riparian Forest
4012	Douglas-fir-Canyon Live Oak Forest Association	Douglas-fir Forest
4014	Douglas-fir-White Alder Forest Association	Douglas-fir Forest
4020	Giant Sequoia Forest Alliance	Giant Sequoia Forest
4021	Giant Sequoia-Sugar Pine/Pacific Dogwood Forest Association	Giant Sequoia Forest
4023	Giant Sequoia-White Fir-California Red Fir Forest Association	Giant Sequoia Forest
4030	Mountain Hemlock Forest Alliance	Mountain Hemlock Forest
4033	Mountain Hemlock-Western White Pine Forest Association	Mountain Hemlock Forest
4035	Mountain Hemlock-(Western White Pine-Sierra Lodgepole Pine) Forest	Mountain Hemlock Forest
4041	Mountain Hemlock-Sierra Lodgepole Pine Forest Association	Mountain Hemlock Forest
4042	Mountain Hemlock-Sierra Lodgepole Pine-Whitebark Pine Forest Mapping Unit	Mountain Hemlock Forest
4043	Mountain Hemlock-Sierra Lodgepole Pine-Western White Pine Forest Association	Mountain Hemlock Forest
4050	California Red Fir Forest Alliance	Red Fir Forest
4051	California Red Fir Forest Association	Red Fir Forest
4056	California Red Fir-(Sierra Lodgepole Pine) Forest Superassociation	Red Fir Forest
4057	California Red Fir-Western White Pine Forest Association	Red Fir Forest
4063	California Red Fir-Sierra Lodgepole Pine/Whiteflower Hawkweed Forest Mapping Unit	Red Fir Forest
4064	California Red Fir-(Western White Pine)/(Pinemat Manzanita-Bush Chinquapin) Forest Mapping Unit	Western White Pine Forest
4069	California Red Fir-(Western White Pine)/(Bush Chinquapin-Huckleberry Oak-Pinemat Man	Western White Pine Forest
4070	California Red Fir-White Fir Forest Alliance	Red Fir Forest
4080	White Fir -Sugar Pine Forest Alliance	White Fir - Sugar Pine Forest
4081	White Fir Forest Mapping Unit	White Fir - Sugar Pine Forest
4082	White Fir Mature Even-age Stands Mapping Unit	White Fir - Sugar Pine Forest
4084	White Fir-(California Red Fir-Sugar Pine-Jeffrey Pine)/Whitethorn Ceanothus-(Greenleaf Manzanita) Forest Mapping Unit	White Fir - Sugar Pine Forest
4085	White Fir East Side Mapping Unit	Jeffrey Pine Forest
4094	White Fir-Sugar Pine-Incense-cedar Forest Superassociation	White Fir - Sugar Pine Forest
4095	White Fir-Sugar Pine/Greenleaf Manzanita-Whitethorn Ceanothus Forest Mapping Unit	White Fir - Sugar Pine Forest
4100	Sierra Juniper Woodland Alliance	High Woodland
4101	Sierra Juniper/(Oceanspray) Woodland Superassociation	High Woodland

Mapping Code	Mapping Community Type	Carbon Type
4107	Sierra Juniper/Curl-leaf Mountain Mahogany-Big Sagebrush Woodland Association	High Woodland
4108	Sierra Juniper Woodland Association	High Woodland
4109	Sierra Juniper/(Oceanspray-Big Sagebrush) Woodland Superassociation	High Woodland
4110	Douglas-fir Forest Alliance	Douglas-fir Forest
4111	Incense-cedar-White Alder Forest Association	Riparian Forest
4510	Western White Pine-(California Red Fir-Sierra Lodgepole Pine) Forest Superalliance	Western White Pine Forest
4520	White Fir-(California Red Fir-Sugar Pine-Jeffrey Pine)/(Pinemat Manzanita-Whitethorn	White Fir - Sugar Pine Forest
4530	White Fir-Sugar Pine-(Incense-cedar-Jeffrey Pine) Forest Mapping Unit	White Fir - Sugar Pine Forest
4540	Western White Pine-Sierra Lodgepole Pine-(California Red Fir) Woodland Superassociation	Western White Pine Forest
4550	Douglas-fir-(White Fir-Incense-cedar-Ponderosa Pine) Forest Mapping Unit	Douglas-fir Forest
5010	Birchleaf Mountain Mahogany Shrubland Alliance	Shrub
5011	Birchleaf Mountain Mahogany-California Redbud-California Flannelbush Shrubland Association	Shrub
5012	Birchleaf Mountain Mahogany-Whiteleaf Manzanita Shrubland Association	Shrub
5020	Chamise Shrubland Alliance	Shrub
5021	Chamise Shrubland Association	Shrub
5022	Chamise-Whiteleaf Manzanita Shrubland Association	Shrub
5023	Chamise-Chaparral Yucca Shrubland Association	Shrub
5025	Chamise-California Yerba Santa Shrubland Association	Shrub
5031	Chamise-Buckbrush Shrubland Association	Shrub
5041	Interior Live Oak-California Buckeye Shrubland Association	Shrub
5050	Buckbrush Shrubland Alliance	Shrub
5060	Chaparral Whitethorn Shrubland Alliance	Shrub
5070	Whiteleaf Manzanita Shrubland Alliance	Shrub
5090	Greenleaf Manzanita Shrubland Alliance	Shrub
5110	Whitethorn Ceanothus Shrubland Alliance	Shrub
5120	Tobacco Brush Shrubland Alliance	Shrub
5130	Mountain Misery Dwarf-shrubland Alliance	Shrub
5131	Mountain Misery-Manzanita spp. Mapping Unit	Shrub
5140	Indian Manzanita Shrubland Alliance	Shrub
5160	Big Sagebrush Shrubland Alliance	Shrub
5200	Timberline Sagebrush Shrubland Alliance	Shrub

Mapping Code	Mapping Community Type	Carbon Type
5210	Low Sagebrush Dwarf-shrubland Alliance	Shrub
5230	Curl-leaf Mountain Mahogany Woodland Alliance	Shrub
5240	Antelope Bitterbrush Shrubland Alliance	Shrub
5250	(Silver Lupine)/Brome spp. Shrubland Mapping Unit	Herbaceous
5260	Big Sagebrush-(Silver Sagebrush) Shrubland Mapping Unit	Shrub
5270	Chaparral Yucca Shrubland Alliance	Shrub
5280	Pinemat Manzanita Dwarf-shrubland Alliance	Shrub
5300	Water Birch Shrubland Alliance	Shrub
5510	Mountain Big Sagebrush & Timberline Sagebrush & Oceanspray & Red Mountainheather Shrubland Superalliance	Shrub
5530	Bitter Cherry-Gooseberry spp.-(Mountain Maple) Shrubland Mapping Unit	Shrub
5550	Red Mountainheather Dwarf-shrubland Alliance	Shrub
5560	Chamise-(Buckbrush-Whiteleaf Manzanita) Shrubland Mapping Unit	Shrub
5570	Greenleaf Manzanita & Bush Chinquapin & Huckleberry Oak Shrubland Superalliance	Shrub
5580	Birchleaf Mountain Mahogany & Buckbrush & Whiteleaf Manzanita Shrubland Superallianc	Shrub
5590	Greenleaf Manzanita-Bush Chinquapin-Whitethorn Ceanothus Shrubland Superalliance	Shrub
6010	Deerbrush Shrubland Alliance	Shrub
6012	Deerbrush-Whiteleaf Manzanita Shrubland Association	Shrub
6020	Oregon White Oak Shrubland Alliance	Shrub
6022	Oregon White Oak-Birchleaf Mountain Mahogany Shrubland Association	Shrub
6030	California Grape Association	Shrub
6110	Sierra Willow/Swamp Onion Seasonally Flooded Shrubland Alliance	Shrub
6210	Oceanspray Shrubland Alliance	Shrub
6300	Bitter Cherry Shrubland Alliance	Shrub
6500	Willow spp./Meadow Shrubland Mapping Unit	Riparian Shrub
6600	Willow spp. Riparian Shrubland Mapping Unit	Riparian Shrub
6700	Willow spp. Talus Shrubland Mapping Unit	Riparian Shrub
6900	Mesic Montane Shrubland Mapping Unit	Shrub
7000	Upland Herbaceous	Herbaceous
7120	Shorthair Sedge Herbaceous Alliance	Herbaceous
7260	California Annual Grassland/Herbland Superalliance	Herbaceous

Mapping Code	Mapping Community Type	Carbon Type
7550	Upland herbaceous	Herbaceous
7701	Post-clearcut Shrub/Herbaceous Mapping Unit	Herbaceous
7702	Mesic Post Fire Herbaceous Mapping Unit	Herbaceous
7703	Post Fire Shrub/Herbaceous Mapping Unit	Shrub
8000	Intermittently to Seasonally Flooded Meadow	Herbaceous
9000	Semi-permanent to Permanently Flooded Meadow	Herbaceous
9030	Bullrush-Cattail Mapping Unit	Herbaceous

Appendix C. Forest type carbon summaries.

The following pages include data summaries for each forest community type. The ‘distribution of mean carbon density estimates’ figure is a histogram of the carbon density estimates from the 10,000 Monte Carlo realizations for each park. The vertical solid lines are the medians of the estimates, and the vertical dashed lines are the 2.5% and 97.5% percentiles of the estimates, which bound a 95% confidence interval. The ‘cumulative distribution of plot carbon densities’ figure is an empirical cumulative distribution of carbon densities for the plots used in the analysis. The ‘carbon-cover relationship’ figure shows the relationship between carbon density and the cover density (i.e., canopy cover) class used in the vegetation maps. The points are the observed plot values; the black line is the estimated fit and the gray error band is the 95% confidence interval derived from the Monte Carlo realizations. The ‘species composition’ table lists the total carbon (kg), number of trees, percentage of total carbon, and percent of total trees for each species across all plots in that forest type. If >15 different tree species were present within a forest type, only the 15 most abundant are shown.

Deciduous Oak Forest and Woodland (n = 88)

distribution of mean carbon density estimates

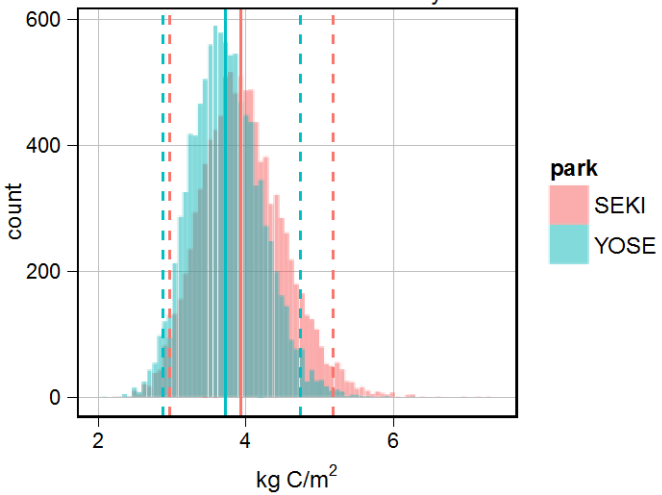

cumulative distribution of plot carbon densities

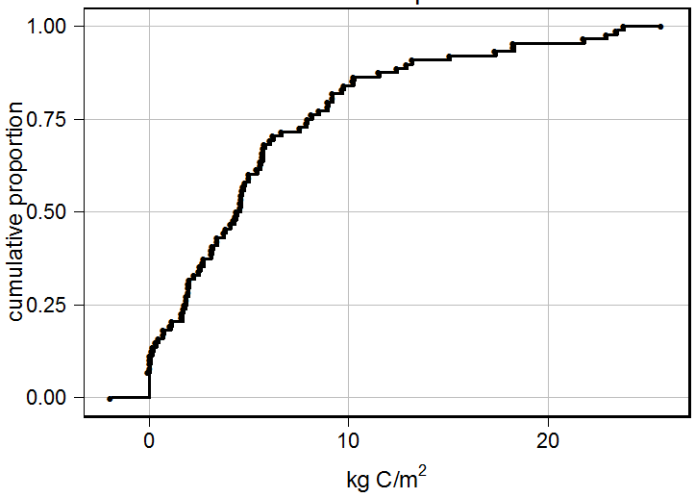

carbon−cover relationship

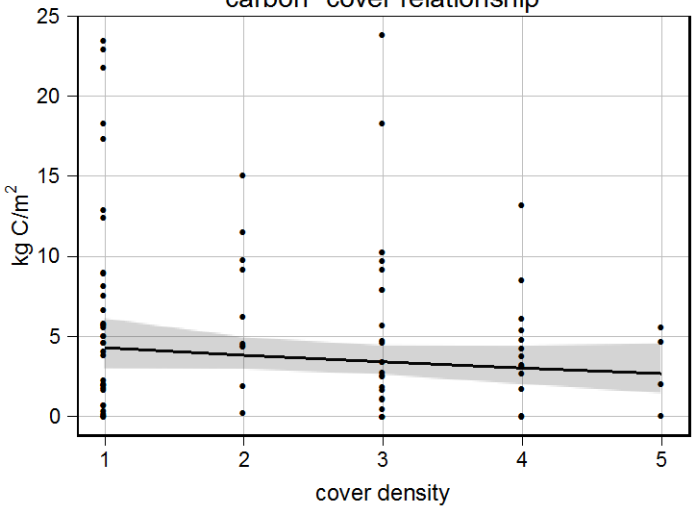

species composition

code	carbon	nTrees	carbonPct	nTreesPct
QUKE	169,908	846	35.6	31.9
QUDO	129,201	378	27	14.3
CADE27	56,740	525	11.9	19.8
QULO	36,726	25	7.7	0.9
ABCO	21,665	179	4.5	6.8
QUCH2	11,674	121	2.4	4.6
treeDead	9,640	186	2	7
PIPO	8,667	34	1.8	1.3
AECA	7,521	97	1.6	3.7
QUWIW	7,883	111	1.6	4.2
QUWI2	5,884	55	1.2	2.1
PIJE	4,096	3	0.9	0.1
PILA	2,999	26	0.6	1
FRLA	2,325	11	0.5	0.4
PISA2	1,425	8	0.3	0.3
...	...	...	...	...

Douglas-fir Forest (n = 7)

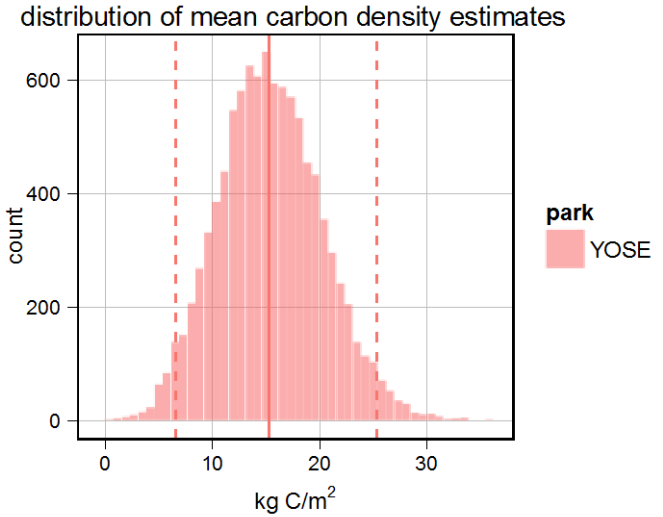

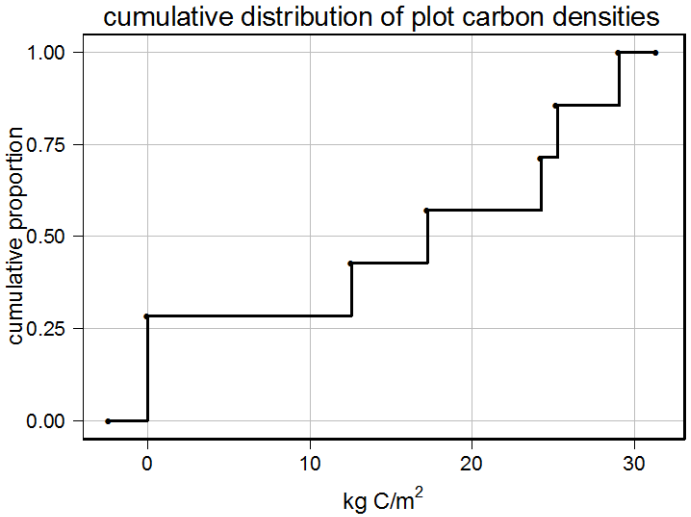

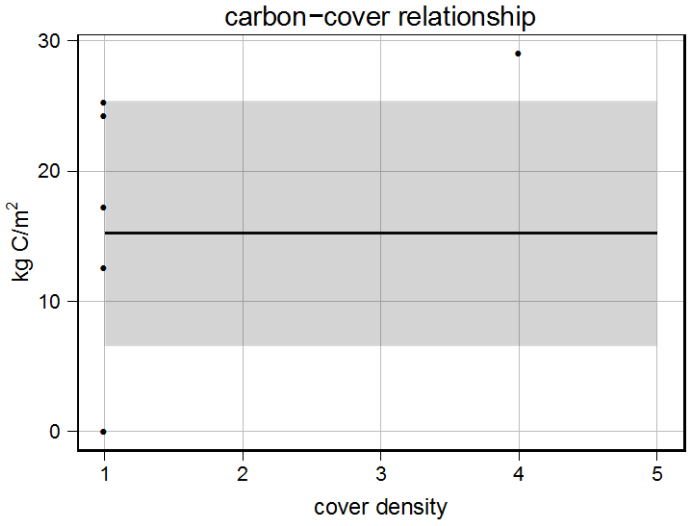

species composition

code	carbon	nTrees	carbonPct	nTreesPct
PSME	40,767	113	47.1	29.7
CADE27	20,126	102	23.2	26.8
PIPO	8,423	13	9.7	3.4
QUCH2	8,096	81	9.3	21.3
ABCO	4,812	21	5.6	5.5
QUKE	1,665	12	1.9	3.2
ALRH2	1,202	7	1.4	1.8
PILA	502	3	0.6	0.8
treeDead	447	14	0.5	3.7
ACMA3	333	2	0.4	0.5
CONU4	213	10	0.2	2.6
treeNone	0	2	0.0	0.5

Evergreen Oak Forest and Woodland (n = 110)

distribution of mean carbon density estimates

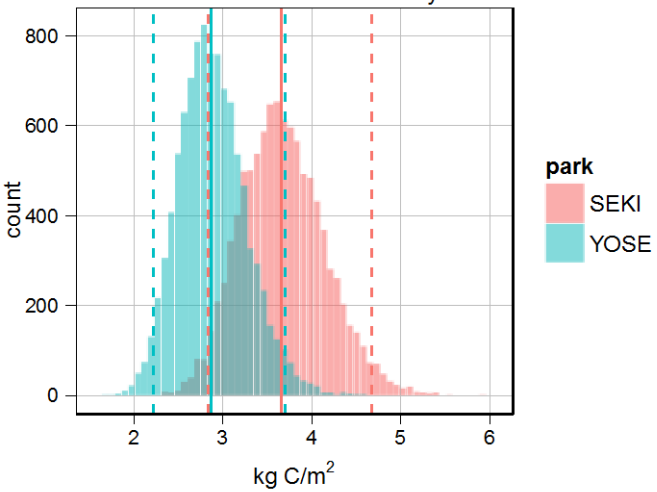

cumulative distribution of plot carbon densities

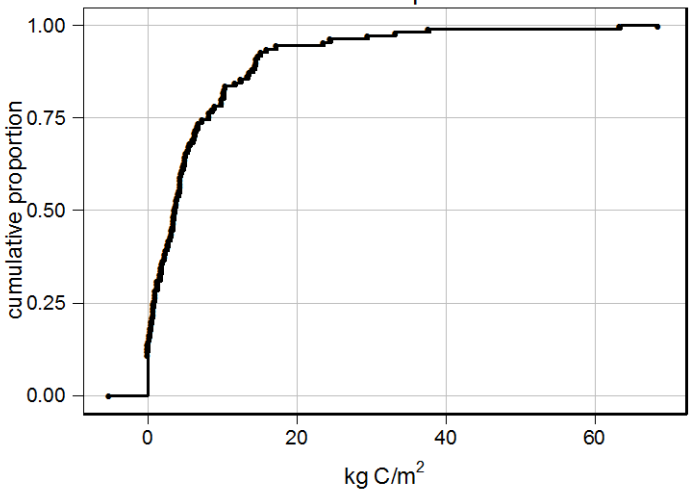

carbon−cover relationship

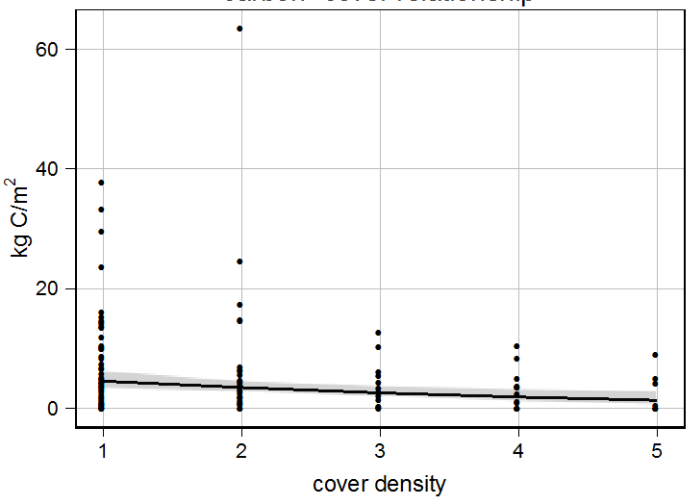

species composition

code	carbon	nTrees	carbonPct	nTreesPct
QUCH2	286,176	1,754	50.8	45.4
QUWIW	82,351	348	14.6	9
AECA	37,330	258	6.6	6.7
PIPO	24,675	39	4.4	1
QUWI2	20,179	185	3.6	4.8
CADE27	18,224	118	3.2	3.1
QUKE	17,824	71	3.2	1.8
treeDead	16,223	158	2.9	4.1
PISA2	11,702	19	2.1	0.5
PSME	12,045	20	2.1	0.5
TOCA	8,927	45	1.6	1.2
UMCA	7,945	676	1.4	17.5
PLRA	4,421	4	0.8	0.1
PILA	2,596	6	0.5	0.2
ABCO	1,608	14	0.3	0.4
...	...	...	...	...

Foothill Pine Woodland (n = 11)

distribution of mean carbon density estimates

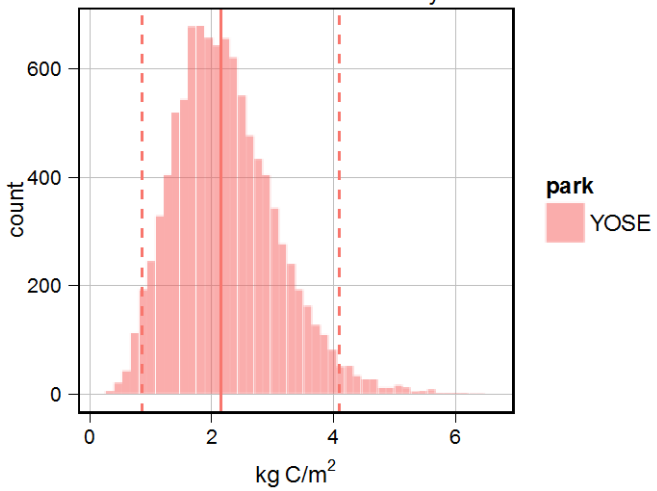

cumulative distribution of plot carbon densities

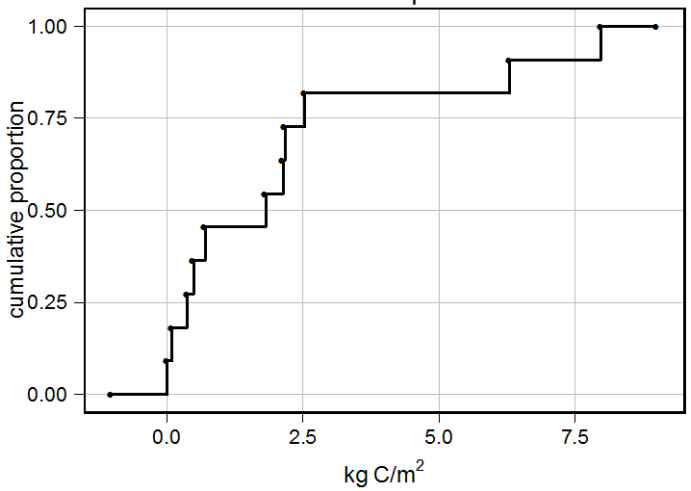

carbon−cover relationship

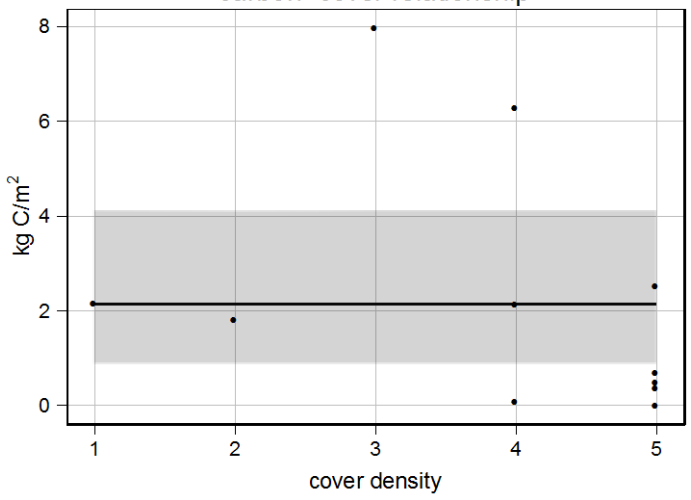

species composition

code	carbon	nTrees	carbonPct	nTreesPct
PISA2	18,126	32	72.3	65.3
QUWI2	2,949	7	11.8	14.3
QUKE	2,718	3	10.8	6.1
QUCH2	964	3	3.8	6.1
QULO	242	1	1.0	2.0
AECA	48	1	0.2	2.0
QUDO	28	1	0.1	2.0
treeNone	0	1	0.0	2.0

Foxtail Pine Forest (n = 58)

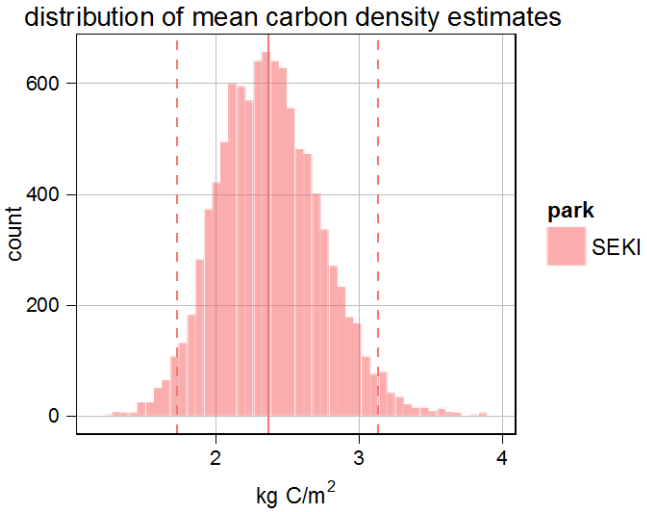

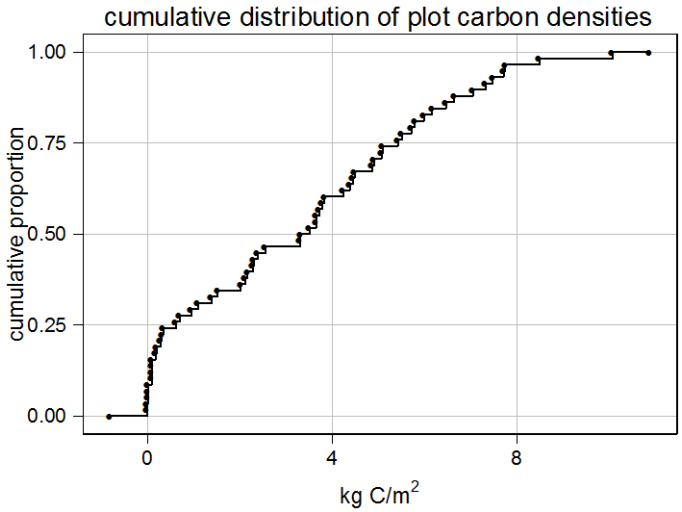

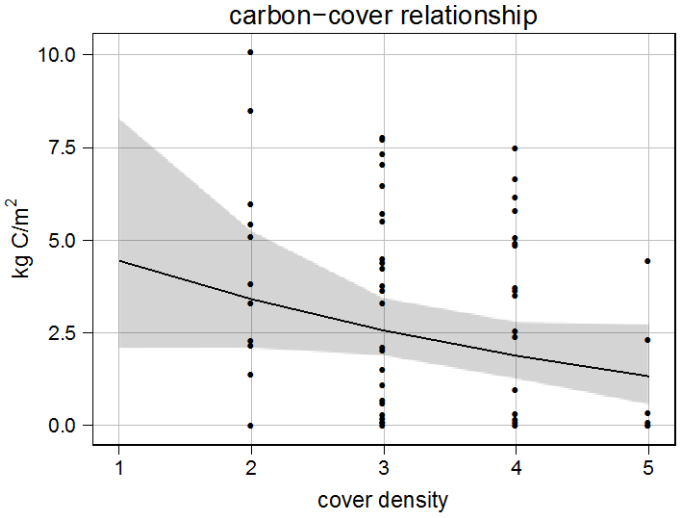

species composition

code	carbon	nTrees	carbonPct	nTreesPct
PICOM	94,108	731	46.4	46.0
treeDead	91,328	109	45.0	6.9
PIBAA	10,595	690	5.2	43.4
PIMO3	6,661	22	3.3	1.4
PIAL	169	35	0.1	2.2
ABMA	48	1	0.0	0.1
treeNone	0	1	0.0	0.1

Giant Sequoia Forest (n = 42)

distribution of mean carbon density estimates

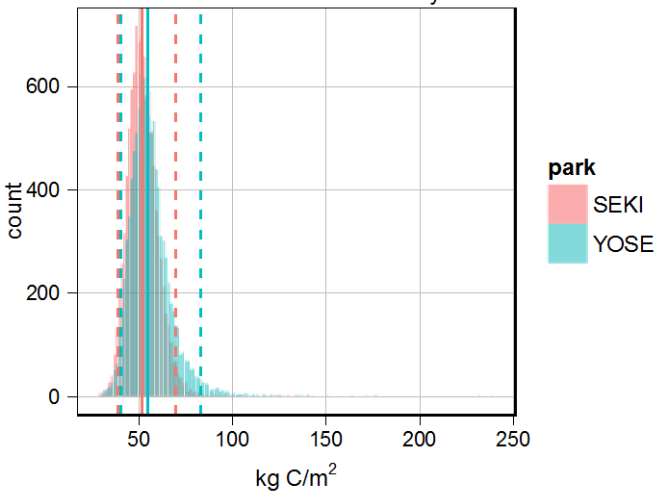

cumulative distribution of plot carbon densities

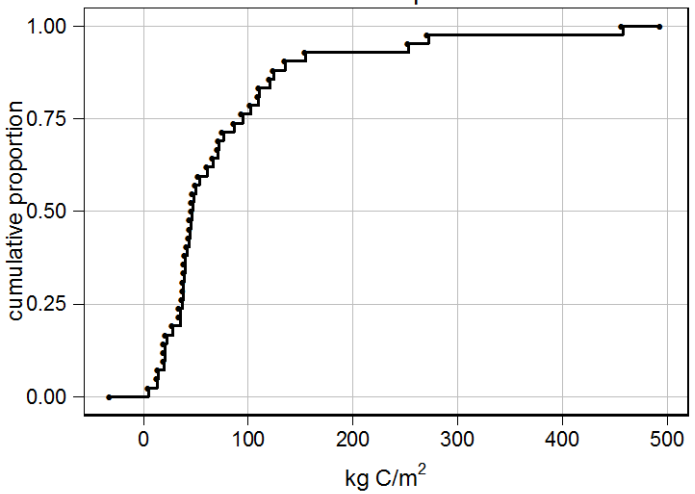

carbon−cover relationship

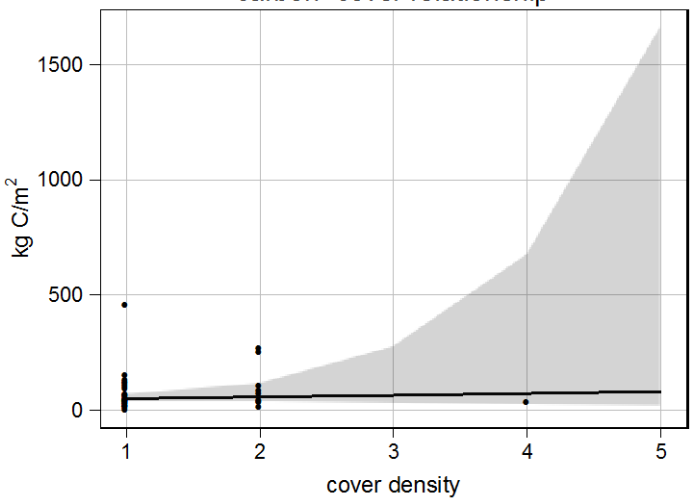

species composition

code	carbon	nTrees	carbonPct	nTreesPct
SEGI2	2,442,130	197	73.1	7.0
ABCO	488,420	1,746	14.6	62.4
treeDead	185,832	341	5.6	12.2
PILA	114,900	251	3.4	9.0
ABMAM	57,362	48	1.7	1.7
PIPO	27,913	13	0.8	0.5
CADE27	17,923	194	0.5	6.9
PINUS	7,486	1	0.2	0.0
CONU4	37	7	0.0	0.2
PIJE	172	1	0.0	0.0
QUKE	18	1	0.0	0.0

High Woodland (n = 89)

distribution of mean carbon density estimates

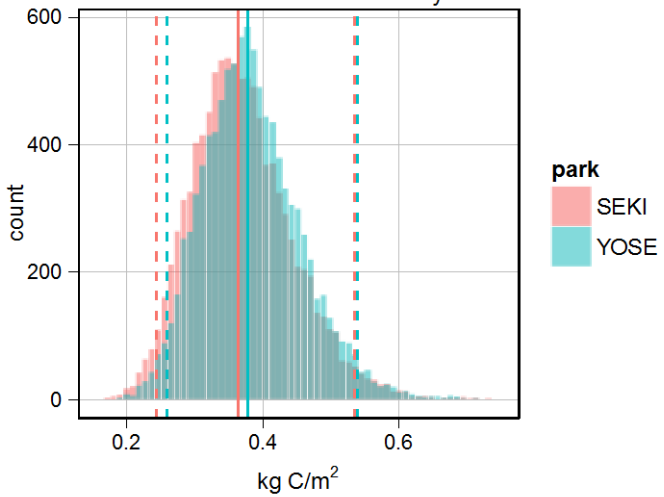

cumulative distribution of plot carbon densities

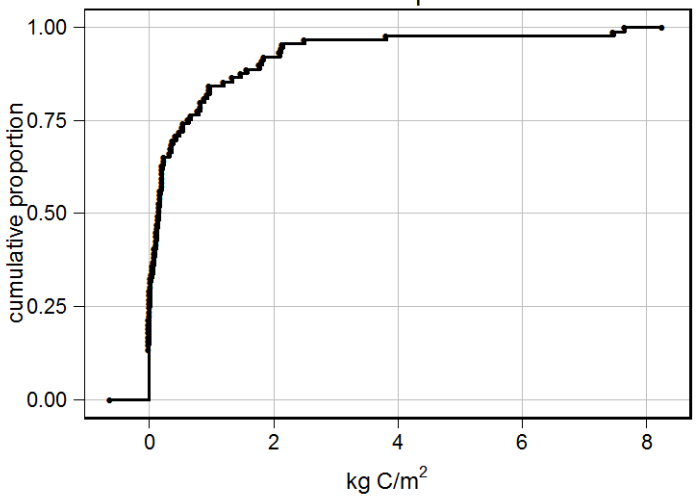

carbon−cover relationship

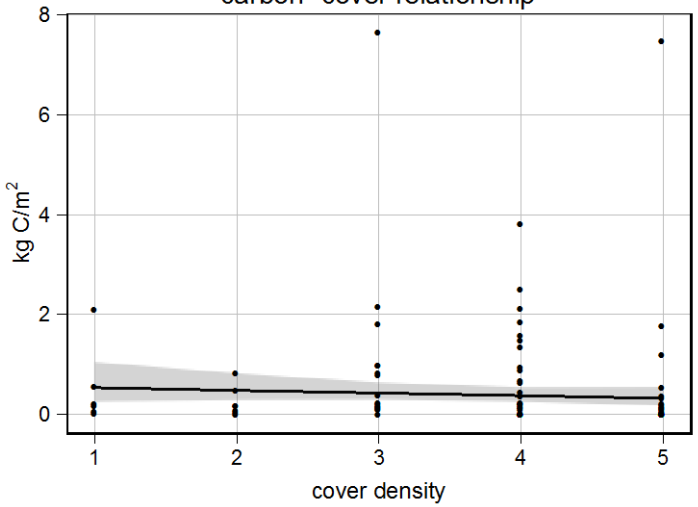

species composition

code	carbon	nTrees	carbonPct	nTreesPct
PICOM	14,939	227	33.6	11.0
treeDead	11,011	52	24.8	2.5
PIAL	6,126	1,552	13.8	75.2
JUOC	5,277	161	11.9	7.8
PIJE	2,125	18	4.8	0.9
PIMO	1,679	7	3.8	0.3
TSME	1,629	13	3.7	0.6
PIMO3	1,160	2	2.6	0.1
CADE27	324	13	0.7	0.6
ABCO	131	3	0.3	0.1
PIBAA	5	1	0.0	0.0
QUKE	14	1	0.0	0.0
treeNone	0	13	0.0	0.6

Jeffrey Pine Forest (n = 111)

distribution of mean carbon density estimates

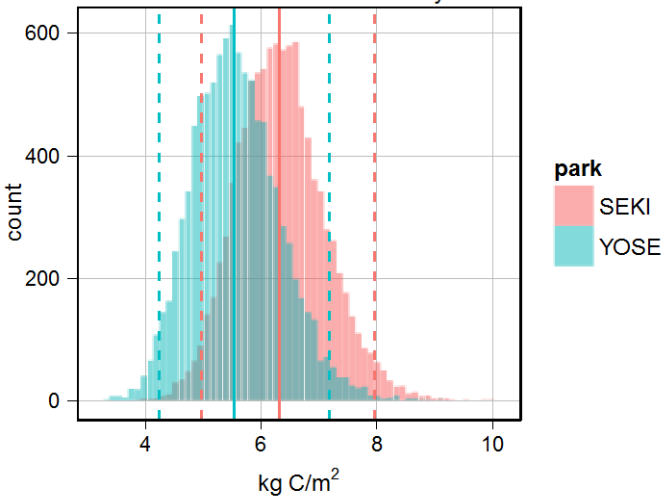

cumulative distribution of plot carbon densities

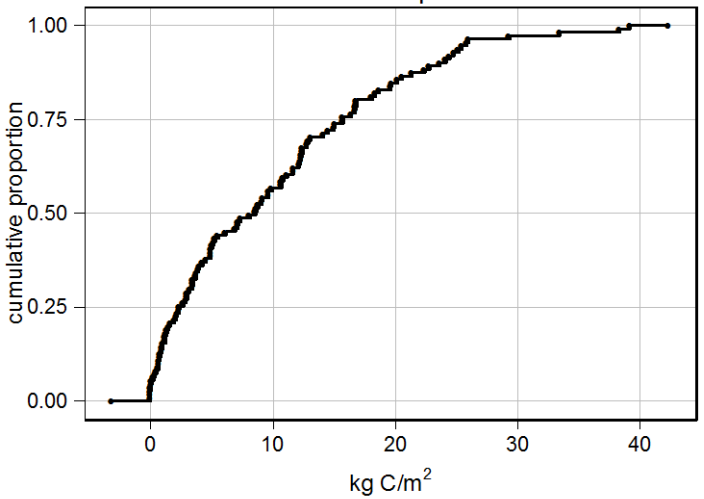

carbon−cover relationship

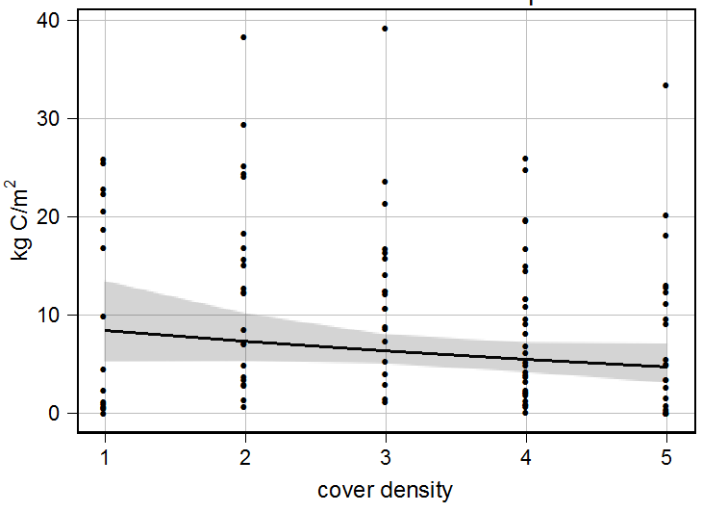

species composition

code	carbon	nTrees	carbonPct	nTreesPct
PIJE	662,498	855	65.3	36.9
ABCO	173,613	435	17.1	18.8
treeDead	65,430	179	6.4	7.7
ABMA	34,960	30	3.4	1.3
CADE27	27,536	162	2.7	7
PILA	14,887	10	1.5	0.4
QUCH2	10,800	200	1.1	8.6
PICOM	10,184	103	1	4.4
QUKE	4,216	88	0.4	3.8
PIPO	2,906	16	0.3	0.7
CELE3	1,929	8	0.2	0.3
PIMO	2,203	17	0.2	0.7
ABMAS	1,281	20	0.1	0.9
POBAT	1,293	5	0.1	0.2
BEOC2	231	6	0	0.3
...	...	...	...	...

Lodgepole Pine Forest (n = 190)

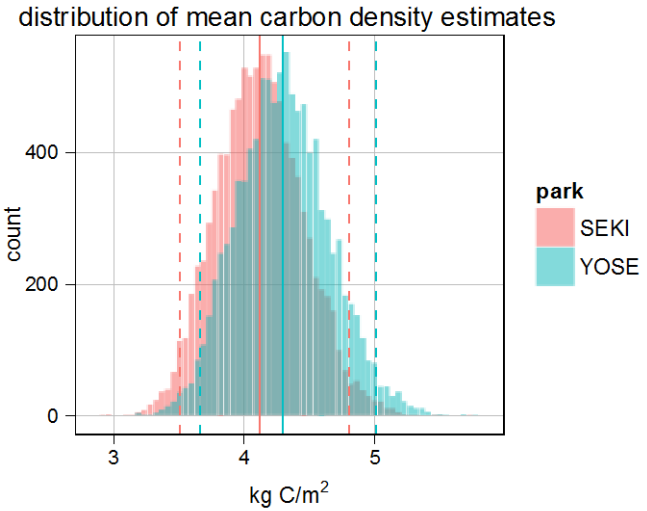

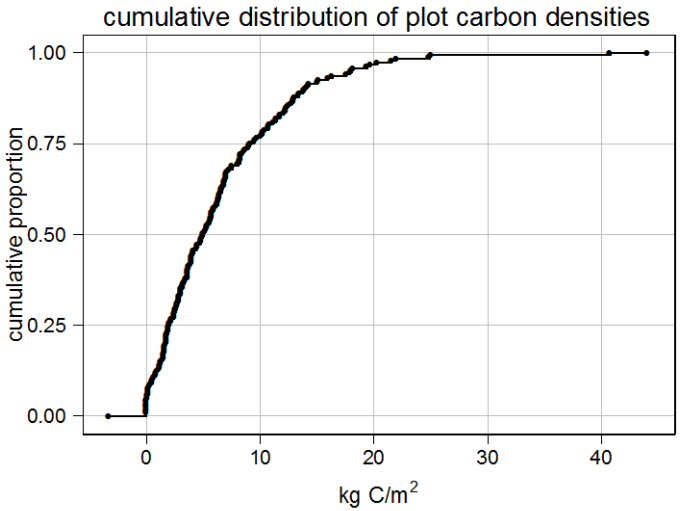

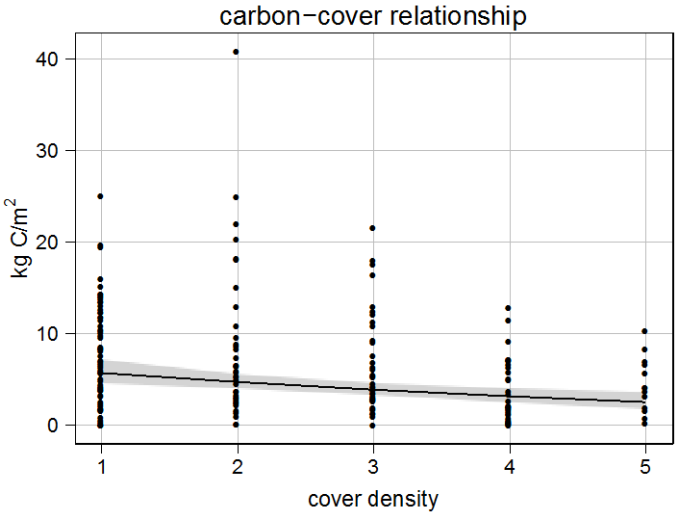

species composition

code	carbon	nTrees	carbonPct	nTreesPct
PICOM	803,220	6,773	73.7	76.7
treeDead	114,283	265	10.5	3.0
ABMA	99,628	735	9.1	8.3
ABMAS	22,410	89	2.1	1.0
PIMO3	22,889	120	2.1	1.4
PIJE	8,085	22	0.7	0.2
ABCO	5,439	39	0.5	0.4
POTR5	5,655	69	0.5	0.8
TSME	5,579	83	0.5	0.9
PIAL	2,140	598	0.2	6.8
JUOC	25	4	0.0	0.0
PIBAA	514	35	0.0	0.4
POBAT	436	2	0.0	0.0
treeNone	0	2	0.0	0.0

Mountain Hemlock Forest (n = 38)

distribution of mean carbon density estimates

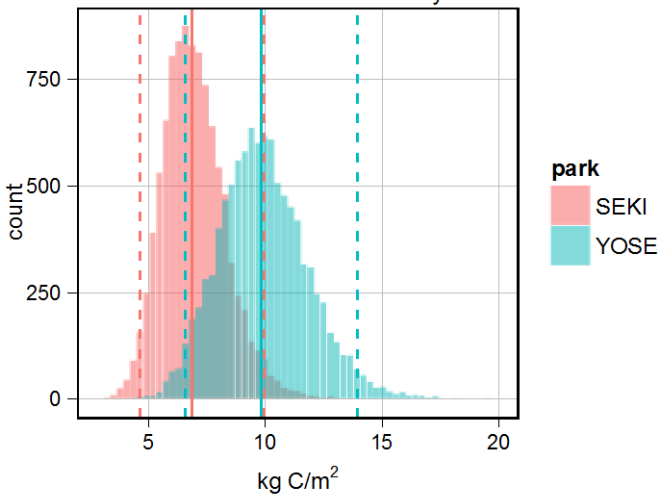

cumulative distribution of plot carbon densities

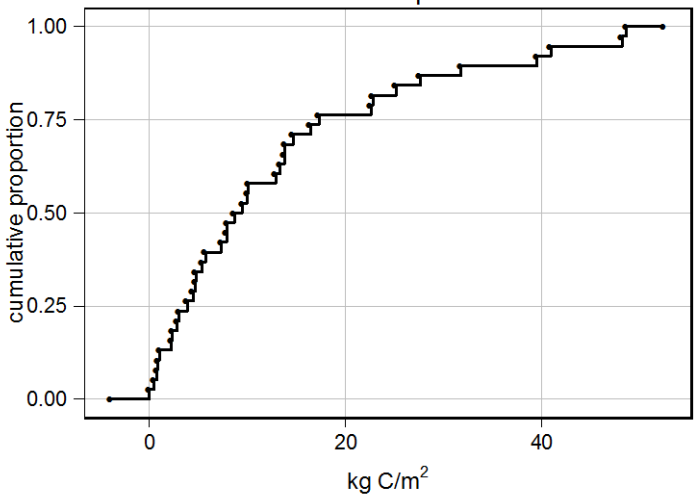

carbon−cover relationship

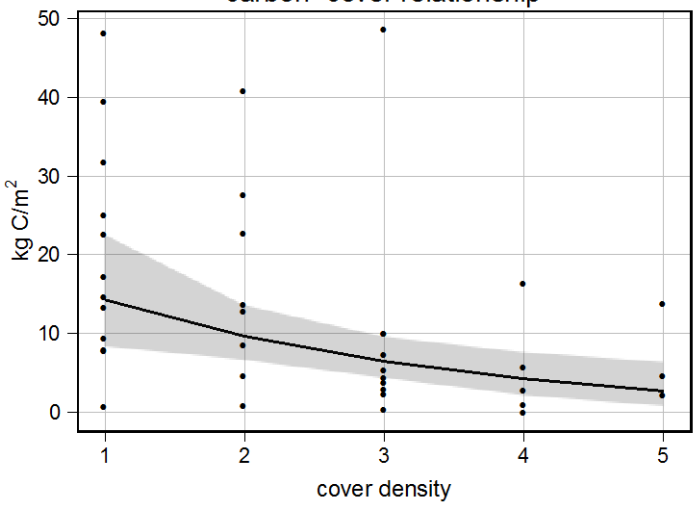

species composition

code	carbon	nTrees	carbonPct	nTreesPct
TSME	375,554	1,389	87.1	73.0
PICOM	18,043	338	4.2	17.8
treeDead	17,714	13	4.1	0.7
PIMO3	11,131	58	2.6	3.0
ABMA	8,227	3	1.9	0.2
PIAL	400	102	0.1	5.4
treeNone	0	1	0.0	0.1

Pinyon Pine Woodland (n = 27)

distribution of mean carbon density estimates

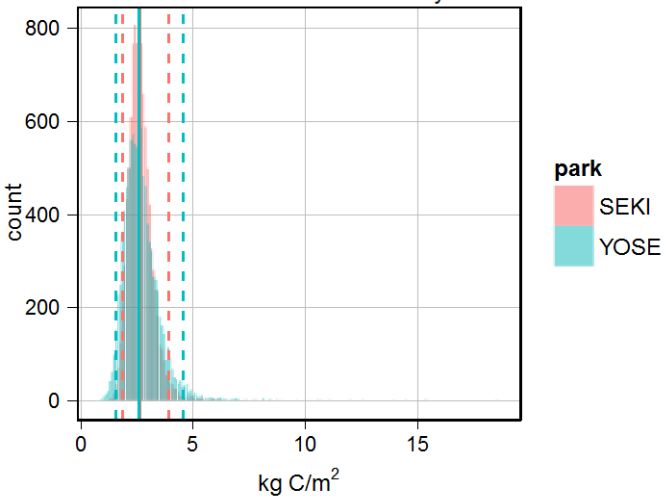

cumulative distribution of plot carbon densities

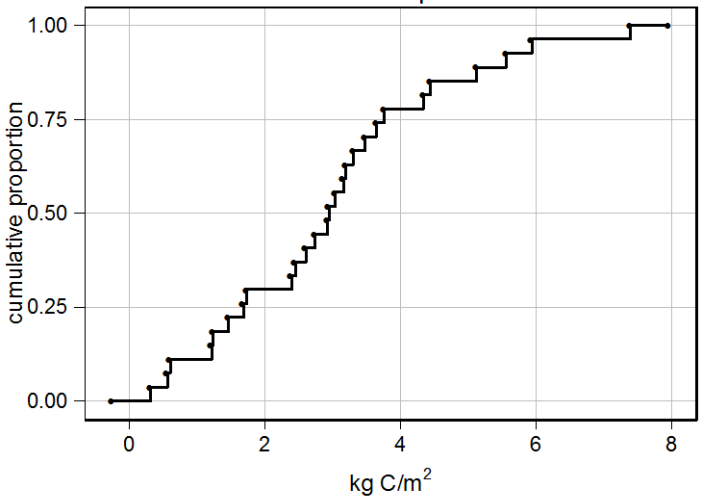

carbon−cover relationship

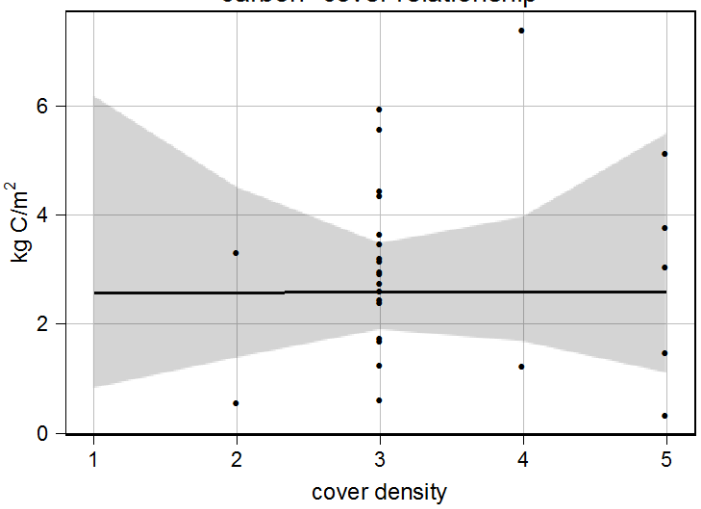

species composition

code	carbon	nTrees	carbonPct	nTreesPct
PIMO	54,971	355	80.4	71.4
QUCH2	4,164	56	6.1	11.3
CELE3	3,962	66	5.8	13.3
CADE27	3,293	7	4.8	1.4
PIJE	1,389	4	2.0	0.8
treeDead	277	2	0.4	0.4
JUOC	200	5	0.3	1.0
PIPO	86	1	0.1	0.2
QUKE	34	1	0.1	0.2

Ponderosa Pine Forest (n = 123)

distribution of mean carbon density estimates

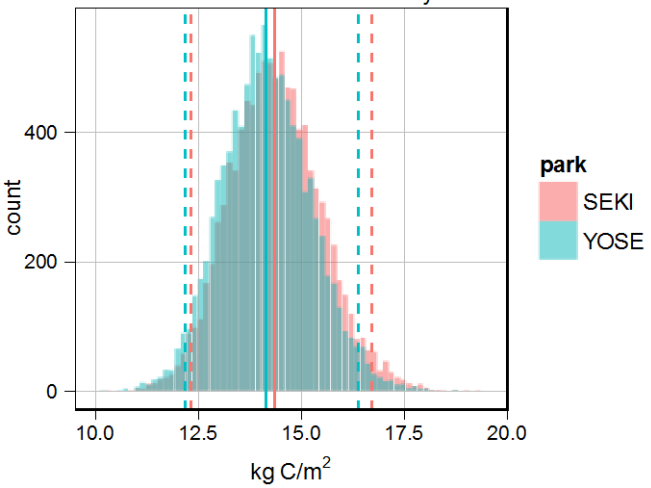

cumulative distribution of plot carbon densities

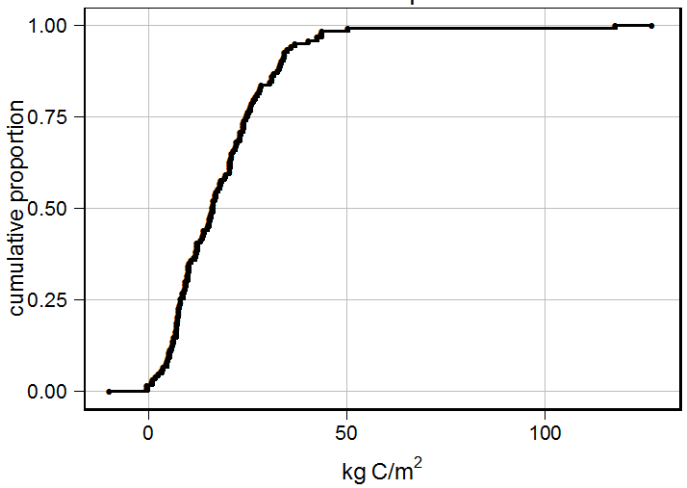

carbon−cover relationship

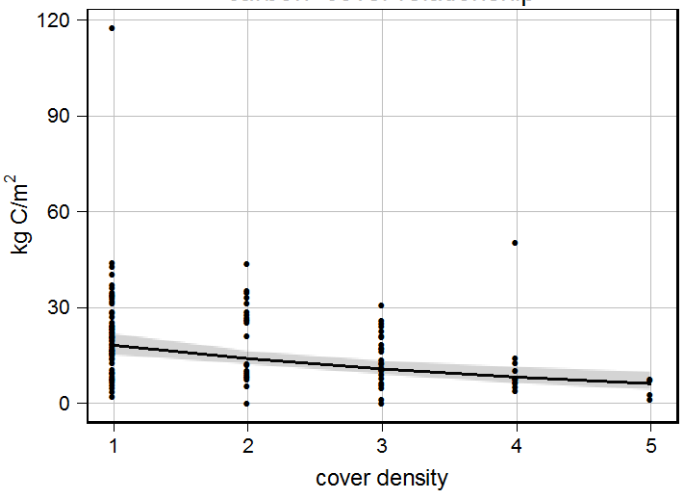

species composition

code	carbon	nTrees	carbonPct	nTreesPct
PIPO	1,058,437	1,827	49.6	23.2
CADE27	410,747	2,878	19.2	36.6
ABCO	225,332	1,204	10.5	15.3
treeDead	177,104	820	8.3	10.4
QUKE	132,868	423	6.2	5.4
PILA	97,653	435	4.6	5.5
QUCH2	15,315	178	0.7	2.3
PIJE	10,859	12	0.5	0.2
PSME	4,375	30	0.2	0.4
ACMA3	918	8	0	0.1
ALRH2	577	7	0	0.1
CONU4	50	4	0	0.1
PIAT	1,008	6	0	0.1
QUWI2	28	1	0	0
treeNone	0	1	0	0
...	...	...	...	...

Ponderosa Pine Woodland (n = 13)

distribution of mean carbon density estimates

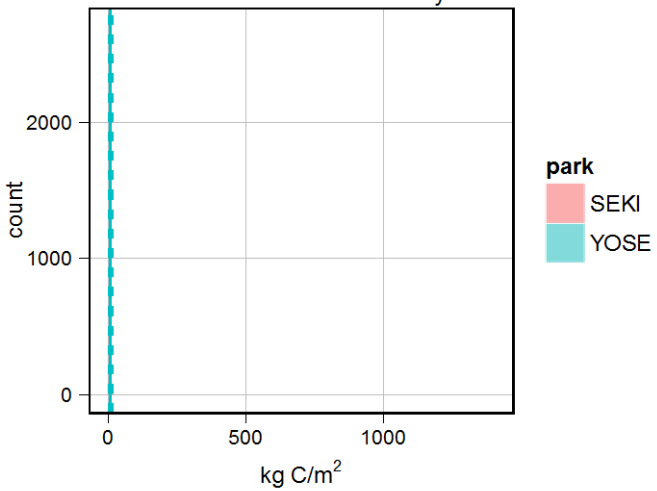

cumulative distribution of plot carbon densities

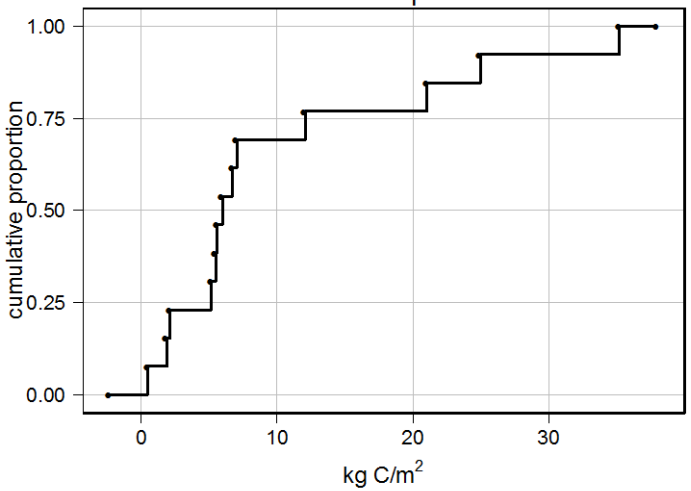

carbon−cover relationship

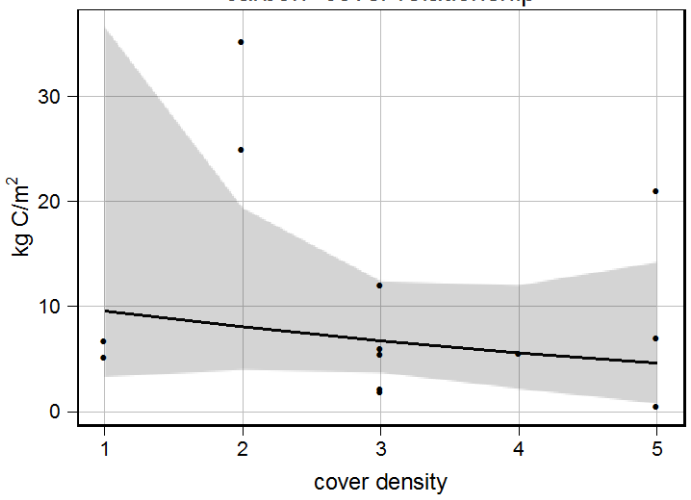

species composition

code	carbon	nTrees	carbonPct	nTreesPct
QUKE	60,719	87	51.8	19.7
PIPO	32,965	89	28.1	20.2
CADE27	12,753	146	10.9	33.1
treeDead	7,497	59	6.4	13.4
PSME	985	13	0.8	2.9
PILA	589	11	0.5	2.5
ABCO	498	7	0.4	1.6
AECA	441	4	0.4	0.9
ARVI4	335	15	0.3	3.4
PIJE	192	2	0.2	0.5
ALRH2	119	1	0.1	0.2
QUCH2	78	4	0.1	0.9
PISA2	7	3	0.0	0.7

Red Fir Forest (n = 116)

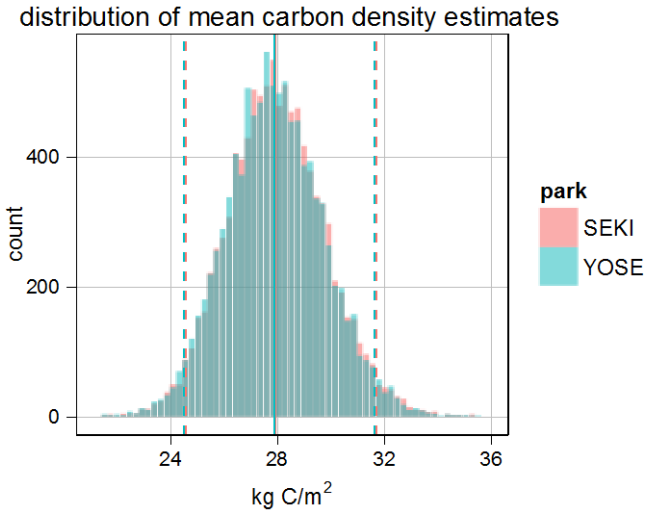

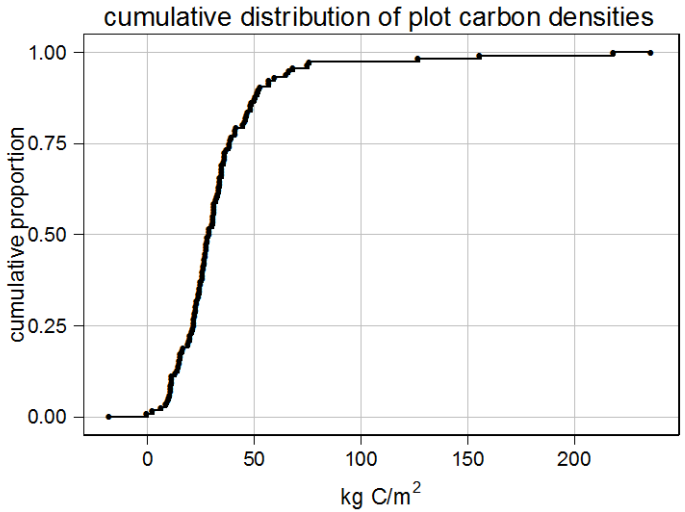

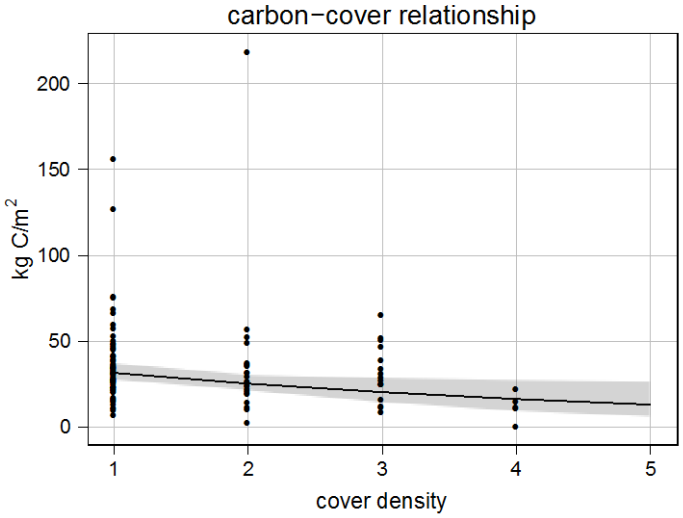

species composition

code	carbon	nTrees	carbonPct	nTreesPct
ABMA	1,911,434	1,600	52.7	29.0
ABMAS	537,531	1,213	14.8	22.0
ABCO	472,044	1,271	13.0	23.1
treeDead	280,782	372	7.7	6.7
ABMAM	215,955	369	5.9	6.7
PIMO3	50,262	124	1.4	2.2
PICOM	46,917	361	1.3	6.5
PILA	42,209	47	1.2	0.9
PIJE	36,350	47	1.0	0.9
PIMO	27,134	33	0.7	0.6
TSME	6,420	42	0.2	0.8
CADE27	1,158	7	0.0	0.1
JUOC	379	3	0.0	0.1
PIBAA	231	18	0.0	0.3
SEGI2	797	7	0.0	0.1

Riparian Forest (n = 87)

distribution of mean carbon density estimates

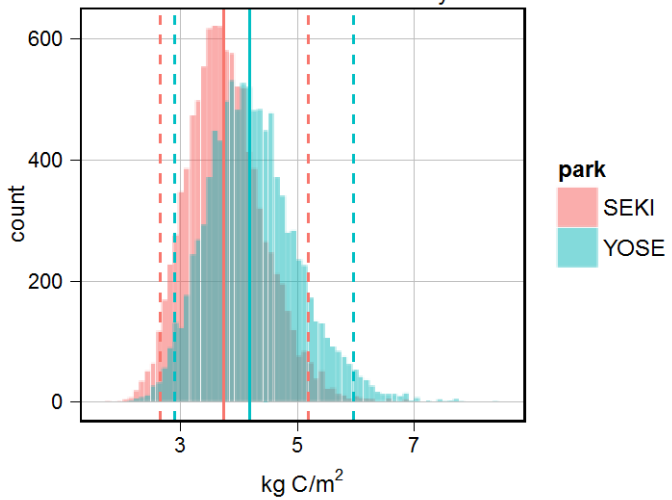

cumulative distribution of plot carbon densities

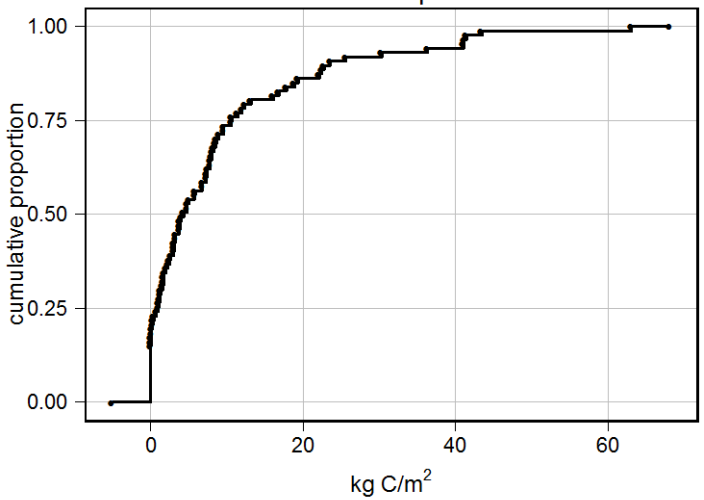

carbon−cover relationship

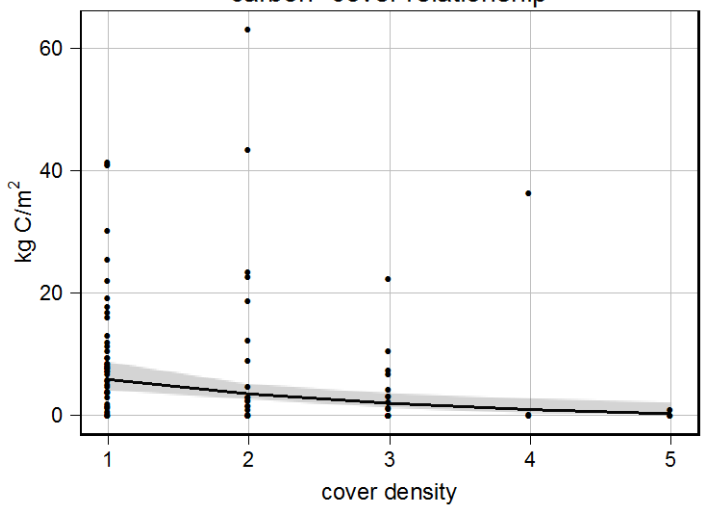

species composition

code	carbon	nTrees	carbonPct	nTreesPct
ABCO	72,250	78	17.7	5.1
POBAT	63,377	136	15.6	8.8
ALRH2	53,730	344	13.2	22.4
PIPO	46,895	13	11.5	0.8
CADE27	44,191	74	10.9	4.8
POTR5	33,056	550	8.1	35.8
PLRA	27,596	35	6.8	2.3
POBA2	16,383	25	4	1.6
QUCH2	13,897	62	3.4	4
treeDead	9,835	27	2.4	1.8
PICOM	5,199	36	1.3	2.3
PIJE	4,913	16	1.2	1
QUKE	4,158	8	1	0.5
CONU4	2,274	37	0.6	2.4
PSME	1,630	5	0.4	0.3
...	...	...	...	...

Riparian Shrub (n = 23)

distribution of mean carbon density estimates

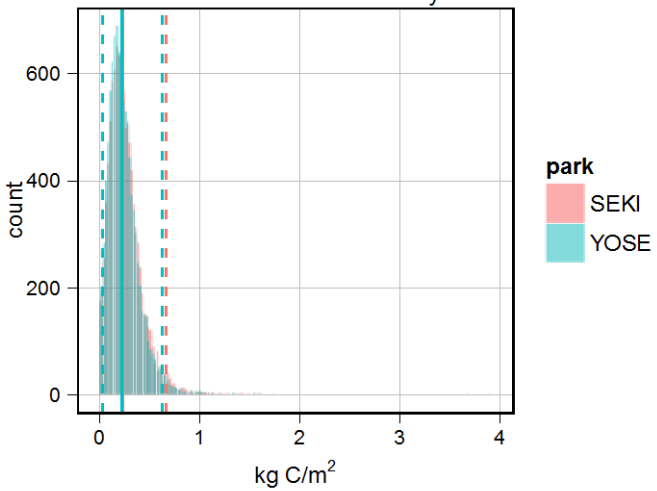

cumulative distribution of plot carbon densities

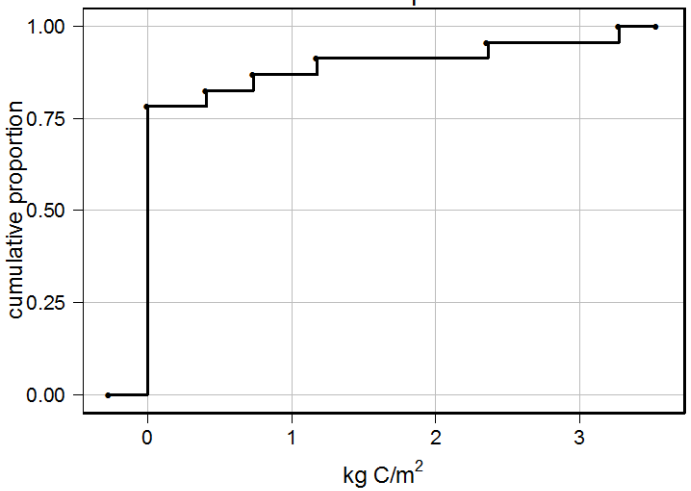

carbon−cover relationship

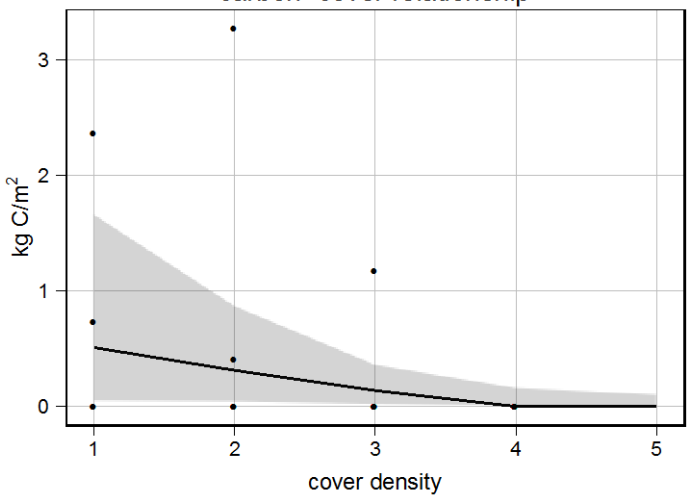

species composition

code	carbon	nTrees	carbonPct	nTreesPct
SALA3	3,985	25	65.7	37.3
SALA6	1,199	8	19.8	11.9
SALUL	473	9	7.8	13.4
ACMA3	226	1	3.7	1.5
ALRH2	97	3	1.6	4.5
QUWI2	64	2	1.1	3.0
PISA2	24	1	0.4	1.5
treeNone	0	18	0.0	26.9

Shrub (n = 258)

distribution of mean carbon density estimates

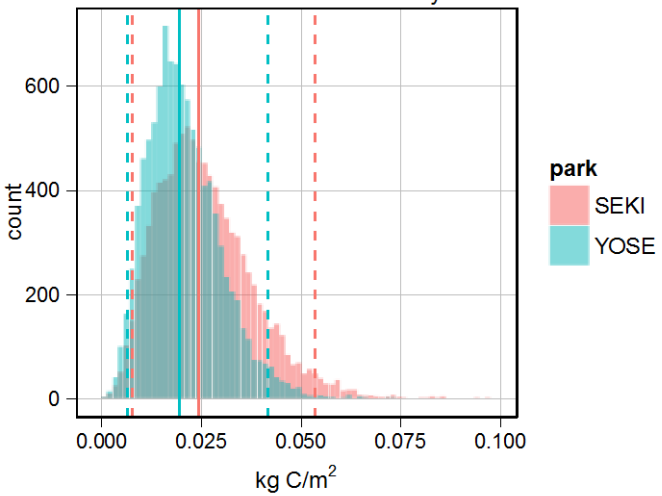

cumulative distribution of plot carbon densities

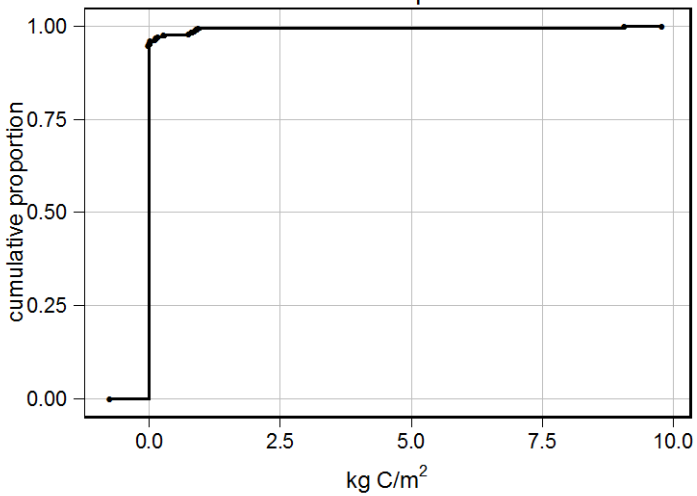

carbon−cover relationship

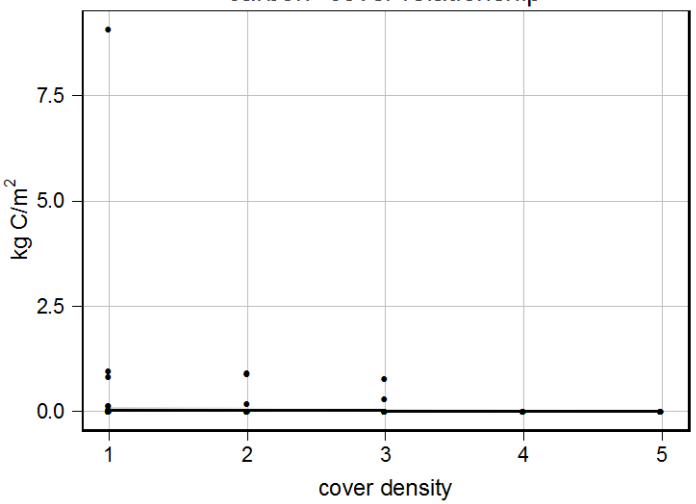

species composition

code	carbon	nTrees	carbonPct	nTreesPct
treeDead	9,258	33	71.9	9.3
PIAT	2,809	65	21.8	18.3
CADE27	367	2	2.9	0.6
ABCO	166	1	1.3	0.3
ABMA	150	3	1.2	0.8
QUCH2	120	3	0.9	0.8
treeNone	0	249	0.0	69.9

Western White Pine Forest (n = 27)

distribution of mean carbon density estimates

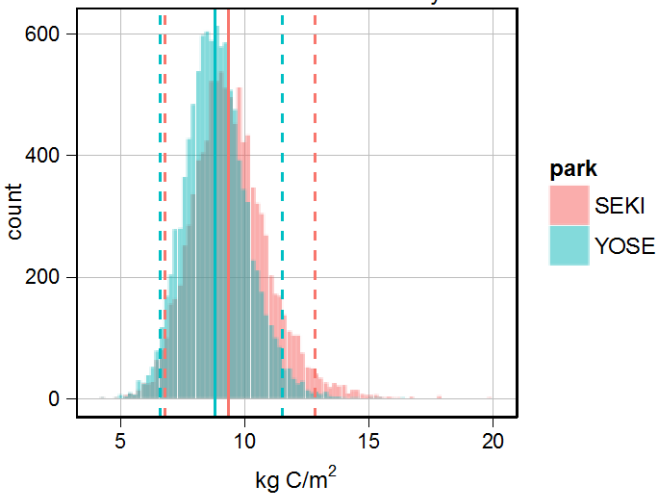

cumulative distribution of plot carbon densities

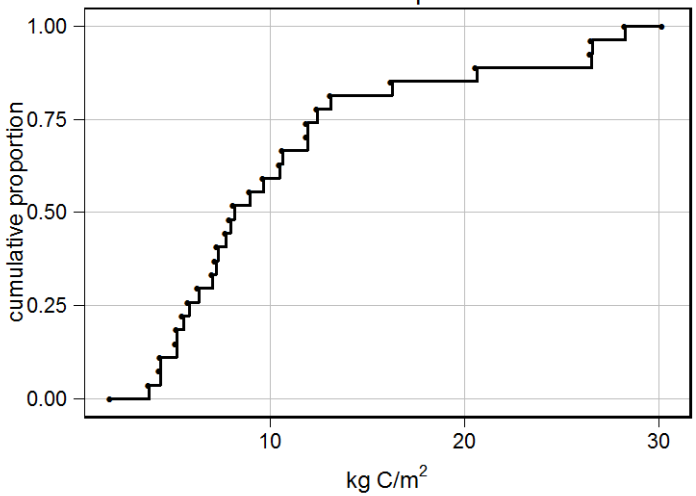

carbon−cover relationship

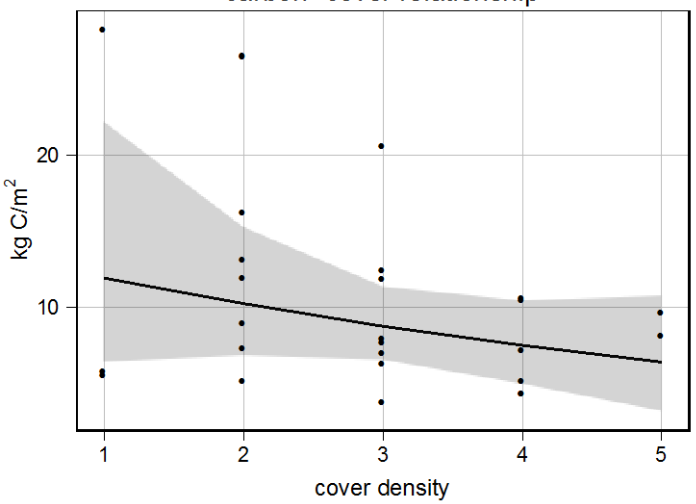

species composition

code	carbon	nTrees	carbonPct	nTreesPct
PIMO3	129,158	136	53.9	43.6
ABMA	48,256	41	20.1	13.1
TSME	31,582	46	13.2	14.7
treeDead	16,572	14	6.9	4.5
PICOM	13,918	74	5.8	23.7
PIJE	181	1	0.1	0.3

Western White Pine Woodland (n = 4)

distribution of mean carbon density estimates

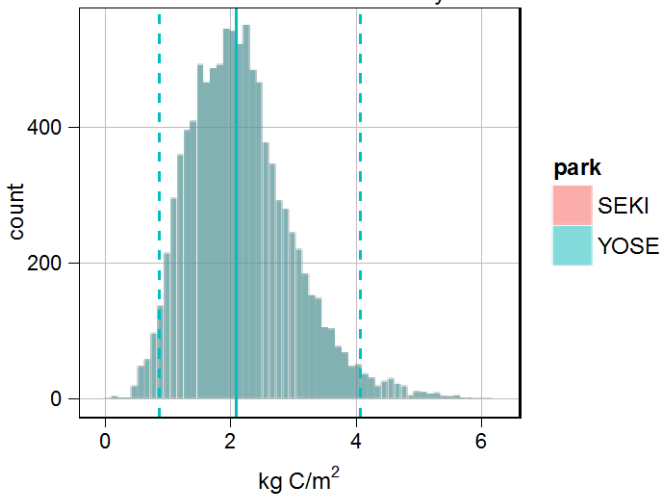

cumulative distribution of plot carbon densities

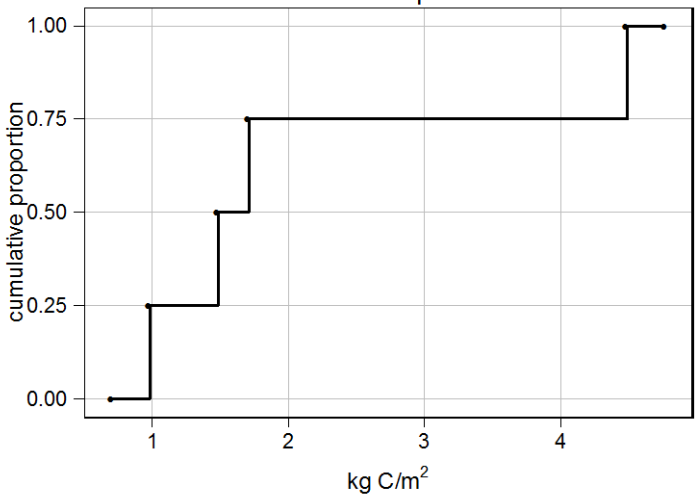

carbon−cover relationship

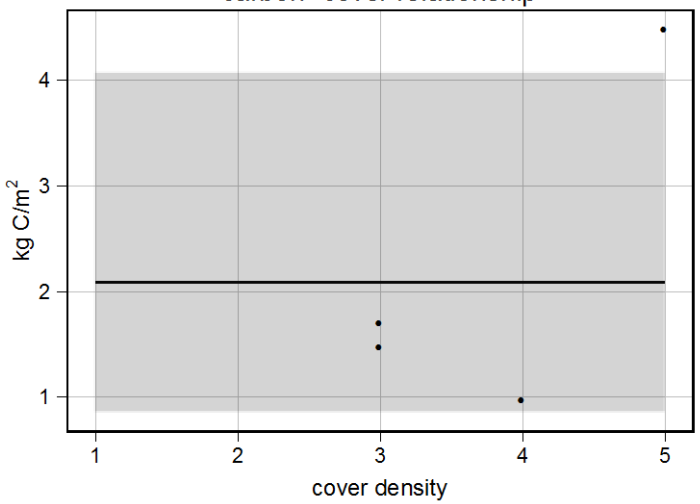

species composition

code	carbon	nTrees	carbonPct	nTreesPct
PIMO3	6,392	53	64.3	80.3
treeDead	3,038	1	30.6	1.5
PICOM	358	8	3.6	12.1
ABMA	137	1	1.4	1.5
ABMAS	6	1	0.1	1.5
PIAL	3	2	0.0	3.0

White Fir − Sugar Pine Forest (n = 224)

distribution of mean carbon density estimates

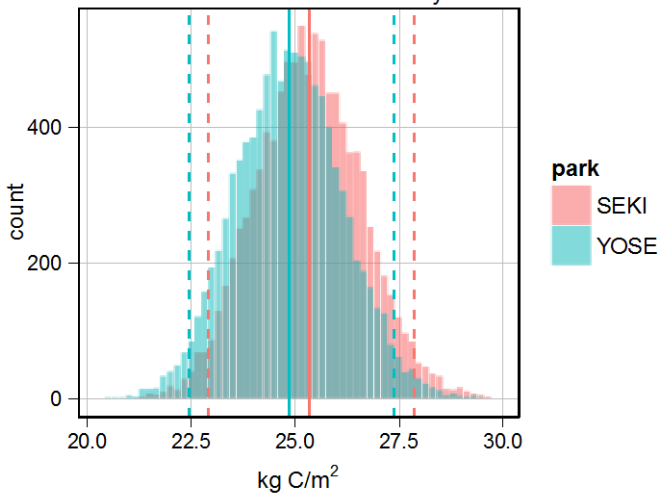

cumulative distribution of plot carbon densities

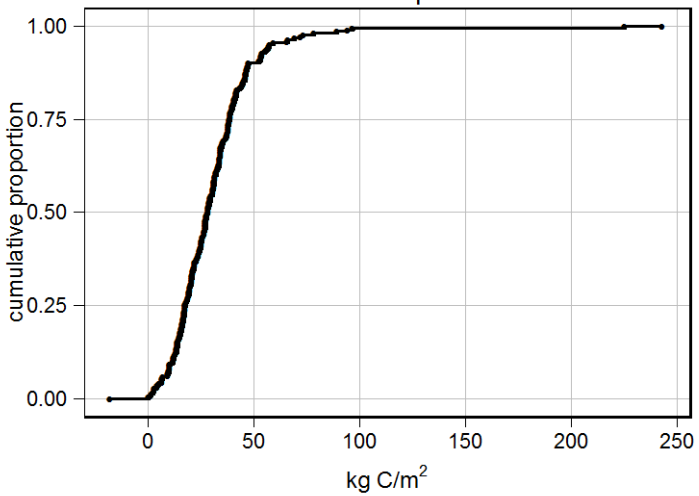

carbon−cover relationship

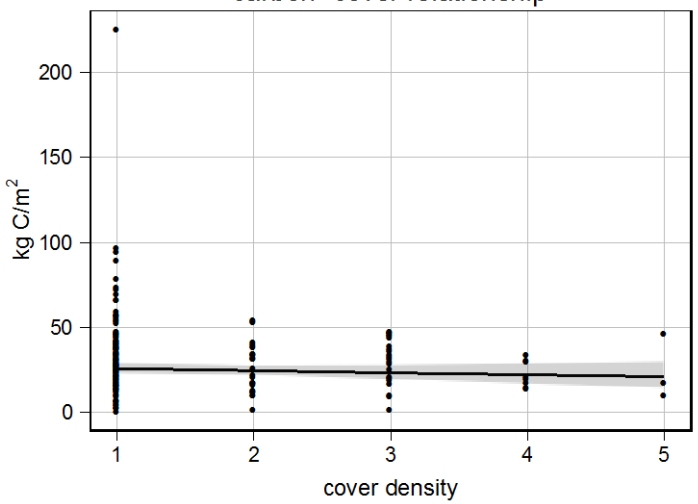

species composition

code	carbon	nTrees	carbonPct	nTreesPct
ABCO	3,331,974	8,376	50.6	56.6
PILA	1,631,938	1,069	24.8	7.2
treeDead	699,566	1,966	10.6	13.3
CADE27	421,130	2,217	6.4	15
PIPO	195,055	219	3	1.5
PIJE	144,698	111	2.2	0.8
QUKE	59,170	282	0.9	1.9
ABMA	29,722	54	0.5	0.4
SEGI2	29,959	24	0.5	0.2
ABMAM	8,504	16	0.1	0.1
ABMAS	6,402	81	0.1	0.5
PICOM	6,012	25	0.1	0.2
POBAT	5,757	6	0.1	0
PSME	5,342	13	0.1	0.1
QUCH2	5,313	116	0.1	0.8
...	...	...	...	...

The Department of the Interior protects and manages the nation's natural resources and cultural heritage; provides scientific and other information about those resources; and honors its special responsibilities to American Indians, Alaska Natives, and affiliated Island Communities.

NPS 104/127729, 102/127729, January 2015

National Park Service
U.S. Department of the Interior

Natural Resource Stewardship and Science
1201 Oakridge Drive, Suite 150
Fort Collins, CO 80525

www.nature.nps.gov